WAVE FORCES ON CYLINDRICAL PILES AND PILE GROUPS

(A critical review)

Robert Shaul, BSc(Eng) in Civil Engineering
University of Cape Town

A thesis submitted in partial fulfilment of the requirements
for the degree of Master of Science in Engineering

Department of Civil Engineering
University of Cape Town

September 1990

DECLARATION OF CANDIDATE

I, Robert Shaul, hereby declare that this thesis is my own work and that it has not been submitted for a degree at another university.

Signed by candidate

Robert Shaul

September 1990

ABSTRACT

This thesis is a critical review of methods of predicting wave forces on vertical piles or groups of piles. It assigns different force prediction theories to different situations or flow regimes and analyses their advantages and disadvantages. The thesis is split into two sections: Section I reviewing the force prediction methods for single piles, and Section II for groups of piles.

Single pile force prediction methods reviewed include the Morison equation, the total force coefficient C_F, vortex theory and diffraction theory. The Morison equation, valid for piles with a diameter which is small in relation to the wavelength ($D/L < 0,2$) consists of two terms, each of which contains a coefficient (C_M or C_D). The accuracy of both the equation and the coefficients are analysed, together with any flaws pertaining either to the equation or to the experimental determination of C_M and C_D. The total force coefficient, C_F, which predicts only the maximum force in a wave cycle, is analysed in a similar way. A totally different approach is through the vortex theory, which predicts the forces on cylinders as a function of the vortices. Diffraction theory relies upon potential flow theory, and is therefore valid only for large diameter cylinders ($D/L > 0,2$). However, it offers a mathematically exact resultant force on a cylinder.

This section concludes that the Morison equation, the total force coefficient and the diffraction theory are all adequate methods of force prediction, though the first two are only accurate to about 25%. Vortex prediction may become more accurate when the theory behind vortex shedding and dissipation is better understood.

Section II examines interference effects between piles, which can significantly affect the forces on the piles. However, much more research needs to be performed in this area before any degree of certainty is achieved.

ACKNOWLEDGEMENTS

The author wishes to acknowledge the invaluable help and assistance given to him throughout the duration of this thesis, and would like to give his special thanks to the following:

Professor F A Kilner, Head of the Department of Civil Engineering, for guidance and expertise.

Mrs P Jordaan, for typing a sometimes illegible script.

Mrs C Welch, for typing the figures.

The Council for Scientific and Industrial Research for the award of a postgraduate bursary,

and all others who have assisted in putting the document together.

TABLE OF CONTENTS

	Page
ABSTRACT	ii
ACKNOWLEDGEMENTS	iii
TABLE OF CONTENTS	iv
NOMENCLATURE	vii
INTRODUCTION	xi
SECTION I : FORCES ON A SINGLE PILE	
1. Physical Processes	1.1
1.1 Regimes of validity for Morison and diffraction theories	1.1
1.2 Vortex formation around a pile	1.4
1.2.1 Comparison with steady flow	1.4
1.2.2 Number of vortices shed per half wave period	1.6
1.2.3 Correlation of the vortices with the length of the pile	1.9
1.3 Shear force around piles	1.12
2. Force Prediction in Real, Viscous Flows	2.1
2.1 The Morrison equation	2.1
2.1.1 Theoretical derivation of Morison's equation	2.2
2.1.1.1 The inertial force	2.3
2.1.1.2 The drag force	2.4
2.1.2 Relative magnitudes of inertia and drag forces	2.4
2.1.3 The Morison force coefficients C_M and C_D	2.6
2.1.3.1 A short historical development of C_M and C_D	2.6
2.1.3.2 Accepted values of C_M and C_D for Morison's equation	2.8
2.1.3.3 Difference between two- and three-dimensional flow	2.18
2.1.3.4 C_M and C_D from field tests	2.21
2.1.4 The accuracy of Morison's equation	2.25
2.1.4.1 Force predictions over a wave period	2.25
2.1.4.2 The accuracy of the coefficients C_M and C_D	2.30
2.1.5 Flows in Morison's equation	2.30

2.2 Extensions of the Morison equation 2.32

2.2.1 An alternative Fourier series approach to the force on a pile 2.32

2.2.2 The four-term Morison equation 2.34

2.2.3 Other variations on the Morison equation 2.34

2.3 Alternatives to the Morison equation 2.35

2.3.1 Force prediction from vortex theory 2.36

2.3.2 Iverson's modulus 2.37

2.4 Total force coefficients 2.39

2.4.1 Total force coefficient C_F 2.39

2.4.2 Differences in C_F between two- and three-dimensional flow 2.40

2.4.3 Total force coefficient C_{F*} 2.40

3. Diffraction Theory 3.1

3.1 Linear diffraction theory 3.1

3.2 Non-linear diffraction theory 3.5

3.3 Extensions of diffraction theory 3.8

3.3.1 Diffraction theory with shallow water cnoidal waves 3.8

4. Transverse Forces on a Pile 4.1

4.1 Parameters governing C_L 4.3

4.2 The magnitude of the transverse force 4.3

4.2.1 The magnitude of C_L 4.4

4.2.1.1 C_L at low Reynolds number 4.4

4.2.1.2 C_L at high Reynolds number 4.5

4.2.2 Field tests of the transverse force 4.8

4.3 Frequency of the transverse force 4.9

4.3.1 Spanwise corrolation of the transverse force 4.9

4.4 Vortex prediction of the transverse force 4.11

5. Conclusions to Section I : Forces on a Single Pile 5.1

SECTION II : FORCES ON PILE GROUPS

6.	Forces on Pile Groups in Steady Flow	6.1
6.1	Forces on piles in a column	6.1
6.1.1	Forces on two piles in a column	6.1
6.1.2	The force on multiple cylinders in a column	6.4
6.2	Forces on piles in a row	6.5
6.2.1	Forces on two piles in a row	6.5
6.2.2	Force on multiple cylinders in a row	6.7
6.3	The force on rectangular arrays	6.7
6.4	Forces on two staggered cylinders	6.8
6.4.1	The drag force	6.8
6.4.2	The transverse force	6.9
6.5	The effect of Reynolds number	6.10
7.	Forces on Pile Groups in Oscillatory Real Flow	7.1
7.1	Forces on a line of cylinders in oscillatory flow	7.3
7.1.1	Forces on a column	7.3
7.1.2	Forces on a row of cylinders	7.4
7.1.3	Forces on a line of cylinders angled to the direction of flow	7.8
7.2	Force on a cylinder in a large array	7.9
7.3	Forces on large arrays	7.10
7.3.1	Solidification	7.10
7.3.2	Resultant forces on complete arrays	7.11
7.3.2.1	In-line forces	7.11
7.3.2.2	Transverse forces	7.14
7.4	Effect of Reynolds number	7.15
8.	Potential Flow Theory around Cylinder Arrays	8.1
8.1	Diffraction theory on cylinder arrays	8.1
9.	Conclusions to Section II : Forces on Pile Groups	9.1
REFERENCES		R.1

APPENDIX A : Bessel Functions

APPENDIX B : Examinations written by the author to complete the requirements of the degree

NOMENCLATURE

a	=	horizontal dimension of wave orbital
A	=	area
C_D	=	coefficient of drag
C_F	=	total force coefficient
C_{F*}	=	total force coefficient as re-defined by Bishop et al (1980)
$(C_{F*})_{RMS}$	=	root mean square value of C_{F*}
C_L	=	coefficient of lift
$C_{L(max)}$	=	coefficient of maximum lift
$C_L(RMS)$	=	root mean square lift coefficient
$C_L(SPP)$	=	semi-peak to peak lift coefficient
C_M	=	coefficient of virtual mass
C_O	=	coefficient of second-order oscillatory force
C_S	=	coefficient of second-order steady force
d	=	water depth
D	=	pile diameter
D_p	=	diameter of a cylinder array
f	=	in-line force per unit length
F	=	total in-line force
$F^{(1)}$	=	first-order force
$F^{(2)}$	=	second-order force
$\bar{F}$	=	second-order steady force
$\tilde{F}$	=	second-order oscillatory force
F_A	=	measured in-line force on a complete array
f_D	=	drag force per unit length
F_D	=	drag force
f_I	=	inertial force per unit length
F_I	=	inertial force
f_L	=	transverse force per unit length
F_L	=	transverse force
f_{max}	=	maximum in-line force per unit length

F_{max} = maximum in-line force

F_o = in-line force on a cylinder in steady flow

F_r = Froude number

f_t = frequency of the transverse force

f_v = vortex pair shedding frequency

g = acceleration due to gravity

H = Wave height

$H_v(z)$ = Hankel function

$H_v^{(1)}(z)$ = Hankel function of the first kind

$H_v^{(2)}(z)$ = Hankel function of the second kind

$H'_v(z)$ = derivative of $H_v(z)$ with respect to z

I = Iverson's modulus

$J_v(z)$ = Bessel function of the first kind

$J'_v(z)$ = derivative of $J_v(z)$ with respect to z

k = $2\pi/L$

k_c = Keulegan-Carpenter number, $= \frac{U_{max}T}{D} = \frac{\pi a}{D}$ (in deep water)

k_D = drag/(drag for a single plate)

k_* = alternate form of k_c number

ℓ = length of pile

L = wave length

M = moment on a pile

MSL = mean sea level

m = mass

m_a = added mass

m_v = virtual mass

N_v = number of vortices shed per half cycle

P = pressure

r = polar co-ordinate

R_e = Reynolds' number

S = spacing (centre-to-centre)
S_L = longitudinal spacing (centre-to-centre)
S_t = Strouhal number
S_T = transverse spacing (centre-to-centre)

t = time
T = period
T_v = lifetime of vortex, ie. time from generation to dissipation
Δt_i = time period used for averaging data

u = velocity component along x-axis
$\bar{u}$ = average velocity along the x-axis
$\dot{U}$ = acceleration in the x-direction
U_m = maximum velocity component along x-axis
U_o = velocity along x-axis remote from pile

v = velocity component long y-axis

w = velocity component along z-axis
W_m = maximum velocity along z axis

x = horizontal co-ordinate in the direction of wave propogation
$|X_i|$ = the amplitude of the in-line force on the ith cylinder
y = horizontal co-ordinate parallel to wave crests
$Y_v(z)$ = Bessel function of second kind
$Y'_v(z)$ = derivative of $Y_v(z)$ with respect to z

z = vertical co-ordinate, positive upwards from MSL

α = a constant
β = frequency parameter = $R_e/k_c = D^2/\nu T$
ϵ = Stokes expansion parameter
$\Gamma(n)$ = the gamma function
σ = $2\pi/T$
θ = $2\pi t/T$, t = 0 when U = 0 as the water level rises

θ	=	angular co-ordinate of cylindrical co-ordinates (in Chapter 3 only)
θ_i	=	angle of approach of incident wave
δ	=	second-order oscillatory force phase difference
ϕ	=	velocity potential
ϕ_i	=	incident velocity potential
ϕ_s	=	scattered velocity potential
ρ	=	density of fluid
ν	=	kinematic viscosity of fluid
Ω	=	$\frac{\text{distance travelled by water particle in x-direction}}{\text{distance travelled by water particle in z-direction}}$
Ψ	=	stream function wave theory

INTRODUCTION

Due to their symmetry with respect to wave direction, circular piles are often favoured as structural members, especially in offshore engineering in deep water. The offshore oil industry, which has expanded rapidly from its beginnings shortly after World War II, has created a need for numerous marine structures which tend to be constructed with multiple circular cylinders. There are also many other examples of the use of circular piles used along our coast, notably within the many harbours that surround it.

Unfortunately, many of the phenomena concerning wave forces on piles are not accurately understood. This is especially true for interference effects between multiple piles in groups. However, even the most common design method for single piles (the Morison equation) relies on empirical data for its results. The diffraction theory is mathematically exact, but, since it relies on potential flow theory is limited in its application. Other theories are needed to deal with real, viscous flows.

This thesis, therefore, contains a critical review of the different methods of force prediction on single and multiple circular cylindrical vertical piles. It is aimed towards deep water conditions, but is valid for non-breaking waves at any depth. The thesis is split into two sections. Section I is a review of methods of in-line and transverse force prediction for single vertical piles. It concentrates on the more common force prediction methods (e.g. the Morison equation) but also includes others, such as the diffraction theory. Section II concerns the forces on pile groups and concentrates on interference effects between piles. Both sections are followed by conclusions which include recommendations for future research.

Several factors that would affect prototype piles were not considered in this thesis. All piles were smooth, rigid, fixed, vertical, circular, cylindrical piles. The following factors were not, therefore, considered:

1. The surface roughness of a pile, including the effect of marine growth.
2. The effect of currents superimposed upon the oscillatory flow due to wave action.
3. Effects due to the flexibility of the piles.
4. Floating cylinders (e.g. part of tethered floating oil platforms).
5. Non-circular cylinders.

When writing this thesis, the general philosophy adopted was to describe an individual method of force prediction, and discuss it. This was followed, in turn, by other methods. Conclusions concerning all methods in various situations were drawn at the end of each section, as well as any recommendations concerning future research.

CHAPTER 1

PHYSICAL PROCESSES

1.1 Regimes of validity for Morison and diffraction theories

There are two main methods to predict the wave force on a single pile. The first is based on experimental investigations, physical insight, and dimensional analysis (for example, the Morison equation). The second is theoretical, based on potential flow theory. The diffraction theory, for example, gives a closed form solution of the force on a single pile based on potential flow theory. The two above-mentioned theories (Morison and diffraction) are, therefore, to a great extent complementary, one valid for real, viscous flow, and the other for ideal, potential flow. The areas of validity of each method are indicated in Fig. 1.1, (from Standing, 1984).

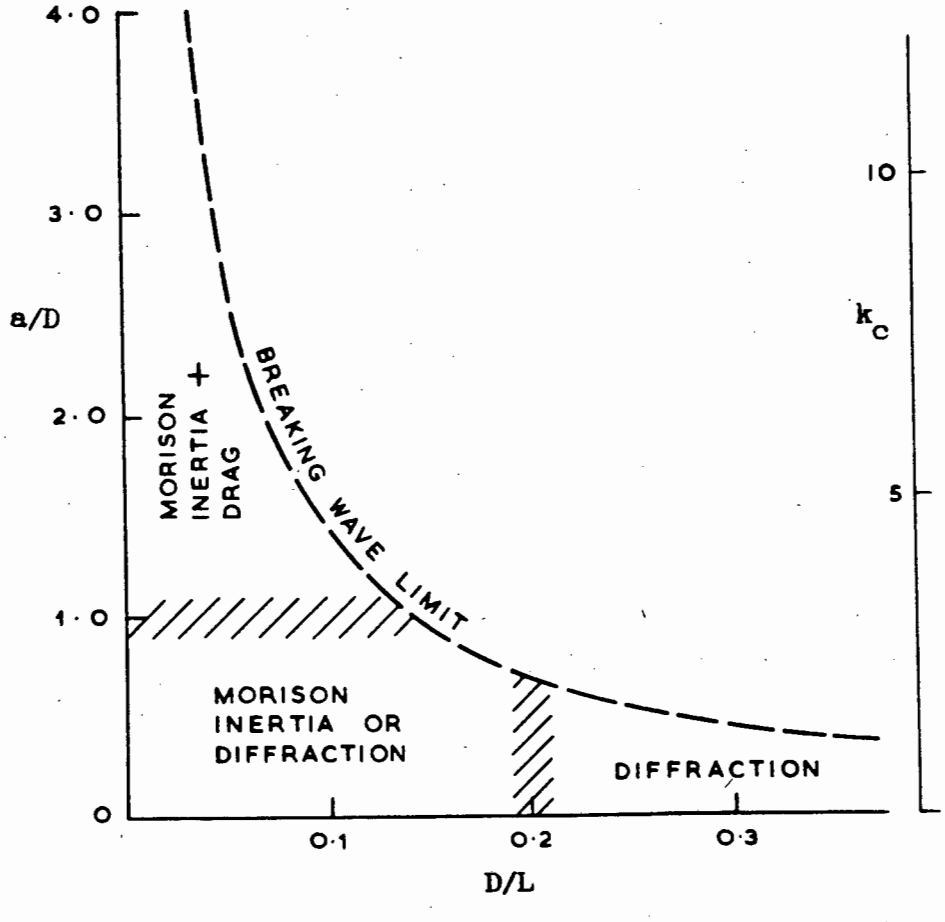

Figure 1.1 : Regions of validity. Force prediction methods for a fixed pile.

Since the diffraction theory is based on potential flow theory, as soon as viscous effects, such as vortices, become apparent, the diffraction theory is no longer applicable. Hogben suggests, in a review paper published in 1974 that, for diffraction theory to apply, the ratio D/L must be $\geq$ 0,2 and this value has been generally accepted. However, several authors (e.g. Chakrabati et al, 1986 and Hayashi and Takenouchi, 1985) have used diffraction theory for values of D/L $\leq$ 0,2. Chakrabati et al plotted the maximum pressures measured around a cylinder and compared this to the maximum pressure predicted by the diffraction theory, shown in Fig. 1.2, (from Chakrabati et al,

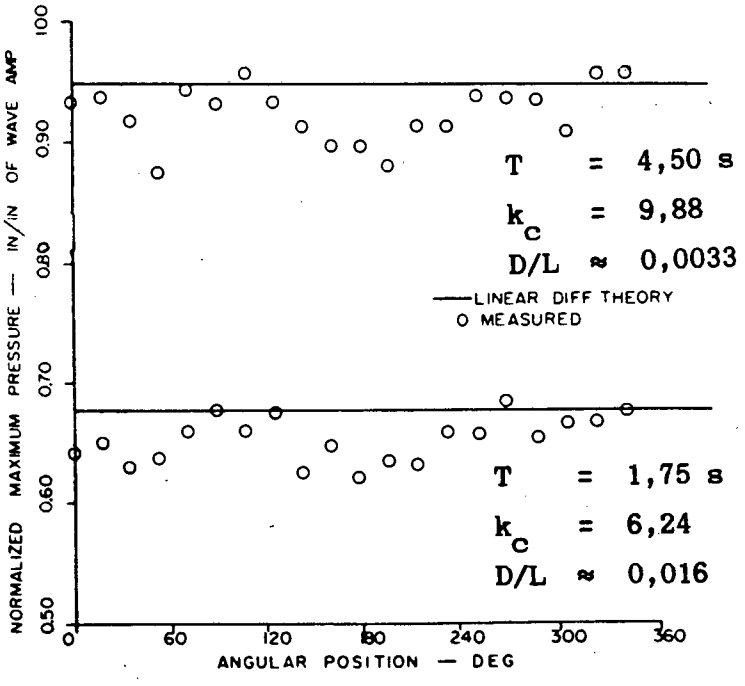

Figure 1.2 : Maximum measured pressures on surface of cylinder correlated with linear diffraction theory at k_c = 6.24 and k_c = 9.88

1986). For these comparisons the Keulegan-Carpenter numbers (k_c numbers) were 6,24 and 9,88, which correspond to D/L ratios of approximately 0,016 and 0,0033 respectively. There was also significant vortex action. In both wave tests the scatter was less than 10%, and the measured pressures were, in general, less than those

predicted by the diffraction theory. Hayashi and Takenouchi used diffraction theory to predict the velocities of water particles around

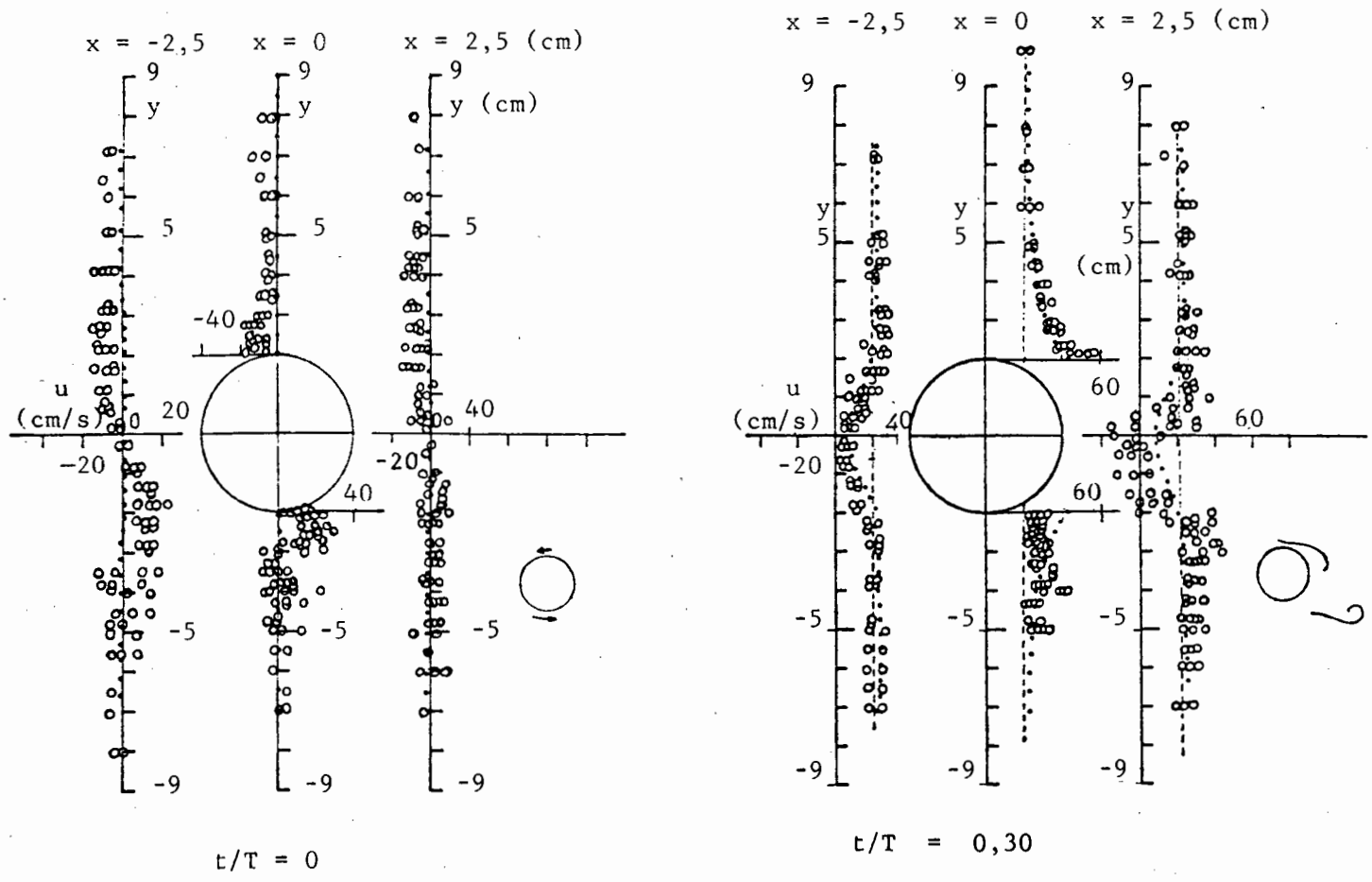

Figure 1.3 : Comparison between the measured water velocity around a pile with Stokes third order wave theory and diffraction theory. D/L = 0,014 k_c = 11,5

a pile, and compared these with experimental values and with Stoke's third-order wave values, as in Fig. 1.3 (from Hayashi and Takenouchi, 1985). The D/L ratio is 0,014 and the k_c value 11,5, and thus there is significant vortex action. The diffraction theory is significantly more accurate than Stoke's third-order wave theory, though errors due to vortex action are apparent. This indicates that, even when the diffraction theory is unable to predict forces accurately, it can still be of use predicting other variables (compared to the Morison equation, which assumes that the water velocity around a pile is undisturbed by the presence of the pile).

1.2 Vortex formation around a pile

The presence of vortices around a pile has a significant effect on the forces experienced by that pile. The transverse pressure differences across a pile (i.e. in a direction parallel to the wave crests) are due solely to the action of vortices, which can also affect the in-line force significantly.

1.2.1 Comparison with steady flow

In steady flow the dimensionless Strouhal number is defined as $S_t = U_o/f_v$ where f_v = the frequency of a vortex-pair shedding, and is almost constant at 0,2 for $300 < R_e < 2 \times 10^5$. This suggests that one vortex-pair is shed in the time that a water particle remote from the pile moves five pile diameters. Therefore, if a is considered to be the horizontal distance that a water particle moves under an oscillatory wave (i.e. the horizontal diameter of the orbit), then $a = \frac{k_c D}{\pi}$. If it is assumed that the same multiple-of-five rule is applicable, and that 2n is the number of vortex pairs shed per wave period, then for

$$
\begin{aligned}
0 < k_c < 7{,}9 \quad &, \quad n = 0 \\
7{,}9 < k_c < 15{,}7 \quad &, \quad n = 1 \\
15{,}7 < k_c < 23{,}6 \quad &, \quad n = 2 \\
23{,}6 < k_c < 31{,}4 \quad &, \quad n = 3 \\
31{,}4 < k_c \quad & \quad n \geq 4
\end{aligned}
$$

The above values of n are an interesting guide to the number of vortex pairs shed during half a period, but there are many other differences between steady and oscillatory flow. Under wave action, the water particle velocities accelerate from rest to a maximum and then decelerate, which causes the rear stagnation points to vary in position. In addition, vortices which are formed and shed in one half period are swept back against the pile when the flow changes direction. This means that even when the velocity of the incident flow is zero, there is a large amount of residual vortex action around the pile. Sarpkaya and

Wilson (1984) found that after 2 waves had passed the pile, there was so much residual vorticity that it was difficult to identify newly shed vortices. Even small vortices not yet shed are swept around the pile, and affect the creation of new vortices. This also means that the flow around a pile is always turbulent, unless no vortices have been formed at all during the previous wave period.

Fig 1.4 (from Sawaragi and Nakamura, 1979) shows the lifetime of

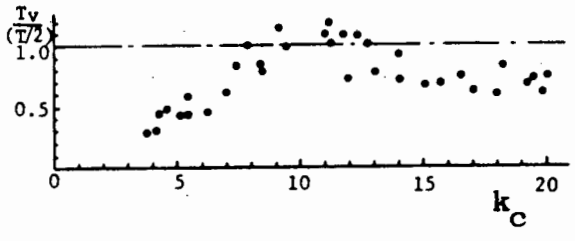

Figure 1.4 : The lifetime of a vortex (in terms of half a wave period) as a function of k_c

a vortex in relation to the half-period of a wave as a function of k_c. It will be noted that when $7 < k_c < 13$ the lifetime of the vortex is longer than the half period and the vortices will be swept back against the pile. However, the vortex may not be "born" at the beginning of the half period (defined as mean water level locally at the pile), although it might then be expected to have a shorter lifetime. Therefore any high value of $T_{v/(T/2)}$ (higher than about 0,7) means that shed vortices might be swept back against the pile. The effect of vortex action is usually quoted to be very significant for $8 < k_c < 20$, so it would be interesting to see Fig. 1.4 extended beyond $k_c = 20$ to see if (and how sharply) the ratio $T_{v/(T/2)}$ diminishes beyond this point.

The final difference between steady and oscillatory flows is that the latter is three-dimensional, as it has a vertical

velocity component, i.e. parallel to the cylinder axis. When this component of velocity is directed downwards, especially in shallow water, the circulation of the vortices increases due to the contraction of the vertical core length of the vortices. This may affect the transverse force or even cause the shedding of a vortex during one half wave period and not in the following half wave period (i.e. one vortex shed during the complete wave period). This may also result in a transverse force with a non-zero average value, but directed to one side of the pile only.

1.2.2 Number of vortices shed per half wave period

For short period waves vortices will not develop around the pile and the flow will closely resemble inviscid, potential flow. At the opposite end of the wave spectrum, for long period waves, a Von Karman vortex sheet, closely resembling that for steady flow, will develop. Usually, though, a small number of vortices will be formed and shed, as shown in Fig. 1.5 (from Sawamoto et al, 1980).

Not presented in this diagram is the case when $k_c < 2$. Here, there is no separation behind the pile and the flow resembles inviscid flow. As k_c increases, the flow separates, as in (a), and then two symmetrical vortices are formed on either side of the pile, as in (b). If the vortices are allowed to grow further (c), one will grow faster than the other, and a pressure differential will be created across the pile, causing a transverse force. For larger k_c as in (d), one vortex (v_1) is shed. This diagram also shows the effect of flow reversal on vortices. Instead of being swept away from the pile and decaying remote from the pile, vortex v_2 is dragged past the back of the pile by vortex v_1, and is then swept past the pile to form a new vortex on the opposite side. This phenomemon also occurs at other k_c values, as indicated by the arrows. In (e), two vortices are shed (or one vortex pair), one vortex being shed from either side of the pile, and in (f) three are shed alternately from each side. As the k_c value increases above 30 as in (g), the wake grows more and more to resemble a Von Karman vortex sheet.

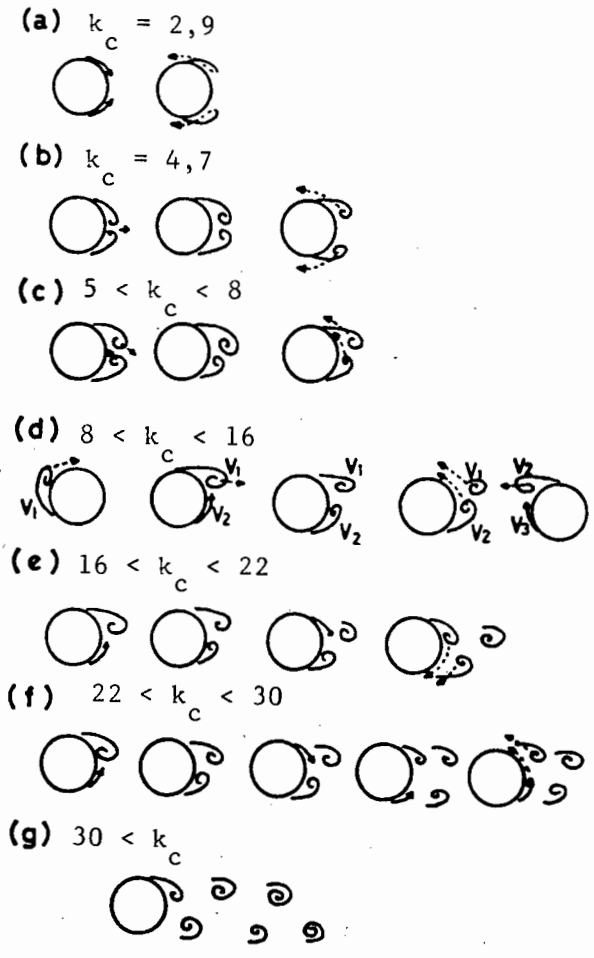

Figure 1.5 : Vortex patterns around cylinders as a function of k_c

The k_c values quoted in Fig. 1.5 are not completely fixed. Due to the inherent instability of vortices, the k_c values are not constant, though they are reasonable approximations. Therefore, a vortex may be shed at k_c = 7, or one (and only one) may be shed at k_c = 17. Furthermore, Figure 1.5 was the result of an experimental study with small Reynolds numbers ($0{,}2 \times 10^3 < R_e < 13 \times 10^3$). Fig. 1.6 (from Sarpkaya 1976c) shows the frequency of the transverse force on a pile (closely related to the frequency of vortex shedding). This figure implies that as the Reynolds

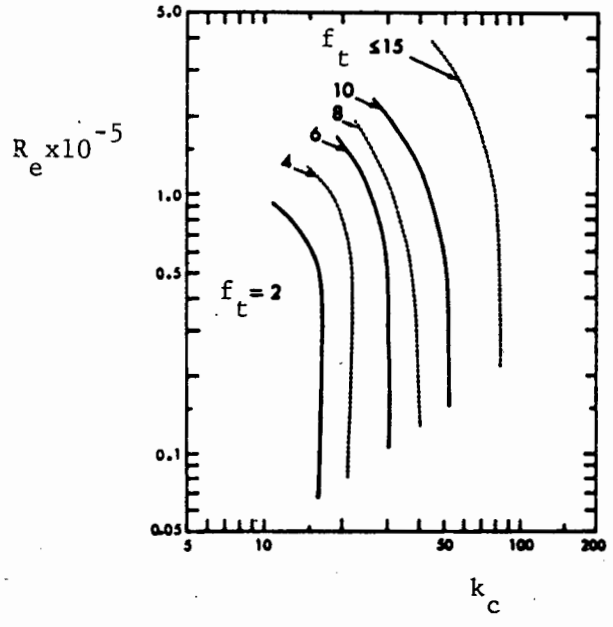

Figure 1.6 : Frequency of the transverse force as a function of R_e and k_c

number increases above 5 x 10^4, the transitions will occur at lower k_c values.

Fig. 1.5 shows the usual vortex action behind a pile, but does not cover every possibility. Figure 1.7 (from Zdrankovich and Namork, 1977) shows a wave (k_c = 5,4) which sheds one vortex throughout its entire period. At A, beneath the crest of the wave, there are two vortices, of which the lefthand one has the higher circulation. As the velocity decreases the righthand vortex decays faster than the left, so that at flow reversal, the lefthand vortex is considerably stronger than the righthand one. After flow reversal the left vortex causes the rapid formation of a new vortex of opposite circulation, also on the left side of the pile, and both these vortices are shed soon after the trough has passed. Thus only one vortex is shed per wave. This is caused both by the vortices swept back affecting new vortices, and by the increase in circulation of vortices in the shallower water trough of the wave caused by the reduction of vortex core length.

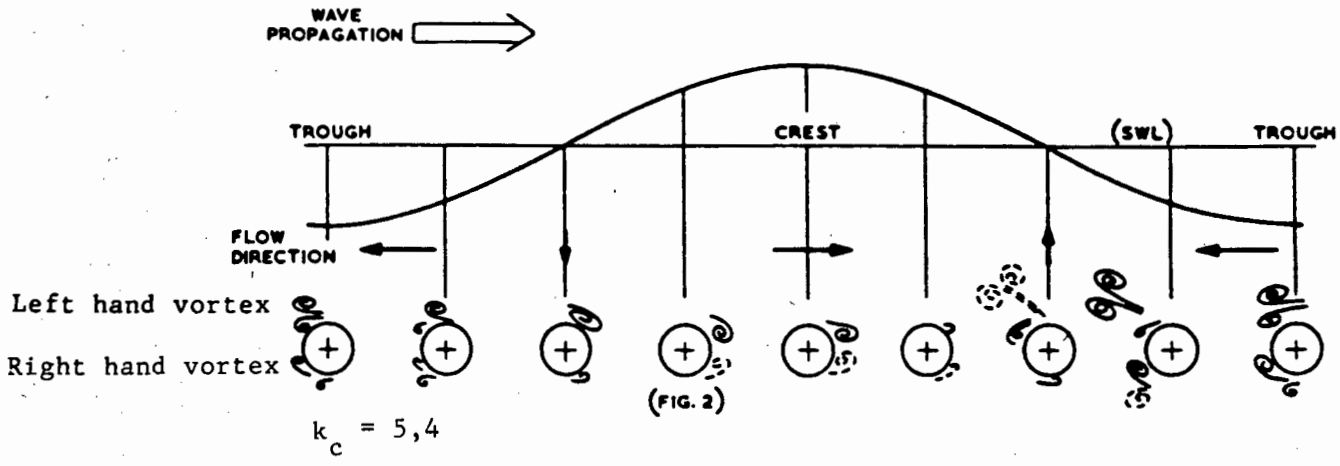

Figure 1.7 : Asymmetric development of vortex shedding.

1.2.3 Correlation of vortices with the length of the pile

Since vortices cause the transverse force on a pile and have a large effect on the in-line force, it is important to know whether vortices form along the entire vertical length of the pile simultaneously or whether they form according to the local k_c number, which will vary with depth. Very little work seems to have been done on this subject, perhaps because it is so difficult to detect vortices underwater.

Dronkers and Massie (1979) estimated the position of vortices by measuring the transverse force along the length of a pile in steady flow. For $R_e < 1,2 \times 10^4$ they found that the vortices "peeled" off the pile from the base (see Fig, 1.8) (from Dronkers and Massie, 1979). However for $R_e > 1,2 \times 10^4$ the vortices were all of the same sense, but broke up axially (Fig. 1.9)(from Dronkers and Massie, 1979).

There are obviously many differences in oscillatory flow: the instantaneous water velocity is a function of depth, but there is a vertical velocity component which will probably increase the spanwise coherence, i.e. increase the amount of simultaneous

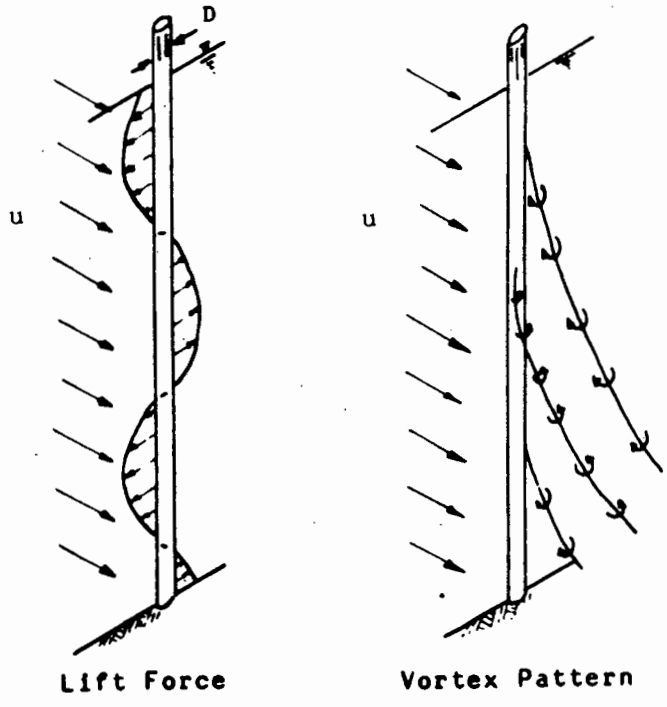

Figure 1.8 : Vortices forming along the length of a pile for $R_e < 1,2 \times 10^4$ in steady flow.

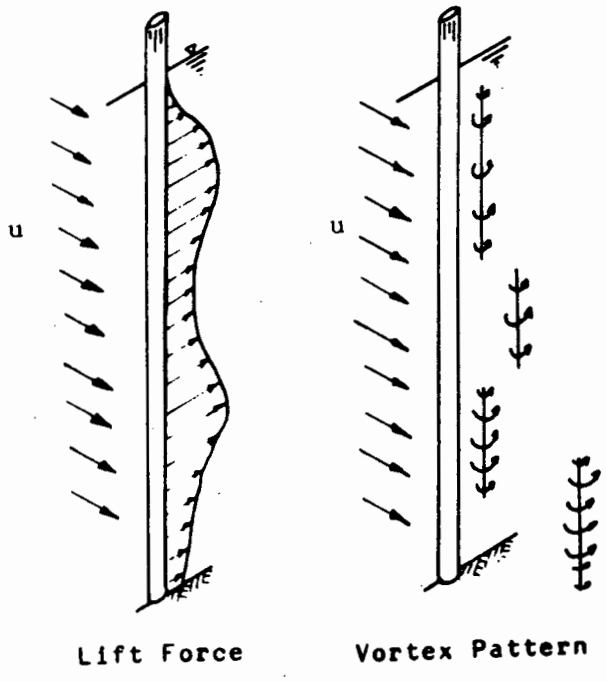

Figure 1.9 : Vortices forming along the length of a pile for $R_e > 1,2 \times 10^4$ in steady flow.

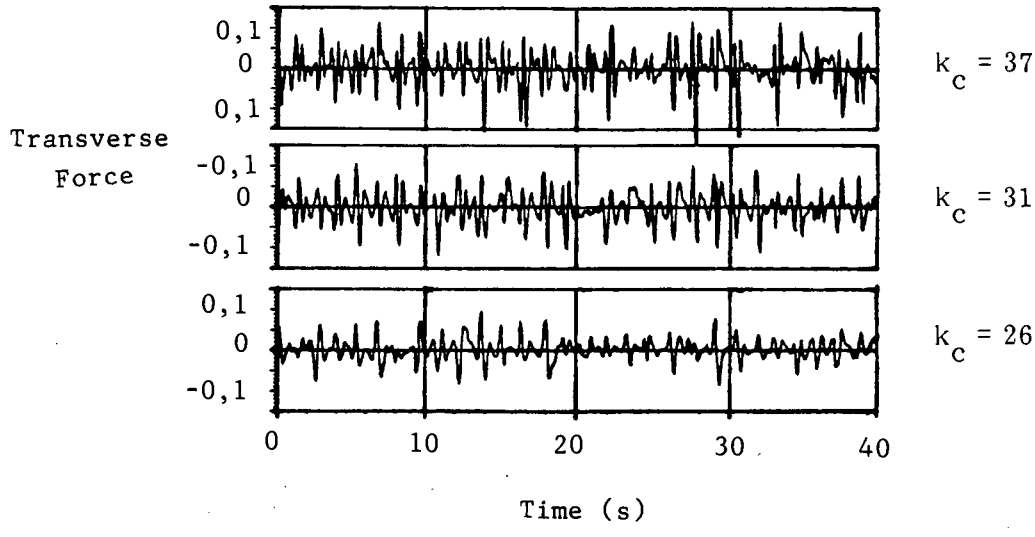

Figure 1.10 : Transverse force measurement. Surface k_c = 51. Local k_c values are given on the right of each recording.

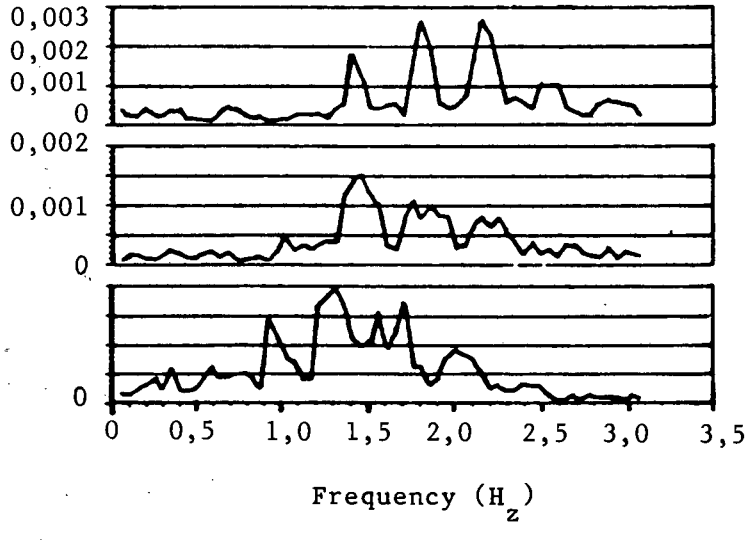

Figure 1.11 : Frequency spectrums from figure 1.10

forming and shedding of vortices along the height of the pile. Torum and Reed (1982) measured the transverse force at three elevations in oscillatory flow to estimate the extent of spanwise coherence of the force, and thus the vortex shedding. The transverse force function for a selected wave is shown in Fig. 1.10 (from Torum and Reed,1982), which is broken up into a

frequency spectrum by Fourier analysis in Fig. 1.11 (from Torum and Reed, 1982). The spectra do show peaks, which correspond with vortex shedding, but they are not well defined.

Finally, Sarpkaya and Wilson (1984) measured the pressure distribution both horizontally and vertically over a pile, and when they integrated the pressure distribution they found larger drag coefficients than those obtained from direct force measurement. This was due to the method of analysis used, since only the pressure data which showed a high degree of coherence were chosen for the calculations. This indicates that a significant amount of variation exists along a pile.

1.3 Shear force around piles

Few investigations have been made into shear stress on vertical cylinders in oscillatory flows, but these have shown that the shear stress is negligible. Fig. 1.12 (from Sawaragi & Nakamura, 1979) plots the pressure and shear stress distributions around a pile. Here $\tau_{max} \approx 0{,}01\ P_{max}$, and is thus insignificant.

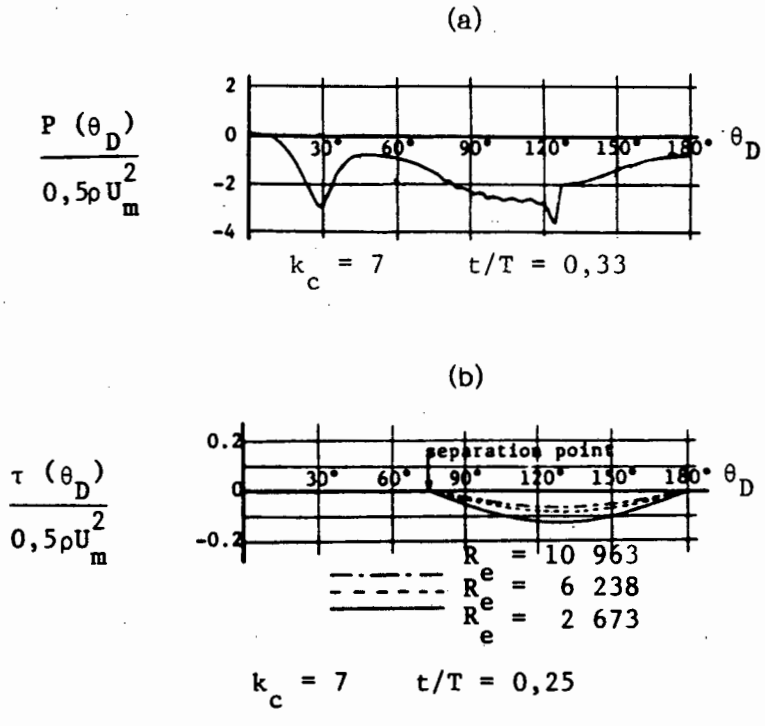

Figure 1.12 : Comparison between the pressure on a cylinder (a) and the shear stress (b).

CHAPTER 2

FORCE PREDICTION IN REAL, VISCOUS FLOWS

Since only very large diameter piles, or piles in very small waves, may be assumed to be in potential flow, most piles are designed with viscous forces in mind. As the oscillatory viscous flow around a blunt object (e.g. a cylinder) has so far defied accurate analysis, most methods of force prediction in real, viscous flow rely on an equation with one or more experimentally determined coefficients. The equation with the greatest collection of experimental evidence, and the one most commonly used, is the Morison equation.

2.1 The Morison equation

The Morison equation to predict the force on a pile is made up of two components, namely

(i) "A virtual mass force proportional to the horizontal component of the accelerative force exerted on the mass of water displaced by the pile". (Morison et al, 1950), and

(ii) "A drag force proportional to the square of the velocity which may be represented by a drag coefficient having substantially the same value as steady flow." (Morison et al, 1950)

$$\text{i.e. } f = C_M \rho \frac{\pi D^2}{4} \frac{\partial u}{\partial t} + \frac{1}{2} C_D \rho D u|u| \qquad (2.1)$$

where f = force per unit length at a selected elevation and $u|u|$ is used instead of u^2 to permit the force to be negative when the flow direction reverses.

This is the most common method of predicting the force on a pile. First suggested by J R Morison et al (1950), it was the first equation to predict, with reasonable accuracy, the force on a pile throughout the wave cycle when the coefficients C_M and C_D were known (see Fig. 2.1, from Morison et al, 1950). Unfortunately, however, due to the empirical nature of Morison's equation, a considerable period of time elapsed after the first publication of the equation before C_M and C_D values could be established accurately.

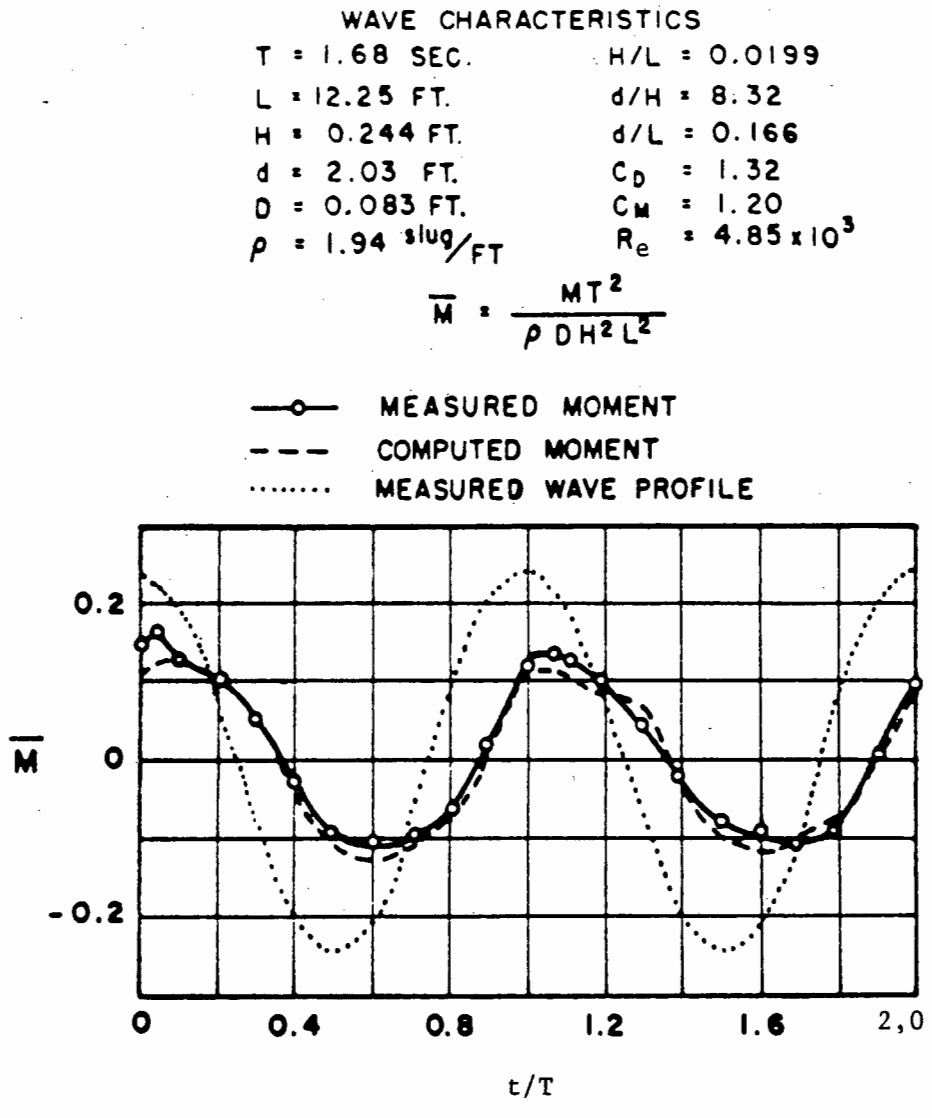

Figure 2.1 : Total moment about the bottom of a single circular pile.

2.1.1. Theoretical derivation of Morison's equation

The equation is made up of two terms; the first term predicts F_I, an inertial force, and the second predicts F_D, the drag force. The total in-line force, F, is equal to the sum of F_I and F_D, i.e.

$$F = F_I + F_D \tag{2.2}$$

2.1.1.1 The inertial force

To consider the inertial force on a body in oscillatory flow it is useful initially to consider simply an oscillating fluid. Also consider a theoretical volume within this fluid, oscillating with the fluid. Such a volume is accelerated in harmony with the flow, and therefore must experience a force, given by (assuming the acceleration is constant throughout the volume)

$$m \frac{\partial u}{\partial t} \tag{2.3}$$

where m is the mass of the fluid volume.

If the volume is now replaced by a solid stationary object, such as a vertical cylinder, extra work must be performed to divert the water around such a cylinder, depending on its shape, and thus a greater force must be exerted on the cylinder : thus the water force on the cylinder can be expressed as

$$(m + m_a) \frac{\partial u}{\partial t} \tag{2.4}$$

where m_a is termed the "added mass" of fluid
and $m + m_a$ is termed the "virtual mass" of fluid

The virtual mass is sensitive to body shape being generally larger for blunter bodies.

The force may also be expressed by a coefficient of virtual mass, such that

$$F_I = C_M m \frac{\partial u}{\partial t} \tag{2.5}$$

and, if the pile dimensions are substituted for the mass, then

$$f_I = C_M \rho \frac{\pi D^2}{4} \frac{\partial u}{\partial t} \tag{2.6}$$

In potential flow for a cylinder, $\frac{m_a}{m}$ has a value of 1,0, and thus, in potential flow, $C_M = 2.0$.

2.1.1.2 The drag force

An additional force, the drag force, is needed in the Morison equation to allow for the viscous drag on an object. This force is expressed in the same way as the drag force in steady flow, i.e.

$$F_D = \frac{1}{2} C_D \rho A u^2 \qquad (2.7)$$

where A = the projected area perpendicular to u

However, because the drag in oscillatory flow changes direction, to calculate the sense of the force correctly, equation (2.7) is changed to

$$F_D = \frac{1}{2} C_D \rho A u|u| \qquad (2.8)$$

or, for a circular cylinder,

$$f_D = \frac{1}{2} C_D \rho D u|u| \qquad (2.9)$$

2.1.2 Relative magnitudes of inertia and drag forces

The inertia and drag components constitute differing proportions of the total in-line force, depending on the period and height of the incident wave and the size of the pile. Drag loads are caused by the relative velocity of the fluid and are more significant when the diameter of the pile is small relative to the wavelength L. Inertial forces are more significant with the larger diameter piles.

The ratio $\frac{(f_D)_{max}}{(f_I)_{max}}$ will show the relative importance of the drag and inertia forces. This can be done by using equations (2.6) and (2.9) and substituting for $\frac{\partial u}{\partial t}$ and u. Considering a linear theory deep water wave at submergence z and wavelength L = 15H (H = wave height) then

$$\frac{(f_D)_{max}}{(f_I)_{max}} = \frac{C_D\, e^{(-2\pi z/15H)}}{C_M} \cdot \frac{H}{D} \qquad (2.10)$$

This is plotted in Fig. 2.2 (from Hogben, 1976) where z = 0, C_M = 2,0 and C_D = 0,6 for the areas marked 'postcritical' and 1,2 for the areas marked 'subcritical'.

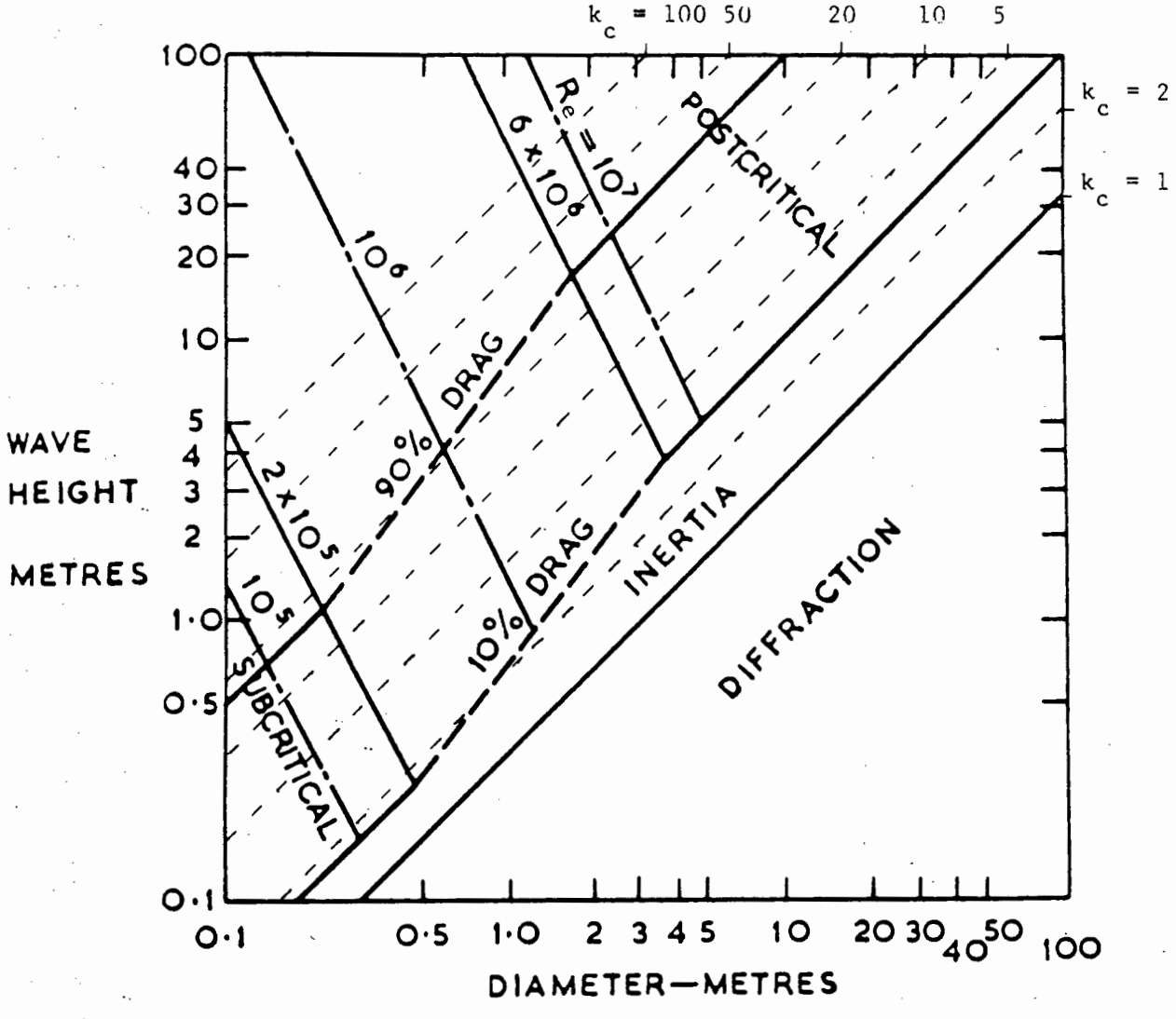

Figure 2.2 : Loading Regimes at the surface for L = 15H

2.1.3 The Morison force coefficients C_M and C_D

2.1.3.1 A short historical development of C_M and C_D

The theoretical value of C_M in a frictionless, incompressible fluid, is 2,0 and that of C_D in a similar fluid is 0. The value of C_D was later assumed to be close to the C_D value in steady flow conditions. Unfortunately none of these assumptions is valid : the flow around a pile is not frictionless (so $C_M \neq 2,0$ and $C_D \neq 0$) and the drag and inertia forces interact such that the drag coefficient in oscillatory flow is not similar to that in steady flow.

The first values suggested for C_M and C_D in oscillatory flow were given by Morison et al (1950). They were

$C_M = 1,508 \pm 0,197$ i.e. approximately 1,3 to 1,7
$C_D = 1,626 \pm 0,414$ i.e. approximately 1,2 to 2,0

where these are regarded as constants through the oscillatory cycle.

However, subsequent investigations (Morison et al, 1953) showed large variations in C_M and they reverted to the theoretical value of $C_M = 2,0$.

The major problem at this time was that there was no method of accurately predicting C_M or C_D. This had to wait until 1958 when Keulegan and Carpenter used dimensional analysis to analyse the force on a pile. This analysis was proposed as $f = f(t, T, u_m, D, \rho, \nu)$

therefore $$\frac{f}{\rho\, u_m^2\, D} = f\left(\frac{t}{T}, \frac{u_m T}{D}, \frac{u_m D}{\nu}\right) \qquad (2.11)$$

where
$\frac{t}{T}$ = phase angle = $\theta/2\pi$
$\frac{u_m T}{D}$ = Keulegan-Carpenter number = k_c
$\frac{u_m D}{\nu}$ = Reynolds number = R_e (based on maximum velocity)

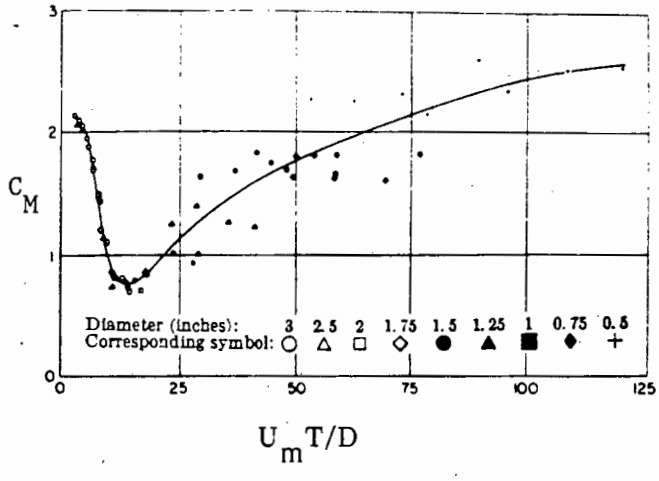

Figure 2.3 : Variation of inertia coefficient with k_c

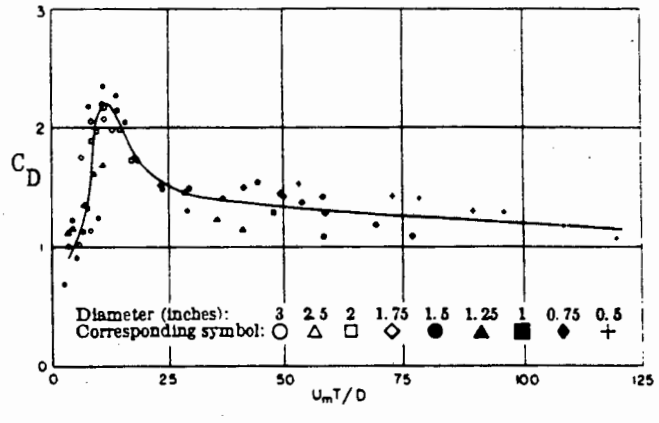

Figure 2.4 : Variation of Drag coefficient with k_c

Following laboratory experiments, Keulegan and Carpenter found that C_M and C_D were, in fact, dependent on k_c (Fig. 2.3 and 2.4)(from Keulegan and Carpenter, 1958), but they could find no relation between C_M and C_D and R_e.

These findings went unchallenged, apart from minor changes to C_M for many years, but many researchers remained unsatisfied ; logically, the coefficients should be affected by Reynolds number, especially considering that Keulegan and Carpenter and several others had shown this through dimensional analysis. However, no researcher was able to find an appropriate relation, largely due to the difficulty of creating oscillatory flow with high

Sarpkaya also introduced a new variable, β, called the "frequency parameter". This was primarily for experimental reasons : it was difficult to keep either $k_c \left(= \frac{u_m T}{D}\right)$ or $R_e \left(= \frac{u_m D}{\nu}\right)$ constant while varying the other. Therefore, β was defined as $\beta = R_e/k_c = D^2/\nu T$, and instead of using

$$f = f(\theta, k_c, R_e) ,$$

he used

$$f = f(\theta, k_c, \beta) . \qquad (2.12)$$

The R_e values were simply recovered by multiplying β by k_c.

The results from these experiments showed C_M and C_D as functions of both k_c and R_e, as shown in Fig. 2.6 - 2.9 (from Sarpkaya, 1976(B)). As can be seen from Fig. 2.8 and 2.9, at high R_e, $C_M \rightarrow 1{,}75$ to $1{,}81$ and $C_D \rightarrow 0{,}62$. The lack of scatter can be seen clearly in the original data plotted in Fig. 2.10 and 2.11 (from Sarpkaya, 1976(B)).

The dependence of C_M and C_D on Reynolds number was confirmed by Garrison et al (1977), who oscillated a cylinder in still water (compared to Sarpkaya, who oscillated the water round a fixed cylinder). Their results are shown in Fig. 2.12 and 2.13 (from Garrison et al, 1977), with Sarpkays's results superimposed. Although both authors show a dependence on Reynolds number, Sarpkaya's values of both C_M and C_D appear to be larger than those of Garrison et al, except for C_M at low Reynolds number ($R_e < 4 \times 10^4$). This is emphasised in Fig. 2.14 and 2.15 (from Garrison, 1990), which have been superimposed on Sarpkaya's data for comparison. These figures combine the data of Garrison et al with the high Reynolds number of Rodenbush and Gutierrez (1983). Fig. 2.16 and 2.17 show typical scatter and also the small amount of data at high R_e ($R_e > 4 \times 10^5$). However, although sparse, the data of Rodenbush et al appears consistent with Garrison's. This is emphasised in Fig. 2.18 and 2.19 where the data from the two sources overlap.

The high Reynolds number data in Fig. 2.14 and 2.15 is important because it creates the largest discrepancy with Sarpkaya's data. Sarpkaya's results converge at high Reynolds number, whilst Garrison's data in Fig. 2.14 and 2.15 diverge. This may be because they show low k_c values ($k_c < 35$) while Sarpkaya uses only high values of k_c at high R_e ($k_d \geq 20$ for $R_e > 10^5$).

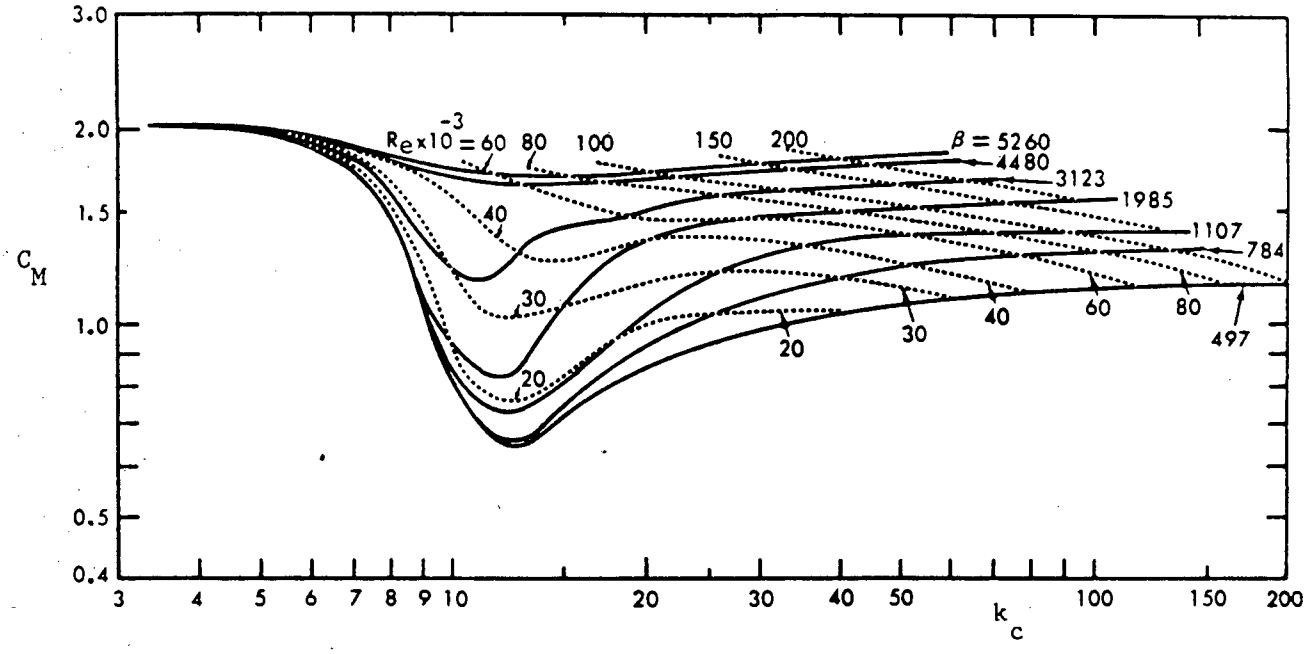

Figure 2.6 : C_M versus k_c for constant values of R_e and β.

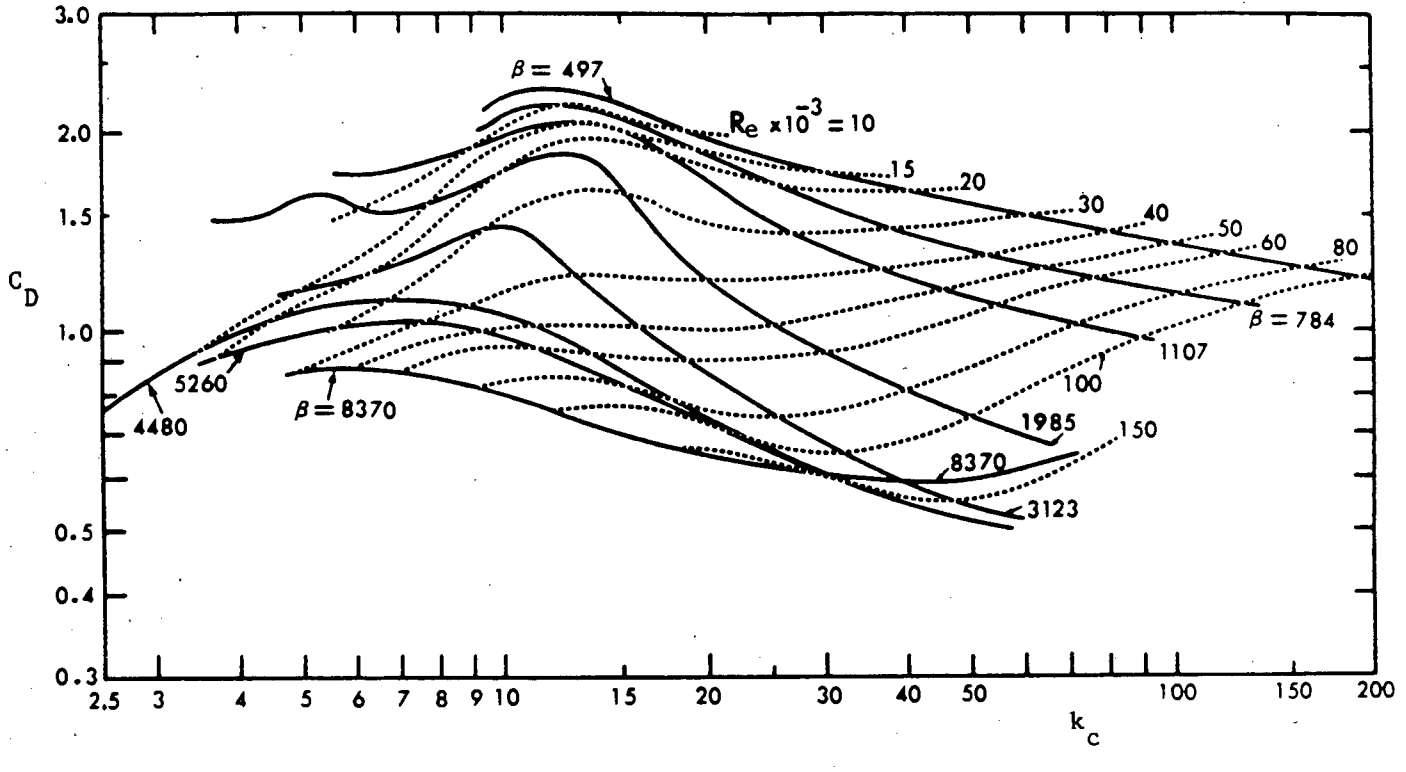

Figure 2.7 : C_D versus k_c for constant values of R_e and β

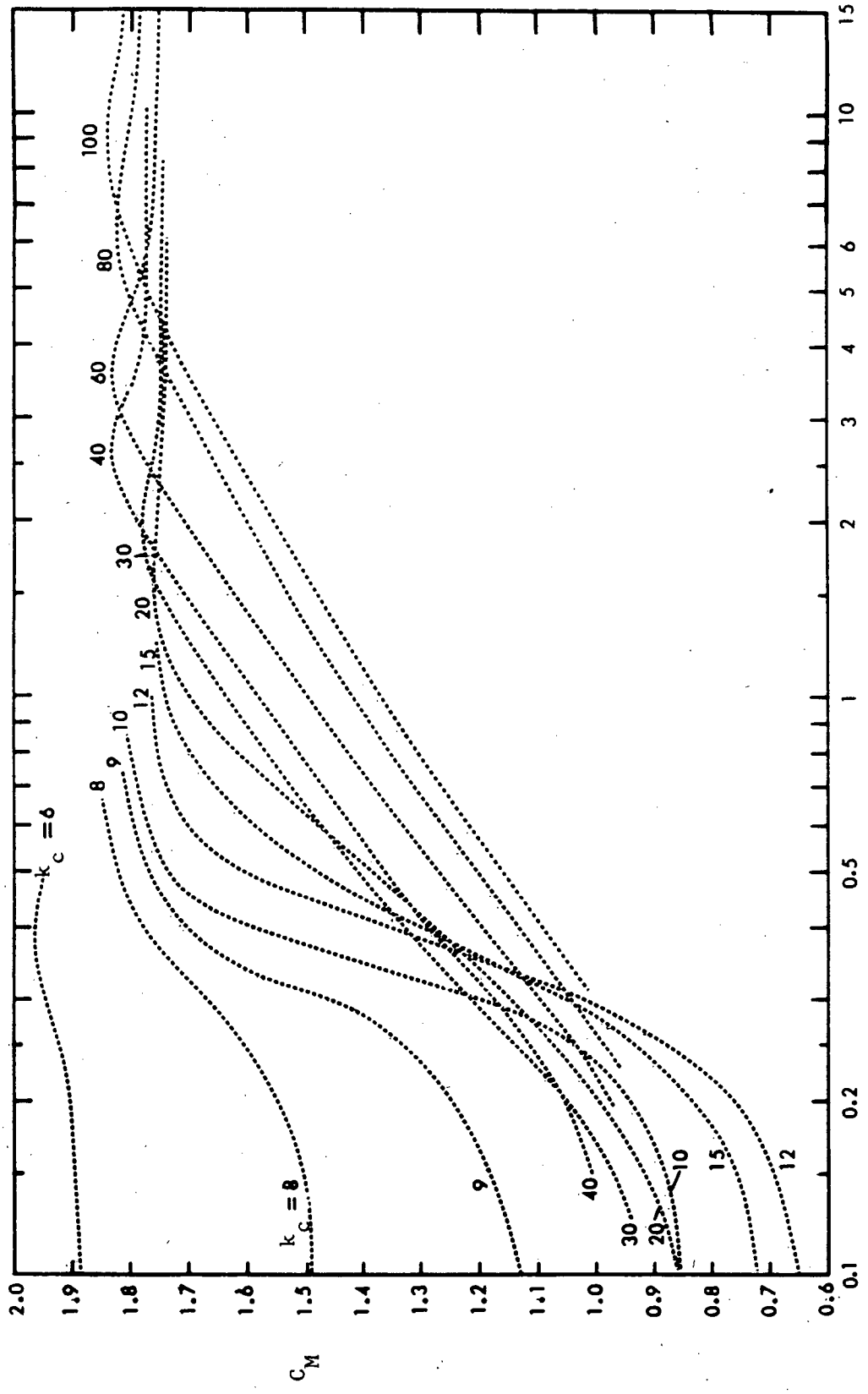

Figure 2.8 : C_M versus R_e for constant values of k_c.

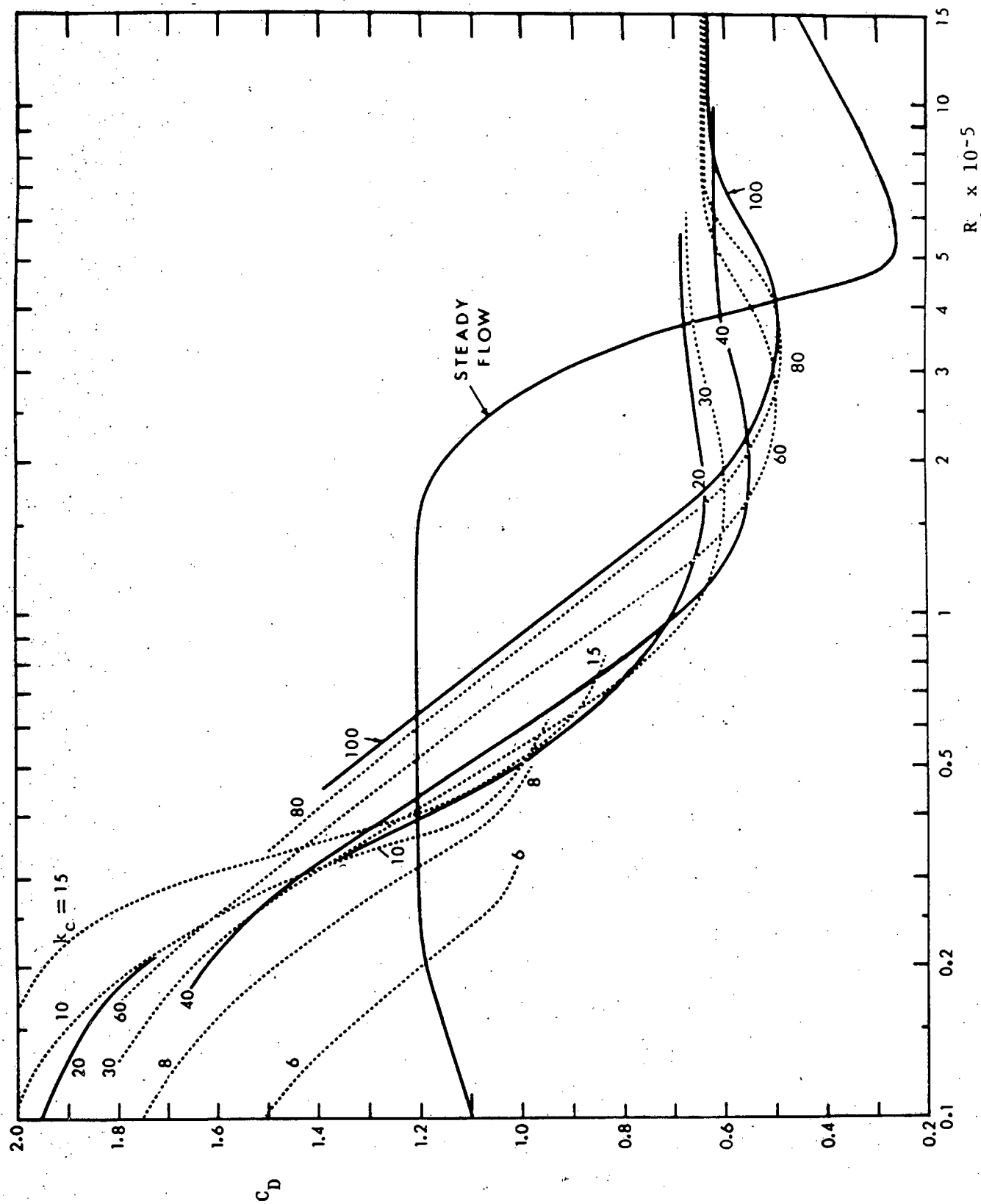

Figure 2.9 : C_D versus R_e for constant of k_c.

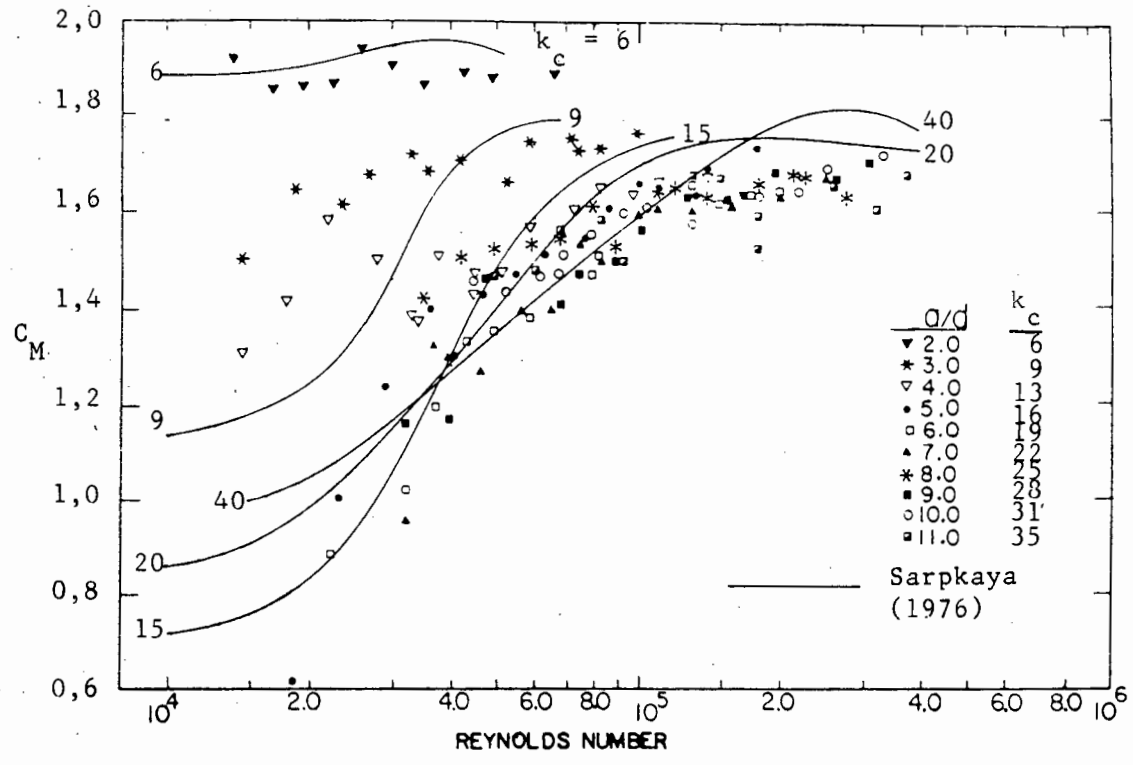

Figure 2.12 : C_M data from Garrison compared to Sarpkaya.

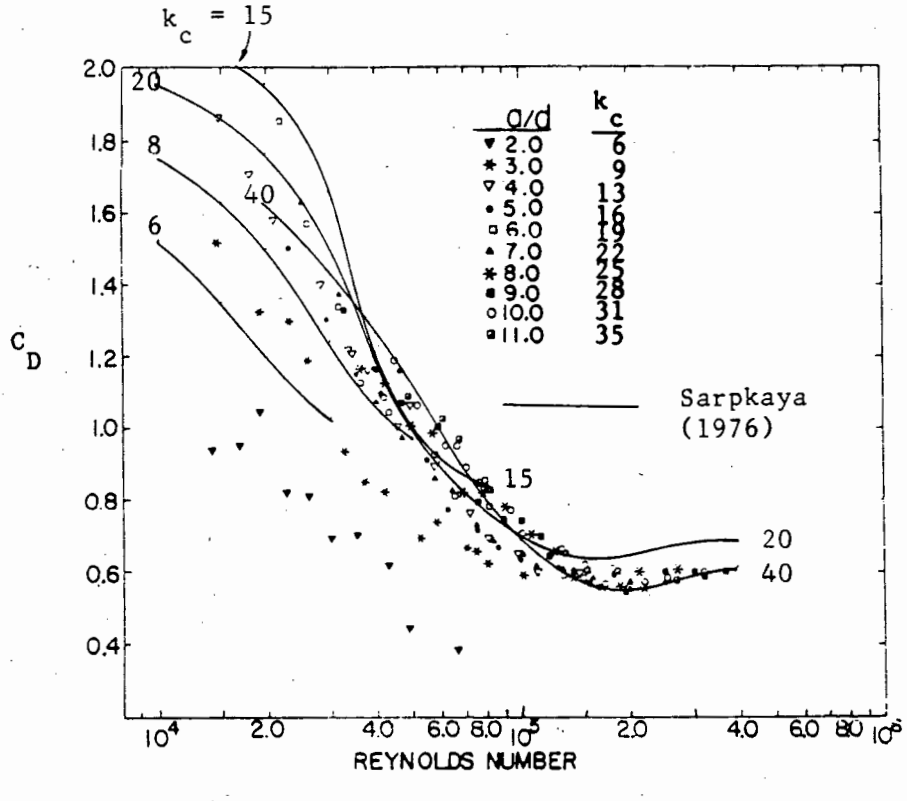

Figure 2.13 : Drag coefficient data of Garrison et al compared to Sarpkaya.

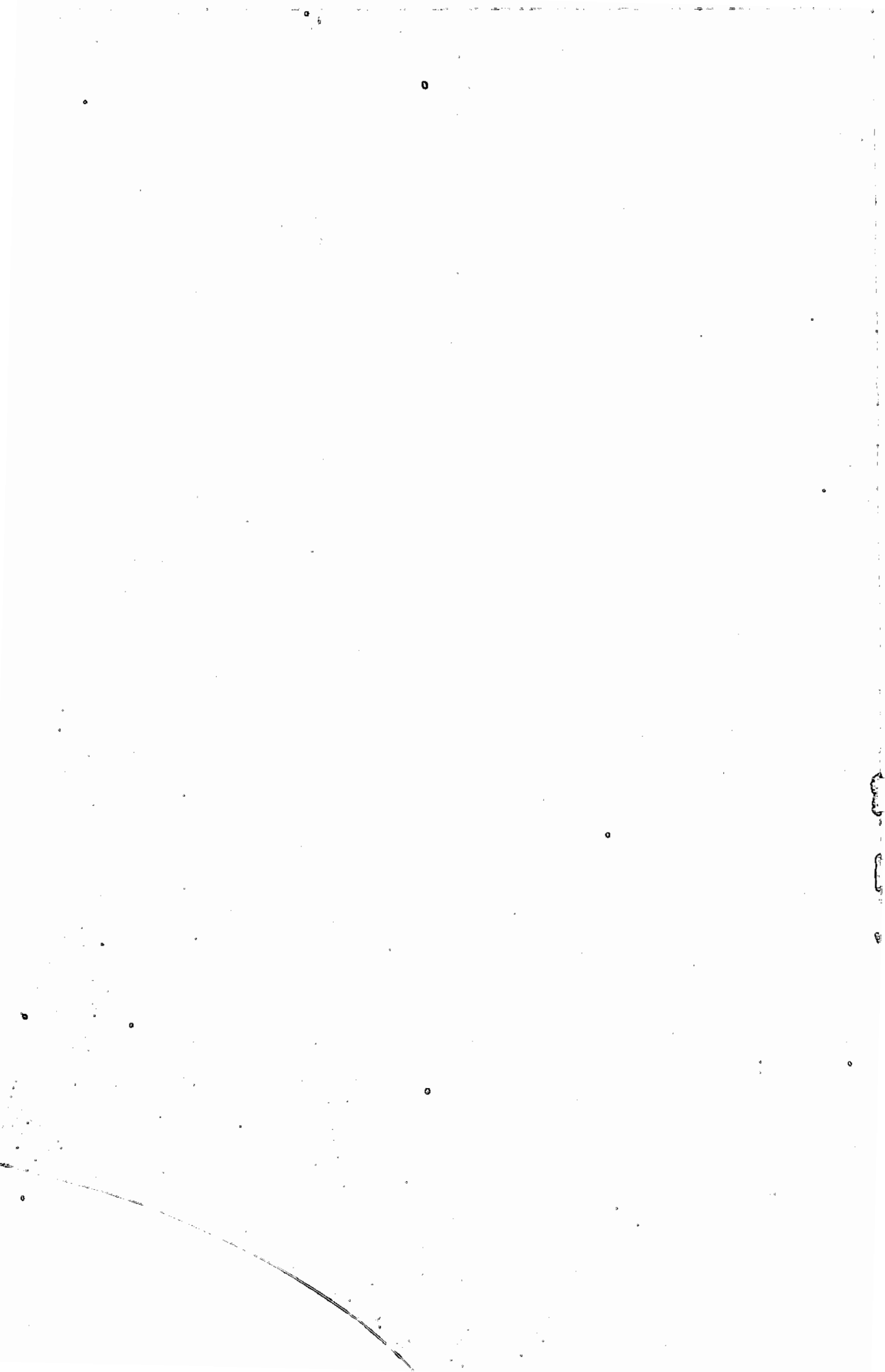

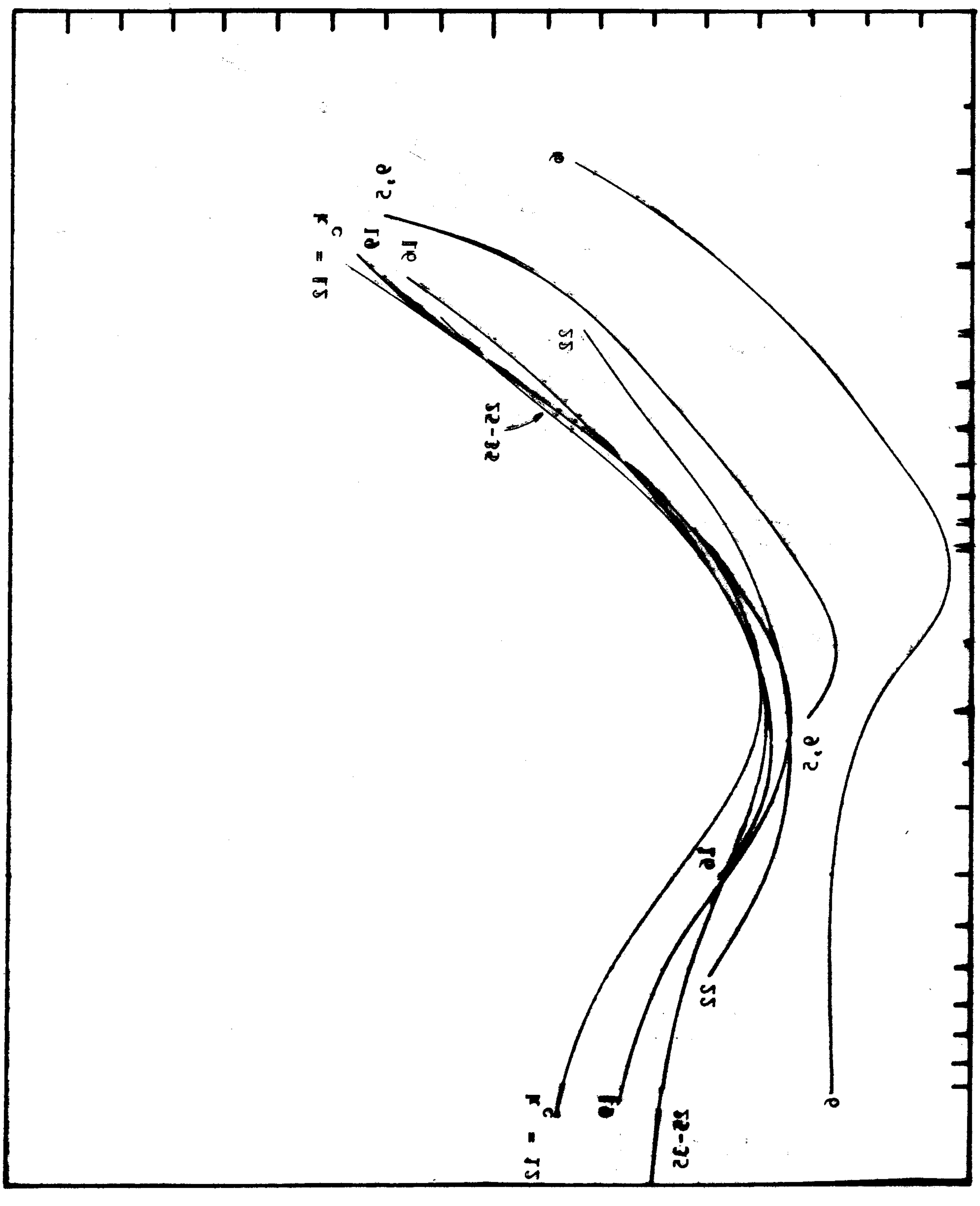

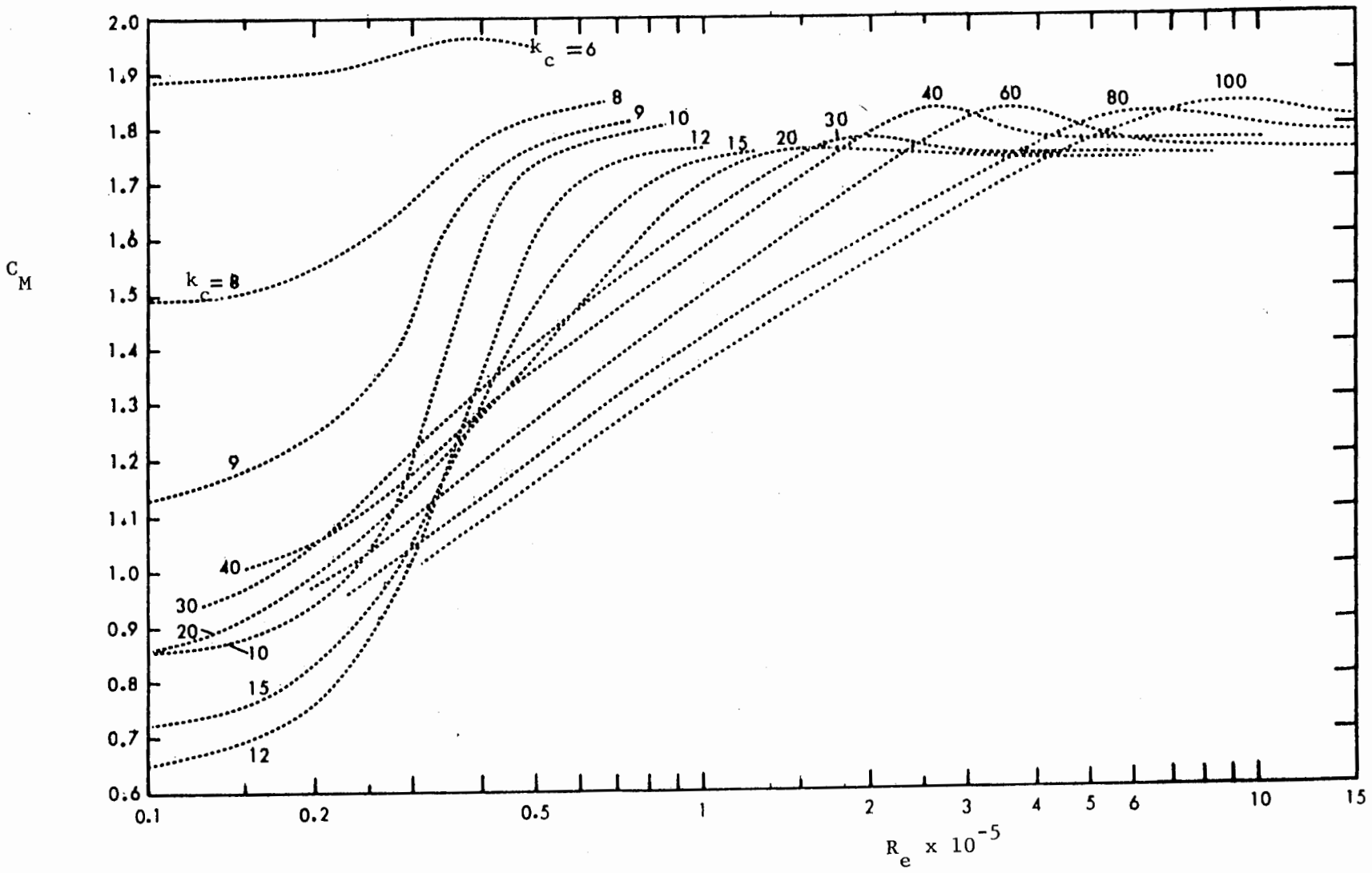

Figure 2.14 : Comparison of Sarpkaya (1976) with Garrison (1990) for C_M.

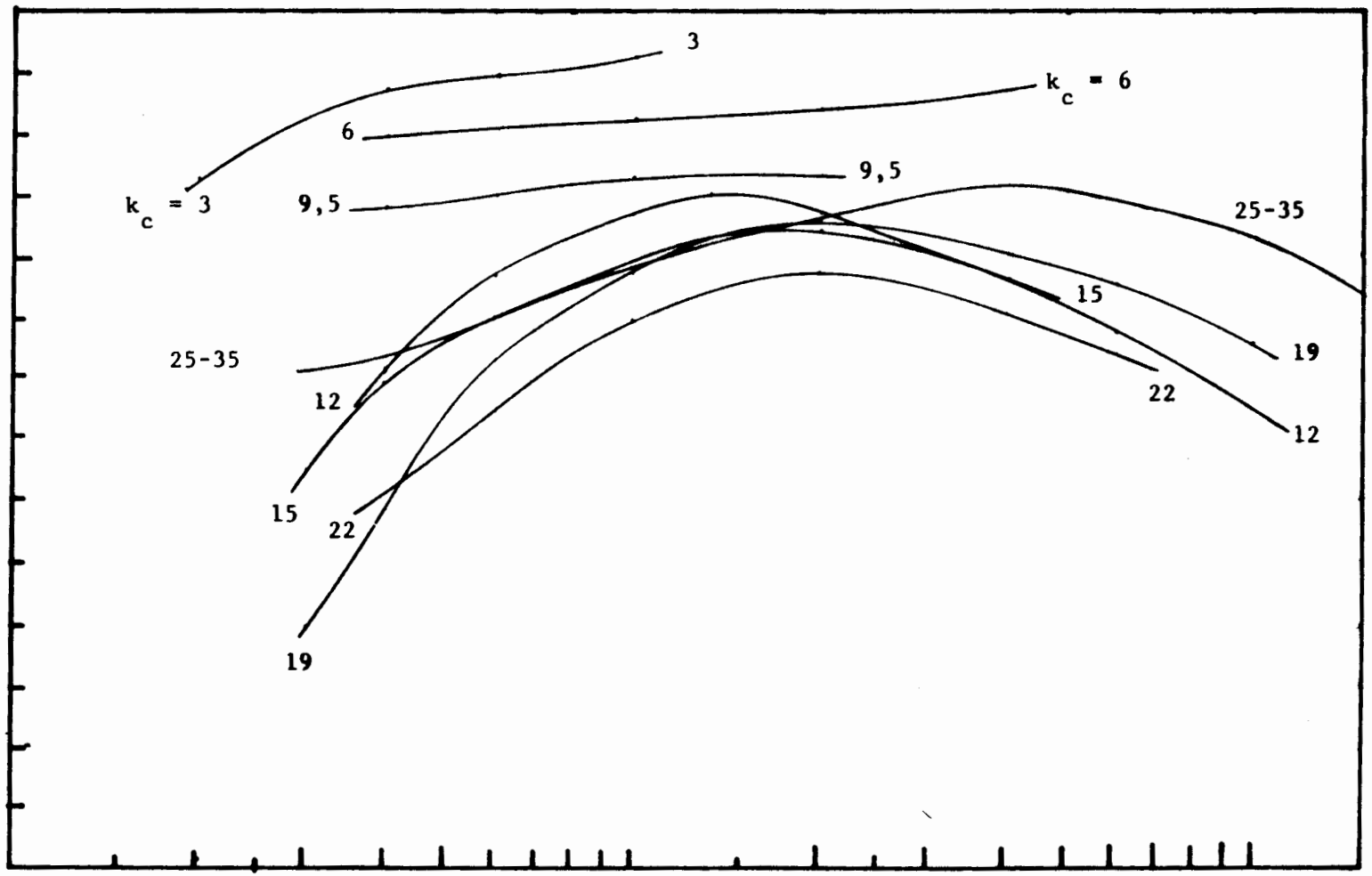
3
6
k_c = 6
9,5
k_c = 3
9,5
25-35
15
19
25-35
12
22
12
15
22
19

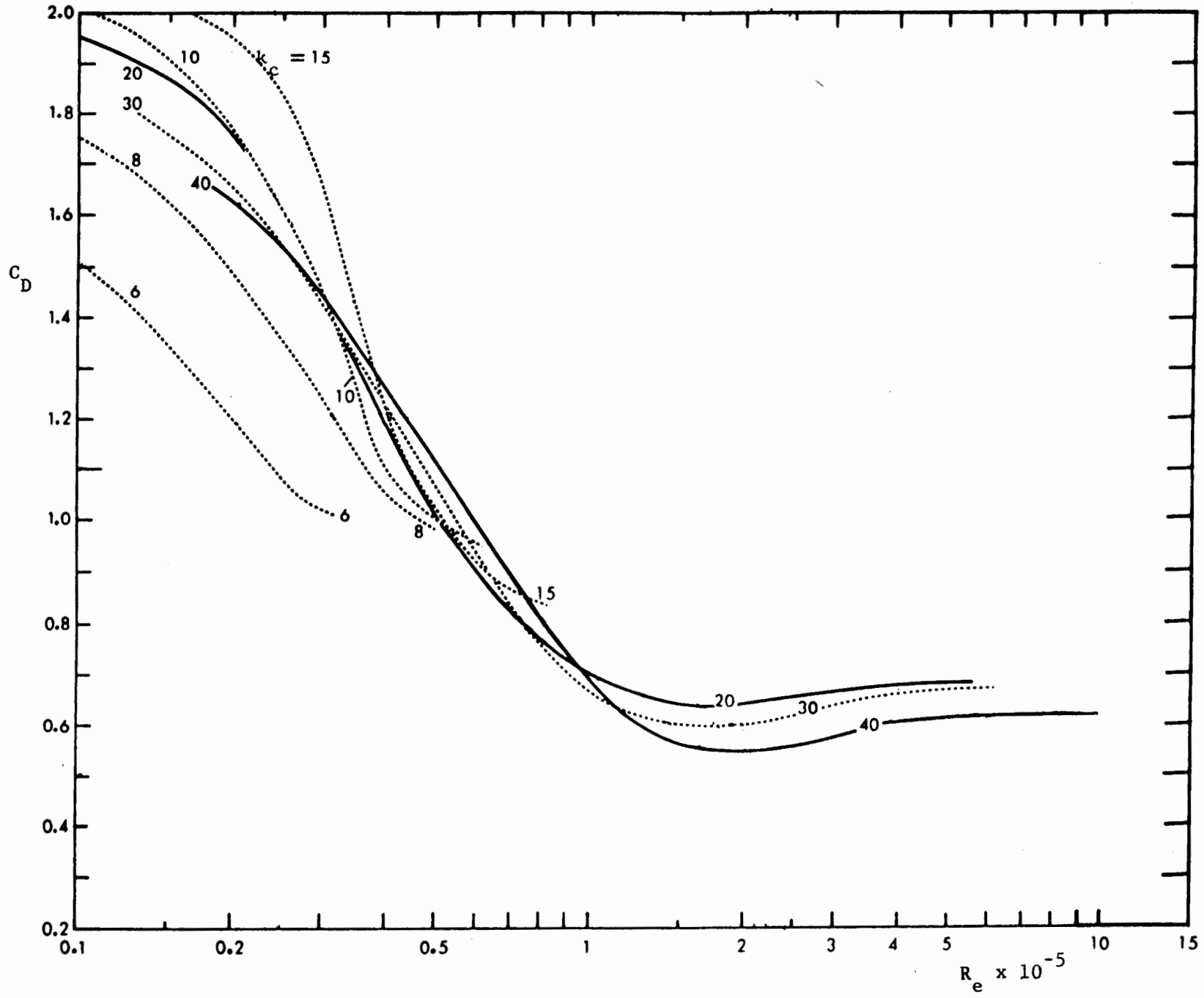

Figure 2.15 : Comparison of Sarpkaya (1976) with Garrison (1990) for C_D .

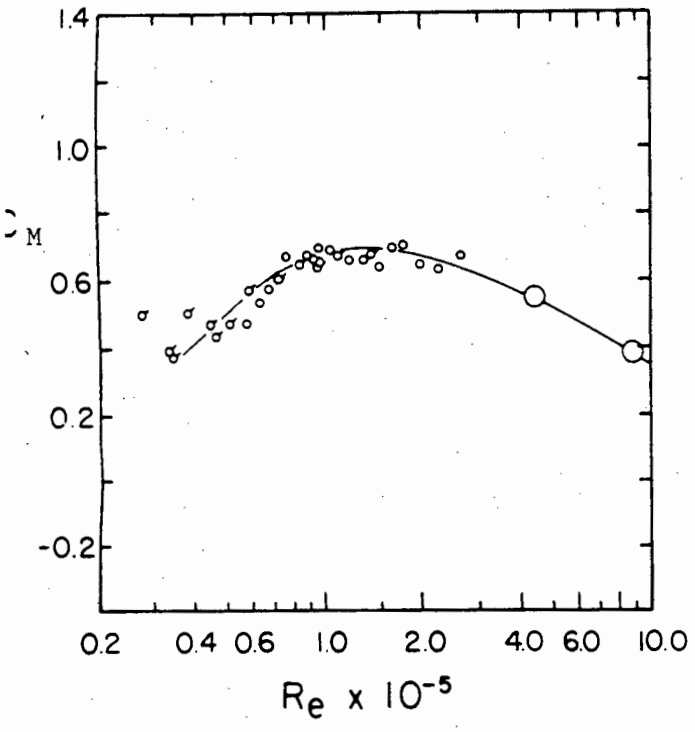

igure 2.16 : Scatter of data for C_M also showing few data points of high R_e. k_c = 2,5

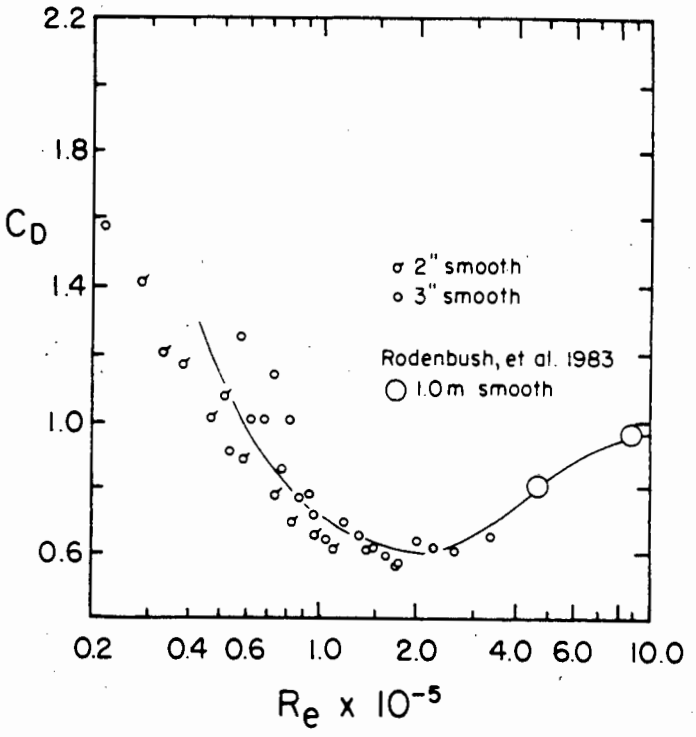

Figure 2.17 : Scatter of data for C_D, also showing few data points at high R_e k_c = 25.

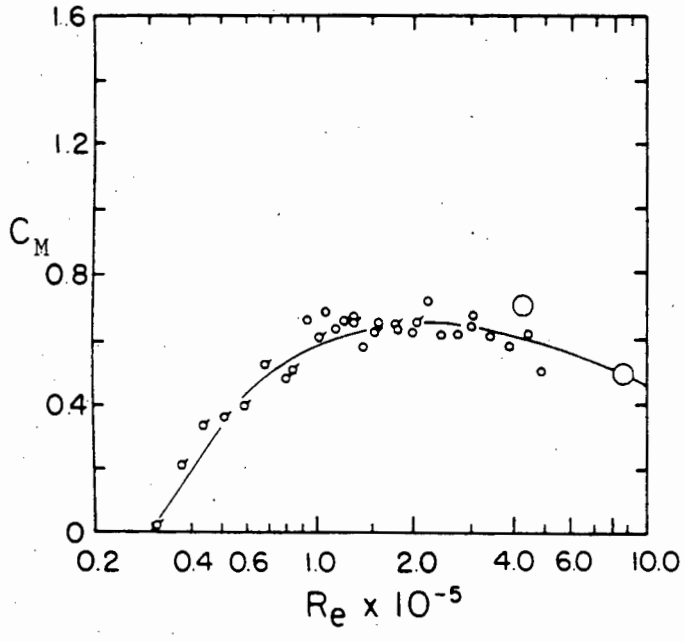

gure 2.18 : Garrison's data (1990) agrees well with that of Rodenbush et al. k_c = 38.

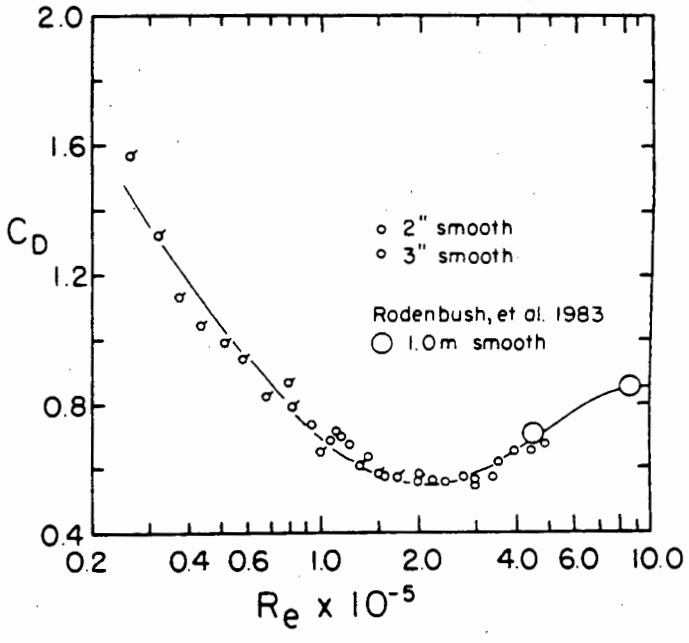

Figure 2.19 : Garrison's data (1990) for C_D agrees well with that of Rodenbush et al. k_c = 38.

But this cannot account for the whole of the discrepancy, especially for C_M. In fact, a close look at Sarpkaya's data indicates that decreasing k_c slightly reduces C_M (agreeing with Garrison and Rodenbush et al) and that decreasing k_c slightly increases C_D (also agreeing with Garrison and Rodenbush et al).

The values of C_M and C_D in Fig. 2.14 and 2.15 have the same trend as Sarpkaya's with respect to Reynolds number, but are, in general, lower. (The exceptions are for C_M for $R_e < 5 \times 10^4$ and $k_c > 10$, and for C_D for $R_e > 5 \times 10^5$ where Sarpkaya's values are lower.) Furthermore, although the trend of C_M and C_D with k_c (for fixed R_e) is not as clear as that shown by Sarpkaya, they do support each other. Therefore, although the measured values of C_M and C_D differ, the trends found by Sarpkaya for both k_c and R_e are confirmed.

Sarpkaya's results are also supported quantitatively by Chakrabati (1980). Chakrabati used oscillatory flow in a wave flume impinging on a fixed, vertical pile, and was thus only able to obtain low Reynolds numbers ($2 \times 10^4 < Re < 3 \times 10^4$). The data, Fig. 2.20 (from Chakrabati, 1980) had a large amount of scatter and are unreliable for values of $k_c > 40$ due to the small amount of data. A comparison of Sarpkaya and Chakrabati is shown in Fig. 2.21 (from Chakrabati, 1980), which shows good agreement for $k_c < 40$, apart from C_M where $k_c < 15$. This is unfortunate, since this is the region where C_M is most important.

2.1.3.3 Difference between two- and three-dimensional flow

The flow in Sarpkaya's experiments was two-dimensional, i.e. it was pure sinusoidal flow with no velocity component parallel to the pile axis. Sarpkaya claimed that his results would give slightly larger forces than oscillatory (three-dimensional) flow because the nature of his experiments caused a far higher amount of spanwise coherence along a pile compared with oscillatory flow (although he did not believe that the difference would be significant). His data is supported by Chakrabati (1980) in three-dimensional flow, and in the field by Heideman et al (1979). However, Stansby et al (1983) showed C_M and C_D as a function of k_c (for limited Reynolds number, $Re < 7{,}5 \times 10^3$) with a parameter Ω, where

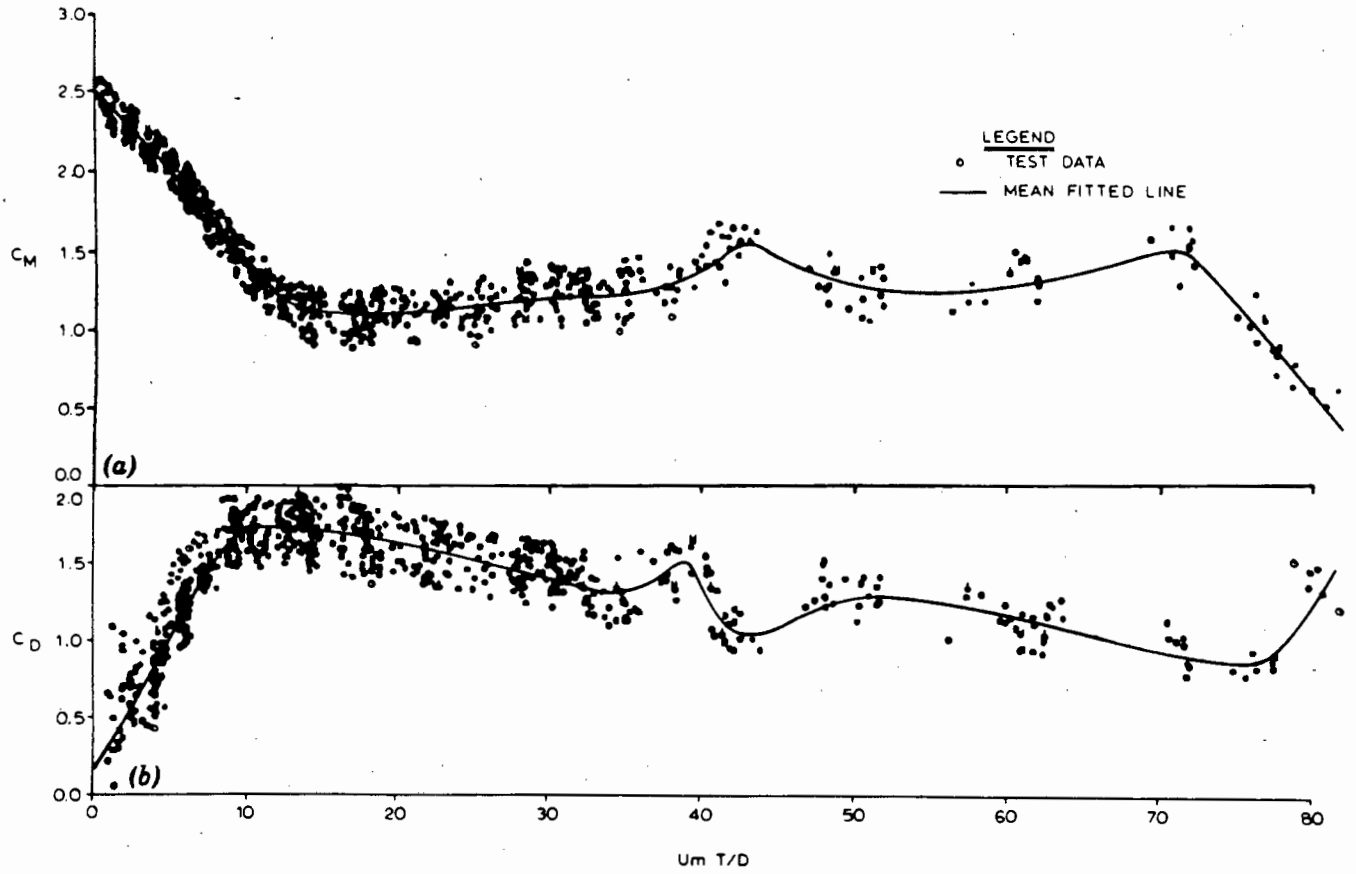

Figure 2.20 : C_M and C_D versus k_c for low R_e ($2 \times 10^4 < R_e < 3 \times 10^4$) from Chakrabati (1980).

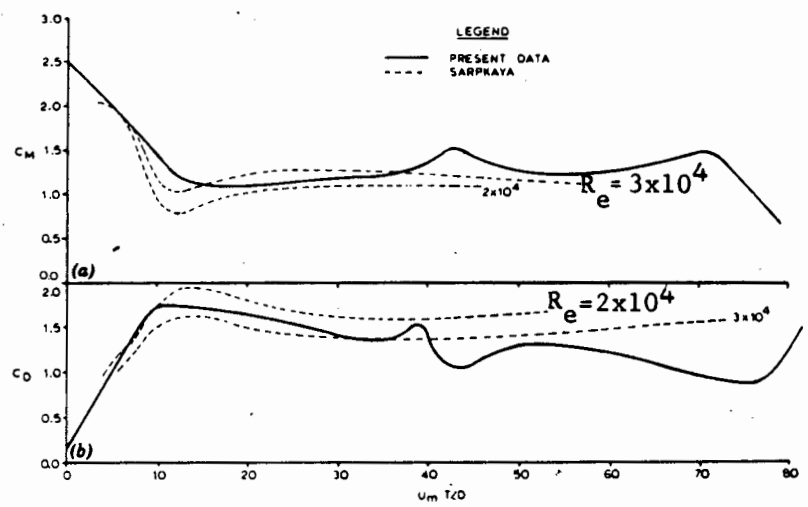

Figure 2.21 : C_M and C_D of Chakrabati (1980) compared to Sarpkaya (1976).

$$\Omega = \frac{\text{Distance travelled by water particle in x-direction}}{\text{Distance travelled by water particle in z-direction}}$$

As can be seen in Fig. 2.22 and 2.23 (Stansby et al, 1983), there is some dependence on Ω, especially for C_D. This is supported by Sarpkaya, at low Reynolds numbers (β = 784) in Fig. 2.24 and 2.25 (from Sarpkaya, discussion of Stansby et al, 1984). For these figures, Sarpkaya used a U-tube, but oscillated the cylinder in an axial direction with the same period as the water oscillations to simulate the vertical movements of the water particles, and therefore his results may not accurately represent three dimensional flow.

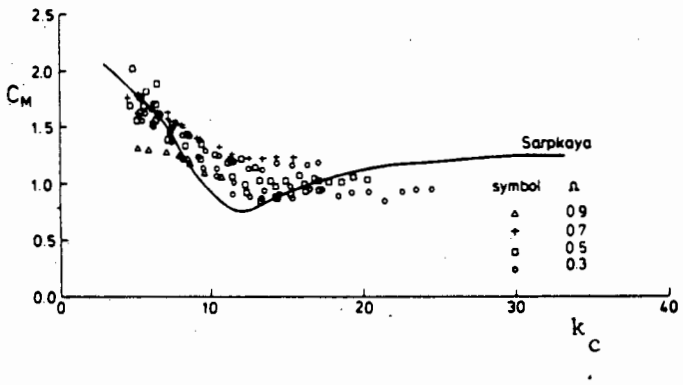

Figure 2.22 : Variation of C_M with k_c for various Ω.

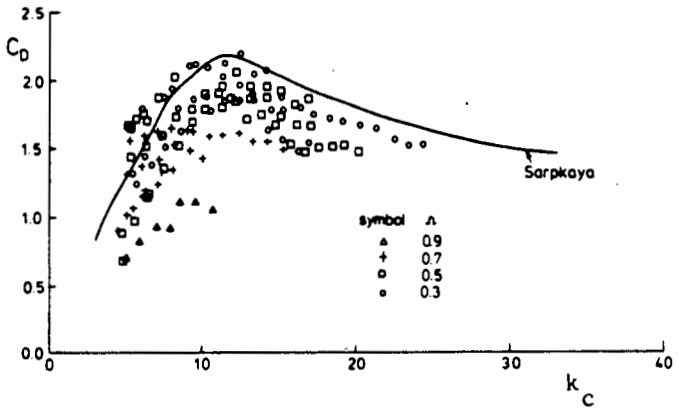

Figure 2.23 : Variation of C_D with k_c for various Ω.

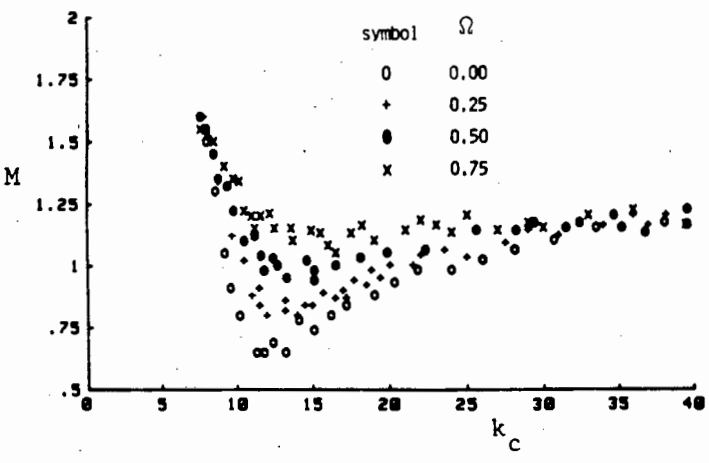

Figure 2.24 : C_D versus k_c for various Ω, from Sarpkaya (1984).

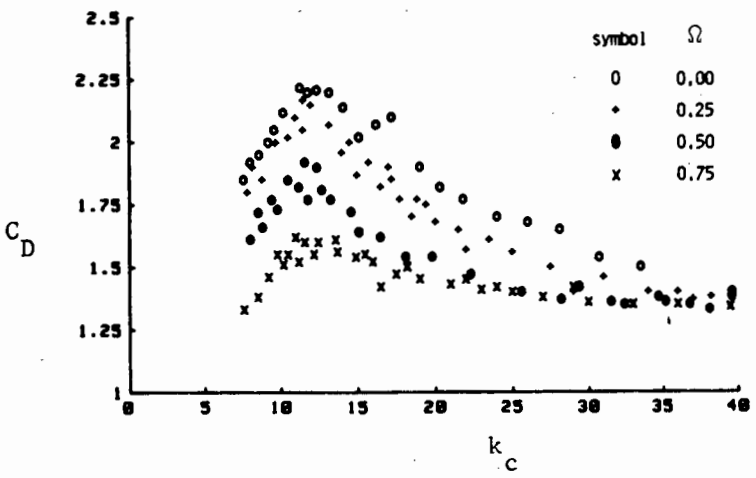

Figure 2.25 : C_D versus k_c for various Ω, from Sarpkaya (1984)

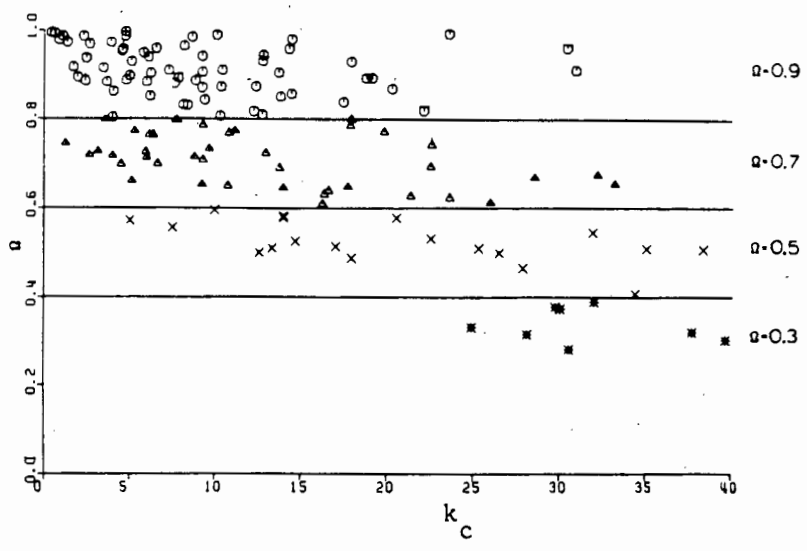

Figure 2.26 : Ω versus k_c

Subsequently, Chakrabati (1985) published the Ω values of the oscillatory flow coefficients shown in Fig. 2.21. The Ω-values, shown in Fig. 2.26 (Chakrabati, 1985), show a large range of Ω for any given value of k_c, without leading to an undue amount of scatter in Fig. 2.21. The greatest difference between Sarpkaya's force coefficients and Chakrabati's (shown in Fig. 2.21) is for C_M when $k_c < 15$. Yet this is the area of least scatter in Fig. 2.20, and has values of Ω ranging from $0,5 < \Omega < 1,0$, so therefore the value of Ω is not the cause of this discrepancy between the two authors. The rest of their data compares very well, except for $k_c > 40$, where Chakrabati's data is unreliable for other reasons. Finally, it must be emphasized that all experimental investigations into the effect of Ω have been performed at low Reynolds numbers, and therefore at high Reynolds numbers, Sarpkaya's force coefficients should be used.

2.1.3.4 C_M and C_D from field tests

Field tests are very important to gather data about force coefficients : they are the only way to collect information at high Reynolds numbers in oscillatory flow. Unfortunately, there are many associated problems : wave directions and water particle velocities and accelerations are unknown. Waves do not arrive in regular swells. Currents, tidal effects, and marine growth may have major effects on the force on a pile. Many of these

variables are measurable, but the measurements may not be a true representation of the desired quantity. If, for example, the water particle velocity is being measured, both the staff holding the velocity meter and the pile itself may cause vortices that impinge upon the meter to give misleading readings, and the distance between the meter and the pile may be such that the actual velocity at the meter is not the relevent local velocity at the pile : certainly, if the meter is very close to the pile, it can alter the flow around the pile. Therefore, the field measurements of wave forces, though very important, are also highly susceptible to errors.

There have been several field tests on piles, reported by, among others, Wiegel (1957), Dean and Aagard (1970), Bishop (1979), Heideman et al (1979) and Ohmart (1984). Fig. 2.27 (from Standing, 1984) shows the average of the measured C_M and C_D values plotted against k*, a version of the Keulegan-Carpenter number, at high Reynolds number, for Bishop, Sarpkaya and Heideman et al. k* is defined as

$$k^* = \frac{2\pi}{0{,}866\ D}\left[\frac{\overline{u^4}}{\overline{u^2}}\right]^{1/2}$$

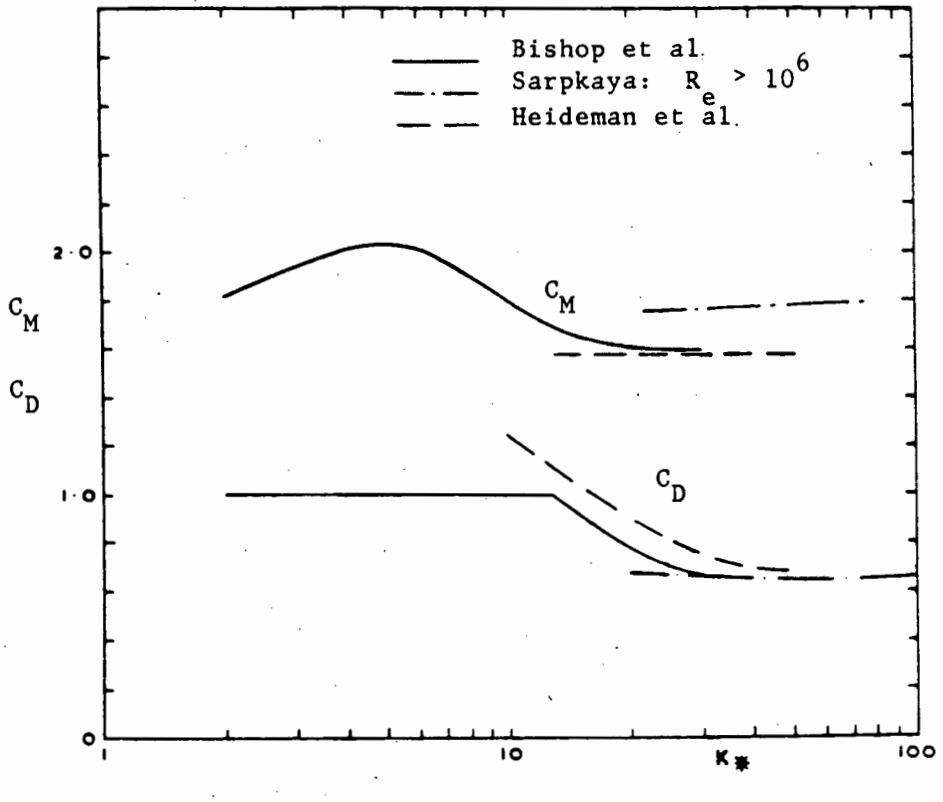

Figure 2.27 : C_M and C_D versus k*.

Bishop found the drag force to be small compared with the inertial force, and that C_D was very variable, for $k_c < 20$, and therefore assumed it to be 1,0. The plots from three different sources show good agreement - the largest difference is in Sarpkaya's C_M values - but these only deviate by 10%, and are on the conservative side. These values were also confirmed by Ohmart, who found the values of C_M and C_D to be 1,7 and 0,7 respectively (at high R_e).

Unfortunately, Fig. 2.27 shows only the average values of C_M and C_D, and thus hides a great deal of scatter. Bishops values, for example, are averaged over a 20 minute time span. As this span reduces, the scatter increases. Figure 2.28 (from Bishop, 1979) shows the increasing scatter for C_M as the time span (Δt_i) decreases from 240 s to 20 s. Note that 20 s is still approximately three wave periods.

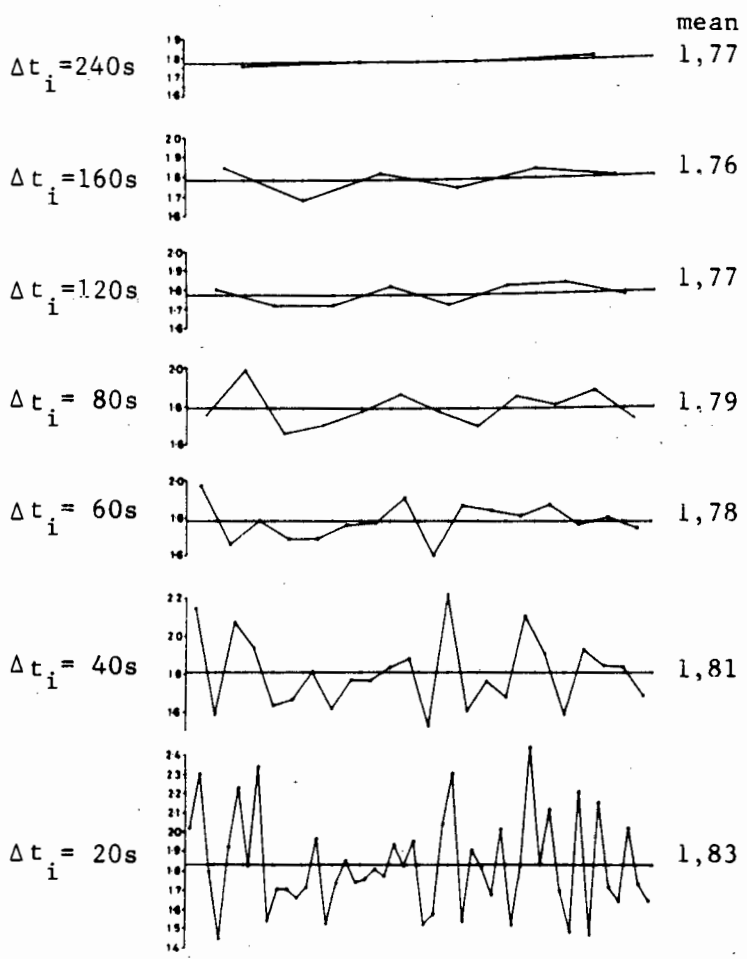

Figure 2.28 : C_M calculated from measured forces for different time periods (Δt_i). C_D forced to 1,0 .

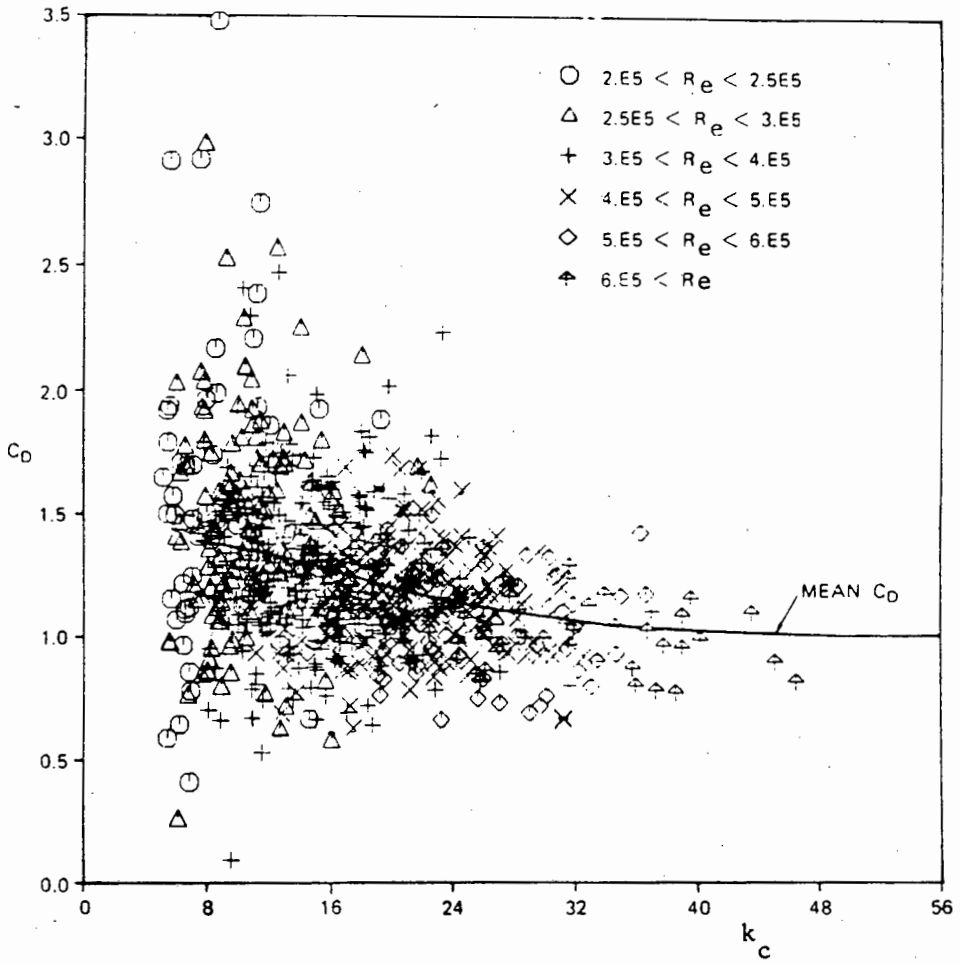

Figure 2.29 : Scatter found in C_D from field tests.

Even larger scatter is shown in Figure 2.29 (from Heideman et al, 1979). This shows C_D as a function of k_c and R_e, but the most noticeable fact is the variation of C_D from 0,1 to 3,5 at $k_c \approx 10$. However, at low k_c ($k_c < 10$) the drag force is a small propor-tion of the total in-line force, and thus a small error in the total in-line force will lead to a much larger variation in C_D. If this is the cause of the scatter, as the k_c numbers increase (i.e. the drag force becomes more significant) then the scatter should reduce (which it does). However there is still a great deal of scatter for large k_c ($k_c > 20$).

Another possible cause of the scatter is vortex action around the pile. Any errors due to this would be aggravated by the relative insignificance of the drag force, as explained above. The largest errors due to vortex action

occur for $8 < k_c < 15$ which also fits the data in the figure. Finally, the forces were measured on a structure with multiple piles and cross members, and therefore interference between piles will probably have occurred.

Due to the inherent unreliability of field test data, the reason for this scatter is unknown. However, since laboratory experiments show that C_M and C_D values are reasonably repeatable, most authors reason that the cause of the scatter is an incorrect measurement of the water particle velocity. But since this has not been proven all C_M and C_D coefficients must be regarded as approximate.

2.1.4 The accuracy of Morison's equation

2.1.4.1 Force predictions over a wave period

Since the drag coefficient in steady flow is a function of Reynolds number, i.e. in part a function of the velocity, it has been suggested that the drag coefficient, if not the inertia coefficient, in oscillatory flow should be a function of the instantaneous velocity. There have been several studies on this, most notably by Keulegan and Carpenter (1958), but also by Sarpkaya (1976) and Sarpkaya and Wilson (1984).

Keulegan and Carpenter expressed the force as a Fourier series, i.e.

$$\frac{f(\theta)}{\rho U_m^2 D} = A_1 \cos\theta + A_3 \cos 3\theta + A_5 \cos 5\theta + \ldots + B_1 \sin\theta + B_3 \sin 3\theta + B_5 \sin 5\theta + \ldots \qquad (2.13)$$

Note that since $f(\theta) = -f(\theta + \pi)$, the terms $A_n \cos n\theta$ and $B_n \sin\theta$ can be dropped when n is even. They then used further Fourier analysis to show that

$$\sin\theta|\sin\theta| = \sum_{n=0}^{\infty} a_n \sin n\theta \qquad (2.14)$$

where $a_n = 0$ for n even.

This identity was used to re-write equation (2.13) as

$$\frac{f(\theta)}{\rho U_m^2 D} = A_1 \cos\theta + A_3 \cos 3\theta + A_5 \cos 5\theta + \ldots + B_1' \sin\theta|\sin\theta| + B_3' \sin\theta + B_5' \sin 5\theta + \ldots \qquad (2.15)$$

Comparing equation (2.15) with the Morison equation,

$$f(\theta) = C_M(\theta) \left(\frac{\rho\pi D^2}{4}\right) u_m \sigma \cos\theta + \frac{C_D(\theta)}{2} D \rho u_m^2 \sin\theta|\sin\theta|, \qquad (2.16)$$

and assuming the cosine series represents the inertia force and the sine series represents the drag force, then

$$C_M(\theta) = \frac{2}{\pi^2} \frac{u_m T}{D} \left[A_1 + \frac{A_3 \cos 3\theta}{\cos\theta} + \frac{A_5 \cos 5\theta}{\cos\theta} \ldots \right]$$

$$= \frac{2}{\pi^2} \frac{u_m T}{D} \left[A_1 + A_3 + A_5 - 2(A_3 + A_5) \sin 2\theta - 2 A_5 \cos 5\theta + \ldots \right]$$

Thus, assuming A_3 and A_5 are small , $C_M(\theta)$ is independent of θ, and therefore

$$C_M = \frac{2}{\pi^2} \frac{u_m T}{T} A_1$$

Furthermore,

$$C_D(\theta) = 2 \left[B_1' + B_3' \frac{\sin 3\theta}{|\sin\theta|\sin\theta} + \frac{B_5' \sin 5\theta}{|\sin\theta|\sin\theta} + \ldots \right]$$

$$= 2 B_1' + \frac{2}{|\sin\theta|} \left[\frac{\sin 3\theta}{\sin\theta} + \frac{\sin 5\theta}{\sin\theta} + \ldots \right]$$

and, therefore assuming coefficients A_3 onwards are small, $C_D(\theta)$ is independent of θ, except where $|\sin\theta| \approx 0$, and

$$C_D = 2 B_1'$$

Fig. 2.30 - 2.32 (from Keulegan and Carpenter, 1958) show the force measured on a vertical cylinder and the force predicted on the same cylinder as a function of $\theta = 2\pi t/T$. The k_c values are 3,0, 15,6 and 44,7 respectively. Also shown are the instantaneous C_D and C_M values. [Note that in this figure, $|\sin \theta| = 0$ at $t/T = 0{,}25$, when Keulegan and Carpenter's analysis assumes that $u = 0$, and therefore that $C_D \to \infty$.]

The Morison equation predicts the force very well in Fig. 2.30 and 2.32. The values of C_M are almost constant, as are the values of C_D, except at $t/T = 0{,}25$ or $0{,}75$ (where $C_D \to \infty$). Note also, at this point, that since $u = 0$, the value of the drag term is very small and a minor error will cause a large change in C_D. Furthermore, in Fig. 2.30, the k_c value is 3,0 and therefore the drag term contributes very little to the total force. Therefore, any experimental error will cause a small error in C_M but a much larger error in C_D. The opposite is true for Fig. 2.32 where C_D is accurately calculable and

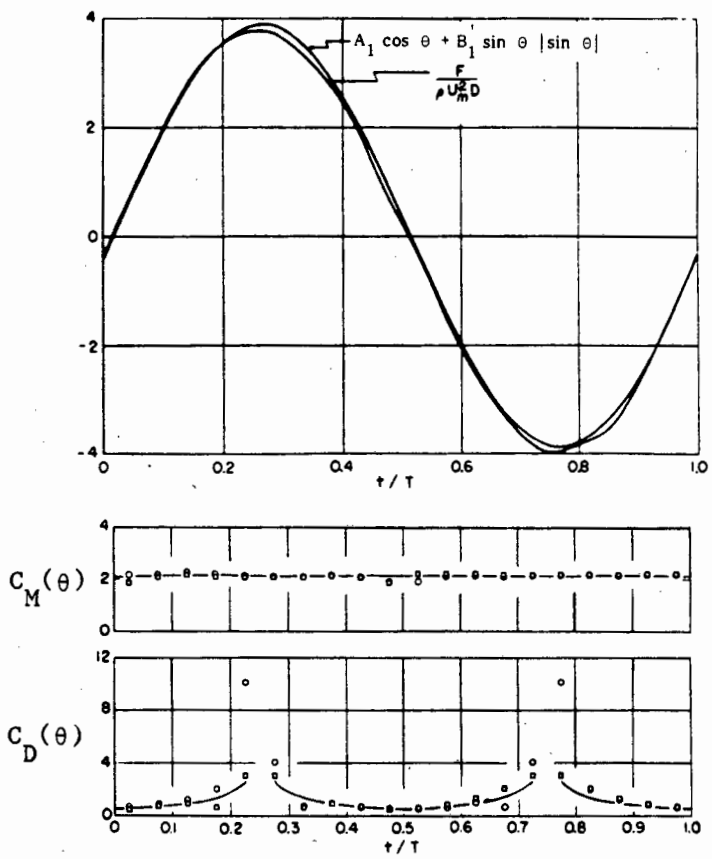

Figure 2.30 : Comparison of measured and computed forces at low k_c with C_M and C_D (for the same wave) as a function of t/T.
$k_c = 3{,}0$; $C_M = 2{,}14$; $C_D = 0{,}70$.

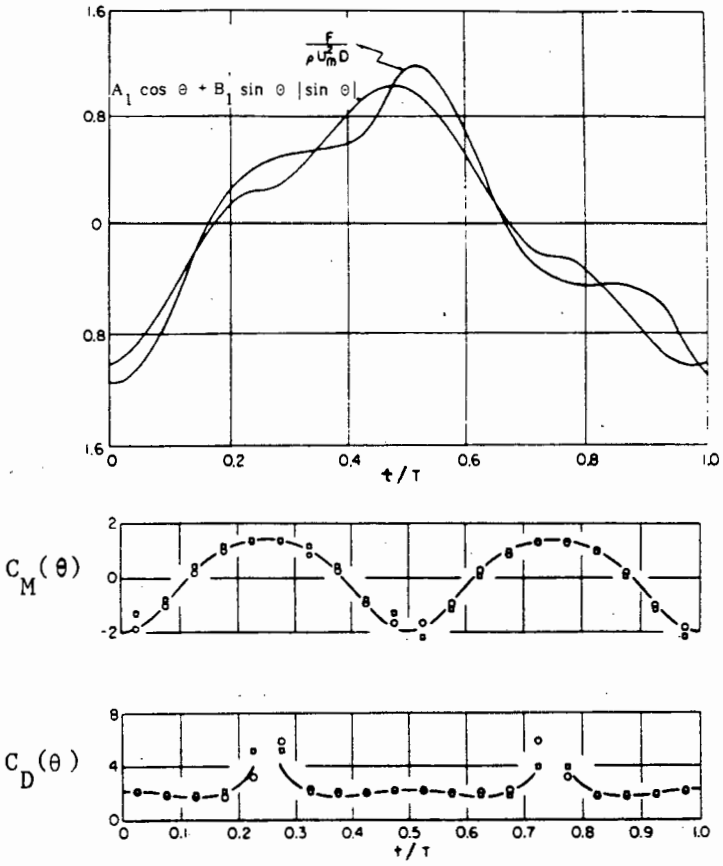

Figure 2.31 : Comparison of measured and computed forces at intermediate k_c, together with C_M and C_D (for the same wave) as functions of t/T

k_c = 15,6 ; C_M = 0,80 ; C_D = 2,05 .

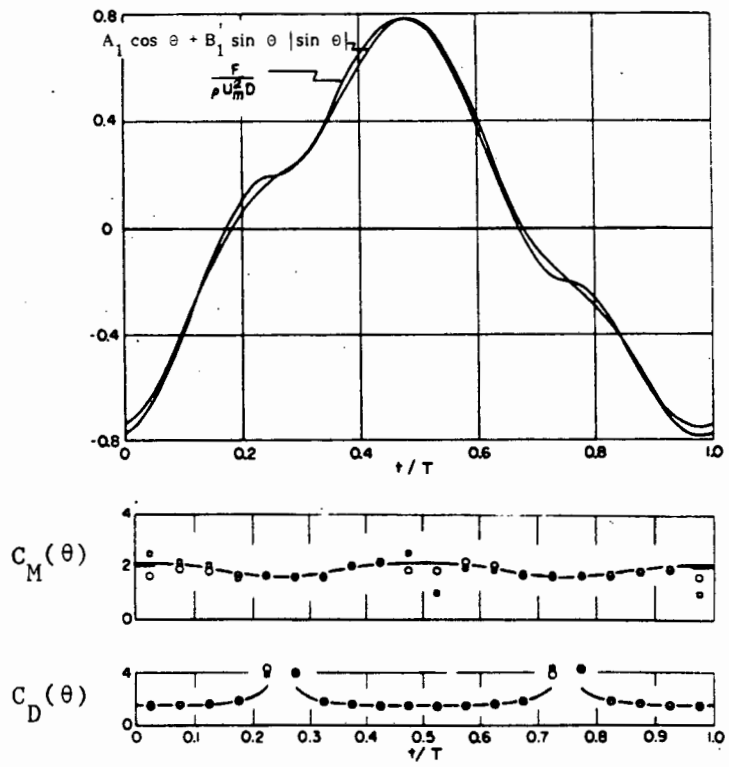

Figure 2.32 : Comparison of computed and measured forces at high k_c, together with C_M and C_D (for the same wave) as functions of t/T

k_c = 44,7 ; C_M = 1,76 ; C_D = 1,54 .

C_M is prone to experimental error. This probably accounts for most of the variation in C_D in Fig. 2.30 and in C_M in Fig. 2.32.

Fig. 2.31, however, shows differences between the predicted and measured forces, and large changes in C_M. This has been studied by several researchers, including Sarpkaya and Wilson (1984) and is fairly typical for k_c values of k_c between 8 and 16. In this region (see Fig. 1.5) one vortex is shed in each half-period. This causes sudden and large changes in velocity, acceleration and pressure around and behind a pile, which the Morison equation does not allow for. It was for this reason that Sarpkaya and Wilson (1984) developed a four-term Morison equation (see section 2.2.2), At higher k_c values more vortices are swept past the left and right hand sides of the pile and rapid changes in the in-line force are not encountered.

Figs. 2.30 to 2.32 were all measured in a laboratory : forces measured at sea will show a far greater scatter due to the greater randomness of the waves, and other experimental errors. Fig. 2.33 (from Heideman et al, 1979)

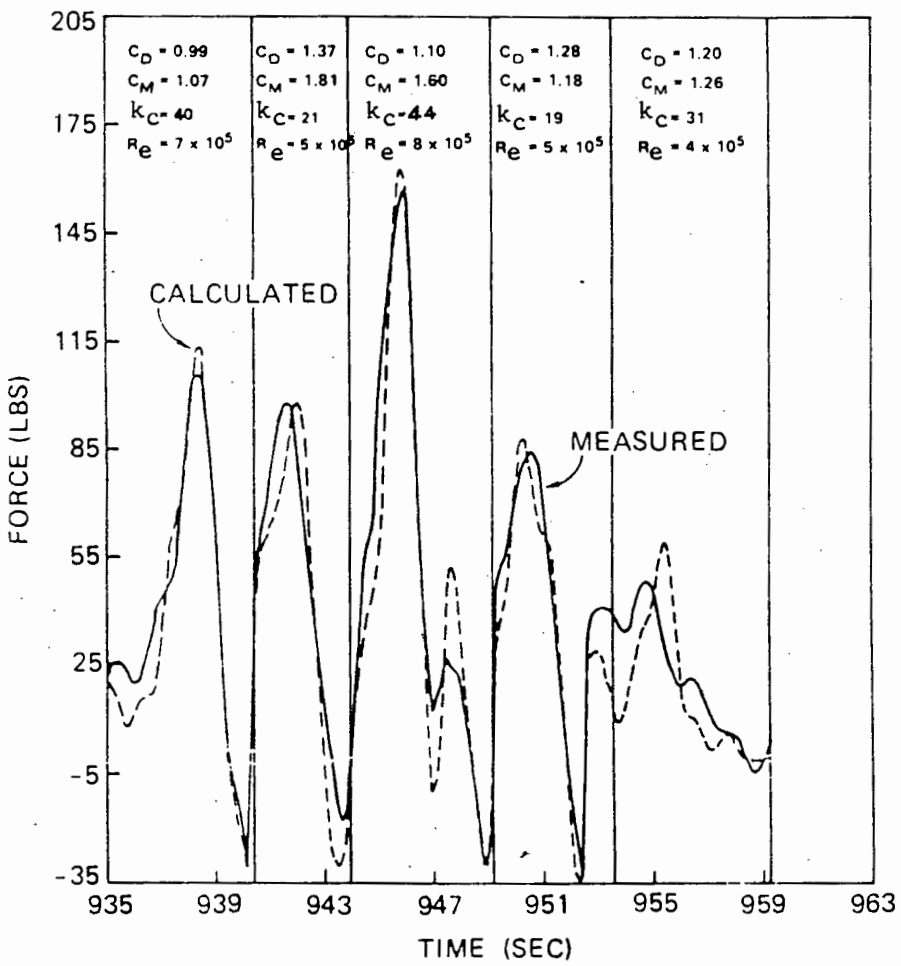

Figure 2.33 : Comparison of computed and measured forces from a field test.

shows closely-fitting force predictions for the first four waves but poor correlation for the last : however, for this wave there was a strong transverse velocity. Note also the variation in C_M, C_D and k_c values, and that C_M varies by 50% (1,07 to 1,60) from the first wave (k_c = 40, R_e = 7 x 10^5) to the third wave (k_c = 44, R_e = 8 x 10^5).

2.1.4.2 The accuracy of the coefficients C_M and C_D

One of the surprising facts about Sarpkaya's force coefficients (Sarpkaya, 1976) is the extremely small amount of scatter. Most experiments have a significant amount of scatter : Chakrabati's data (Fig. 2.20) shows a small amount of scatter compared to Stansby et al (Figs. 2.22 and 2.23) : in each of Stansby's figures one data point represents an average of 200 wave cycles and there is still considerable scatter. The force coefficients gathered in field tests are worse : they usually have extremely large amounts of scatter which can be ascribed to any one of many possible causes of error.

The most reliable and complete force coefficients are those of Sarpkaya (1976) which have been supported by several authors. However there will probably be large variations on these in the field.

2.1.5 Flaws in the Morison equation

The Morison equation is an empirical formula and does not recognise the various physical phenomenon such as vortex shedding which also affect the pile. It separates the total force into two components, which interact. In these circumstances it is surprising that the Morison equation predicts the total force as well as it does, even in the region of k_c values between 8 and 16. The basic flaws are:

1. The drag force is not only dependent on the instantaneous incident velocity. For example at the moment that u = 0, vortex action can cause a low pressure region behind the pile, and thus a drag force may exit.

2. Diffracted and reflected waves are not considered. Therefore the range of the equation is limited to small D/L < 0,2.

3. Vortex action, which can cause significant deviations from predicted forces (as in 1 above) is ignored.

4. The total force is expressed as a function of u and $\frac{\partial u}{\partial t}$. These values must be predicted by wave theory, and different theories give different results, as shown in Fig. 2.34 (from Dean, 1976). Therefore, even with the correct coefficients, the calculated force might not be accurate.

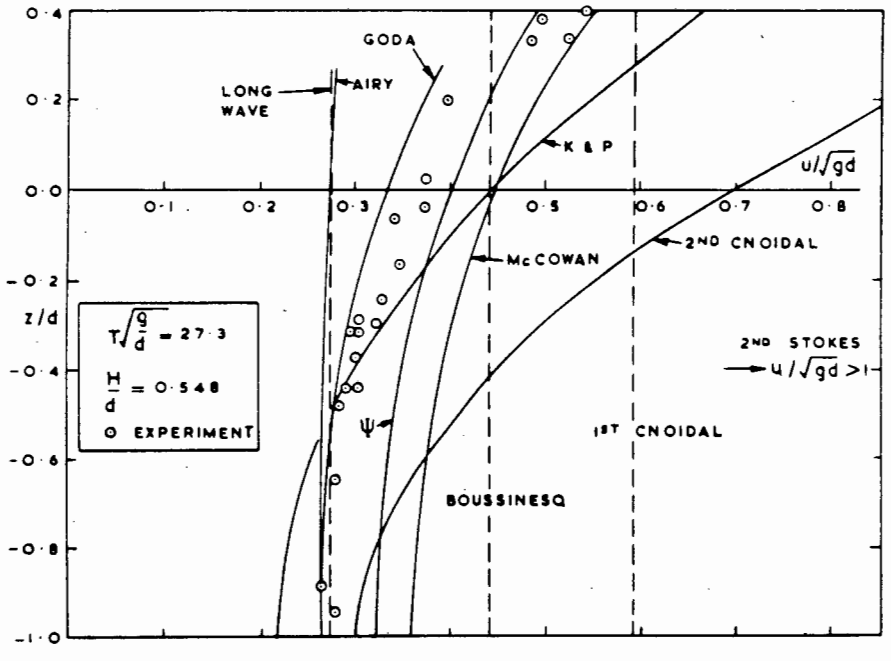

Figure 2.34 : Measured velocities and calculated velocities for several wave theories. K & P = Keulegan and Patterson wave theory.

5. Finally, there are many variables at sea that are not accounted for with the Morison equation. These include, among others, tidal currents, marine growth, and resonance or movement of the pile. Thus the Morison equation can only be regarded as a reasonable guide, and not as totally valid.

2.2 Extensions of the Morison equation

The Morison equation is an empirical attempt to predict the force on a pile, and thus is not as accurate as an analytical equation would be expected to be. There are differences between predicted and measured forces, especially between the k_c values 8 and 16.

2.2.1 An alternative Fourier series approach to the force on a pile

Keulegan and Carpenter (1958) tried to avoid this problem by describing the force as a Fourier series, as shown in equation (2.15) previously, which is repeated below:

$$\frac{f(\theta)}{\rho U_m^2 D} = A_1 \cos\theta + A_3 \cos 3\theta + A_5 \cos 5\theta + \ldots + B_1' \sin\theta|\sin\theta| + B_3' \sin\theta + B_5' \sin\theta + \ldots$$

and, therefore,

$$f(\theta) = C_M(\theta)\,\rho\,\frac{\pi D^2}{4}\,u_m\sigma\cos\theta + \frac{C_D(\theta)}{2}\,\rho\,D\,u_m^2\sin\theta|\sin\theta| + \rho\,U_m^2\,D\,\Delta R(\theta) \qquad (2.17)$$

where $\sigma = \frac{2\pi}{T}$

$\Delta R(\theta)$ = the remainder function (dimensionless)

$$= \sum_{n=1}^{n=\infty} A_{2n+1}\cos(2n+1)\theta + \sum_{n=1}^{n=\infty} B_{2n+1}'\sin(2n+1)\theta \quad \ldots \qquad (2.18)$$

As can be seen, the first two terms in equation (2.17) comprise the Morison equation and $\rho\,u_m^2\,D\,\Delta R(\theta)$ is therefore the difference between the measured and calculated forces. As shown in Fig. 2.35 (from Keulegan and Carpenter, 1958), $\Delta R(\theta)$ is definitely periodic, with a period of approximately T/3 as would be expected from the presence of the third harmonic. Keulegan and Carpenter also calculated (see Figs. 2.36 and 2.37) (from Keulegan and Carpenter, 1958) the values of A_3, A_5 and B_3', B_5' as functions of k_c. These also show the areas of inaccuracy of Morison's equation - values of $|A_n|$ or

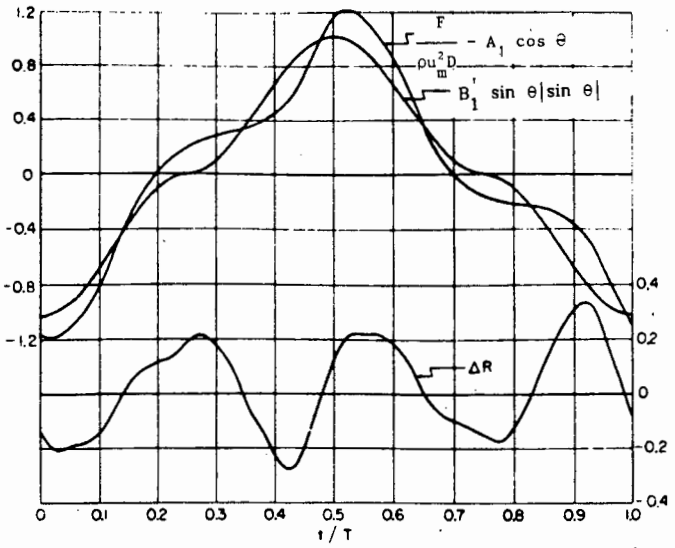

Figure 2.35 : Evaluation of remainder function ΔR for $k_c = 15,6$

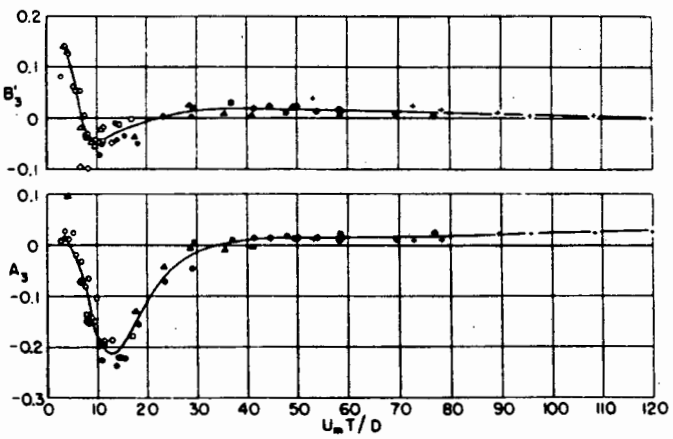

Figure 2.36 : Variation of coefficients of the remainder force with k_c .

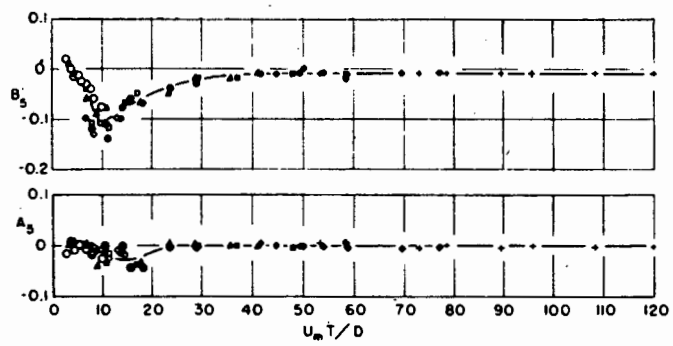

Figure 2.37 : Variation of coefficients of the remainder force with k_c.

$|B_n'| > 0{,}10$ lead to errors in force calculations greater than 5%. Note the relatively large magnitude of $|A_3|$ accounts for most of the errors, as the influence of A_5 is negligible. $|B_5'|$ is similar to $|B_3'|$, but these may still lead to a maximum error of 5% in the measured force.

2.2.2 The four-term Morison equation

A similar examination of the remainder function was performed by Sarpkaya and Wilson (1984) which led to the four-term Morison equation, valid for the same k_c values (i.e. $8 < k_c < 16$). Interestingly, this ignores the sin 3θ term, despite the fact that A_3 was found by Keulegan and Carpenter to be the most influential coefficient after C_M and C_D, but includes cos 3θ and cos 5θ.

It is

$$\frac{f(\theta)}{\frac{1}{2}\rho D u_m^2} = \frac{\pi^2}{k_c} C_M \cos\theta + C_D \sin\theta|\sin\theta| + 2 \text{ extra terms}$$

The effect of this equation is shown in Fig. 2.38 and 2.39 (from Sarpkaya & Wilson, 1984). Fig. 2.38 shows the force predicted by the Morison equation compared to the measured force, while Fig. 2.39 compares the four-term equation to the measured force. While the four-term equation is distinctly better than the original Morison approach, it still shows discrepancies. These may be due to the absence of any term with sin 3θ.

2.2.3 Other variations on the Morison equation

There are several other variations of the Morison equation, or on methods of predicting C_M and C_D: Hogben (1976), for example, suggests that

$$C_M \approx \frac{\sqrt{k_c^2 C_D/\pi^3 + 1/4} + 3/2}{\sqrt{k_c^2 C_D/\pi^3 + 1/4} + 1/2} \quad . \tag{2.18}$$

However, this equation and most of the other variations are either inaccurate or there is insufficient evidence to support them.

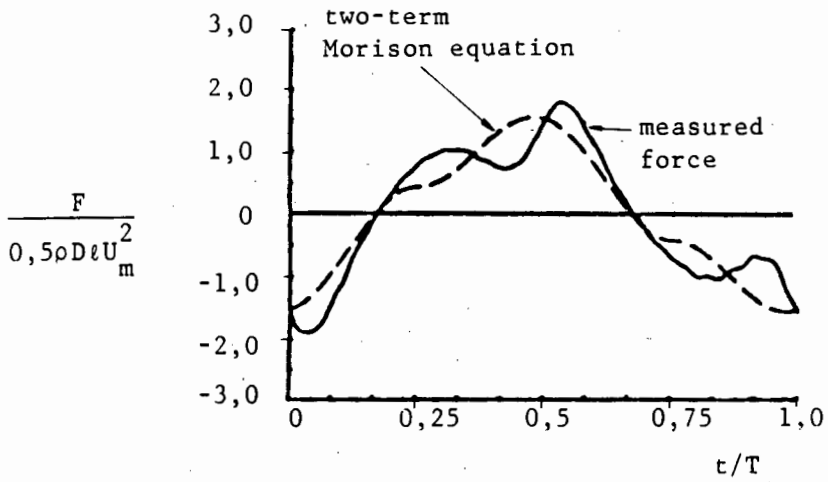

Figure 2.38 : Comparison of Morison equation with measured force for $k_c = 12$.

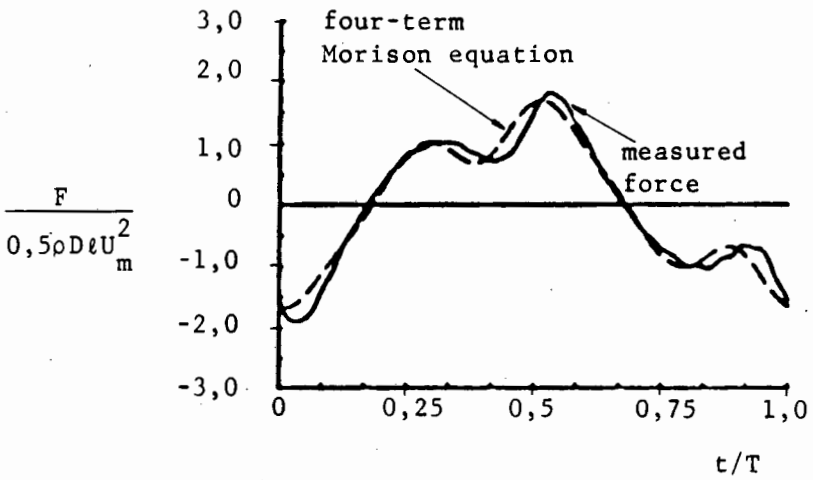

Figure 2.39 : Comparison of four-term Morison equation with measured force for $k_c = 12$.

2.3 Alternatives to the Morison equation

There are several alternative methods to predict the in-line force on a pile apart from the Morison equation. The most important is probably the prediction of the force by predicting the position and movement of vortices.

2.3.1 Force prediction from vortex theory

Since the force on a pile is a function of the pressures surrounding the pile, and the pressures are significantly affected by the vortex action around the pile, it should be possible to predict the force on a pile by predicting the vortex action around it. Although the formation and propagation of vortices is not fully understood, there have been several attempts to solve these problems with approximate solutions. Stansby (1977) and Sawaragi and Nakamura (1979) have both tried to predict the force on a pile by this method. Stansby's results, compared with the Morison equation, are shown in Fig. 2.40 (from Stansby, 1977). Stansby's results follow the

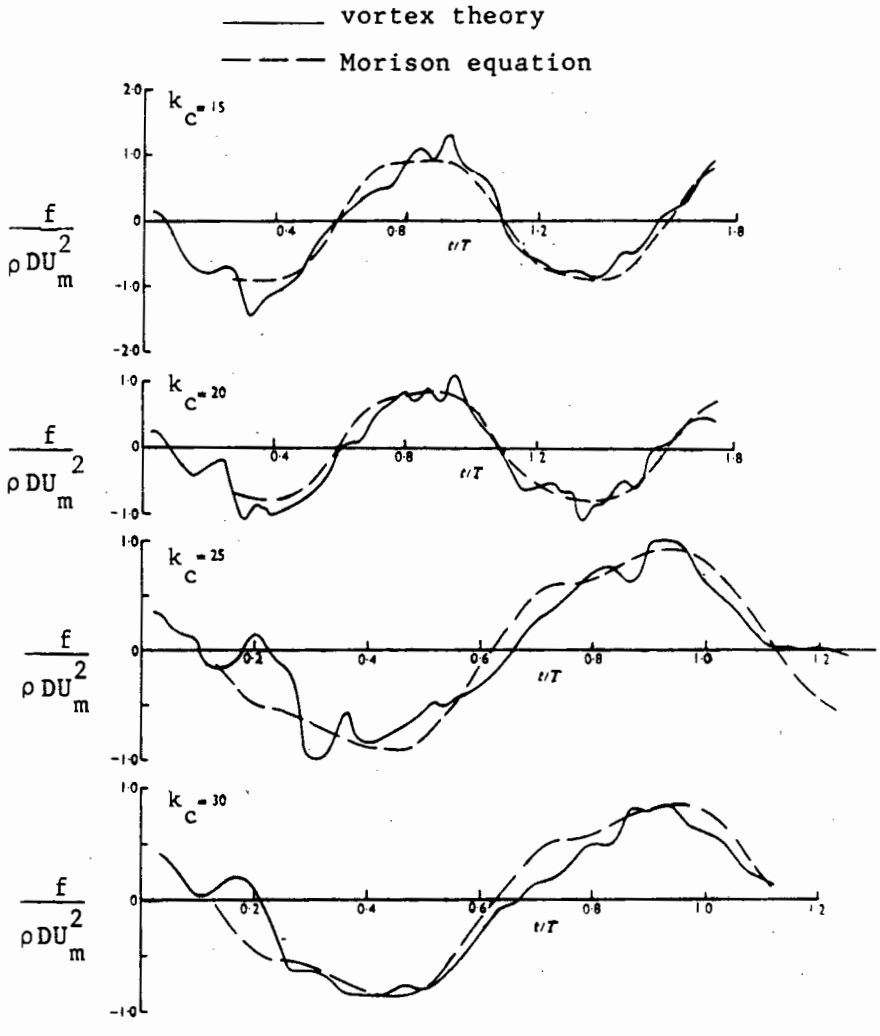

Figure 2.40 : Forces predicted by vortex theory compared to those predicted by Morison's equation.

trend of the Morison equation closely, but there are large differences at isolated moments within the wave period.

Although this method of force prediction is in some ways inaccurate, as our knowledge concerning vortices increases, and as vortex theory improves, the associated force predictions will become more accurate, and may, in time replace the Morison equation.

2.3.2 Iverson's Modulus

Iverson's modulus was proposed as an alternative to the Morison equation early in the 1950's (Iverson and Balent, 1951). Iverson and Balent claimed that

$$F = C \frac{1}{2} \rho V^2 S \qquad (2.19)$$

where V = velocity
S = area
and C = a coefficient, a function of Iverson's modulus,

where Iverson's modulus = $\frac{A D}{V^2}$
and A = acceleration

Although Laird and Johnson (1956) showed that the modulus could not predict forces accurately, it was revived by Jen (1980), who showed by dimensional analysis that

$$F = f(R_e, I, F_r) \qquad (2.20)$$

where I = Iverson's modulus
and F_r = the Froude Number

Unfortunately, Jen did not compare his method of force prediction with either experimental results or with Morison's equation. However, since it is an empirical equation with experimental coefficients, it is unlikely that it will be significantly more accurate than the Morison equation.

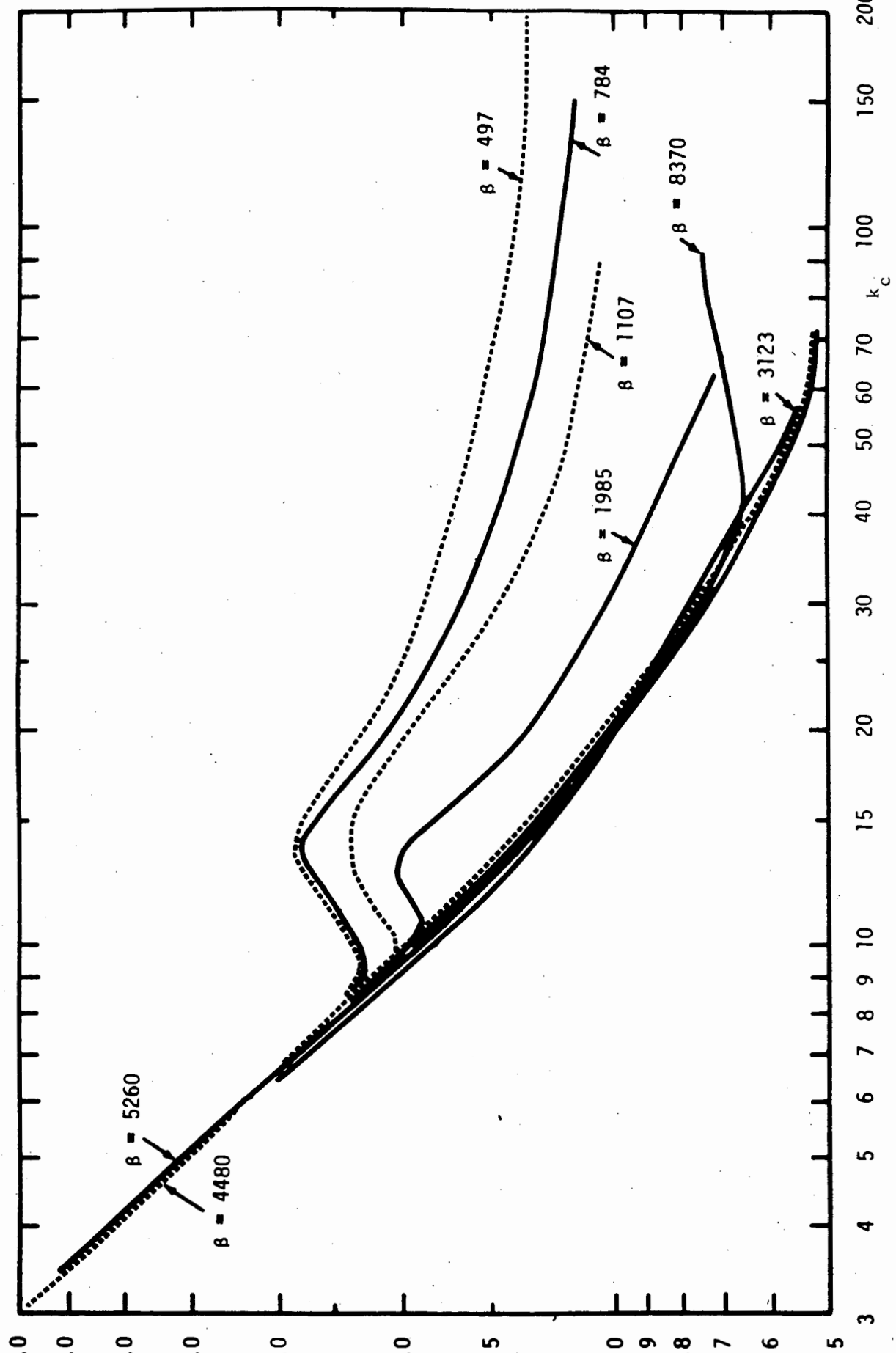

Figure 2.41 : C_F versus k_c for various β

2.4 Total force coefficients

2.4.1 Total force coefficient C_F

The total force coefficient, C_F, is defined as

$$C_F = \frac{\text{Maximum of the measured force per unit length within a cycle}}{0{,}5\ \rho\ D\ U_m^2}$$

$$= \frac{f_{max}}{0{,}5\ \rho\ D\ U_m^2}$$

The values of C_F are shown as functions of k_c and β in Fig. 2.41 (from Sarpkaya, 1976A) and the amount of scatter about a typical line is shown in Fig. 2.42 (from Sarpkaya, 1976A) for one value of β (β = 1985). These experiments were performed in Sarpkaya's U-tube (see Section 2.1.3.2) in sinusoidal two-dimensional flow, and the amount of scatter is very similar to the amount of scatter that Sarpkaya measured in the C_M and C_D coefficients.

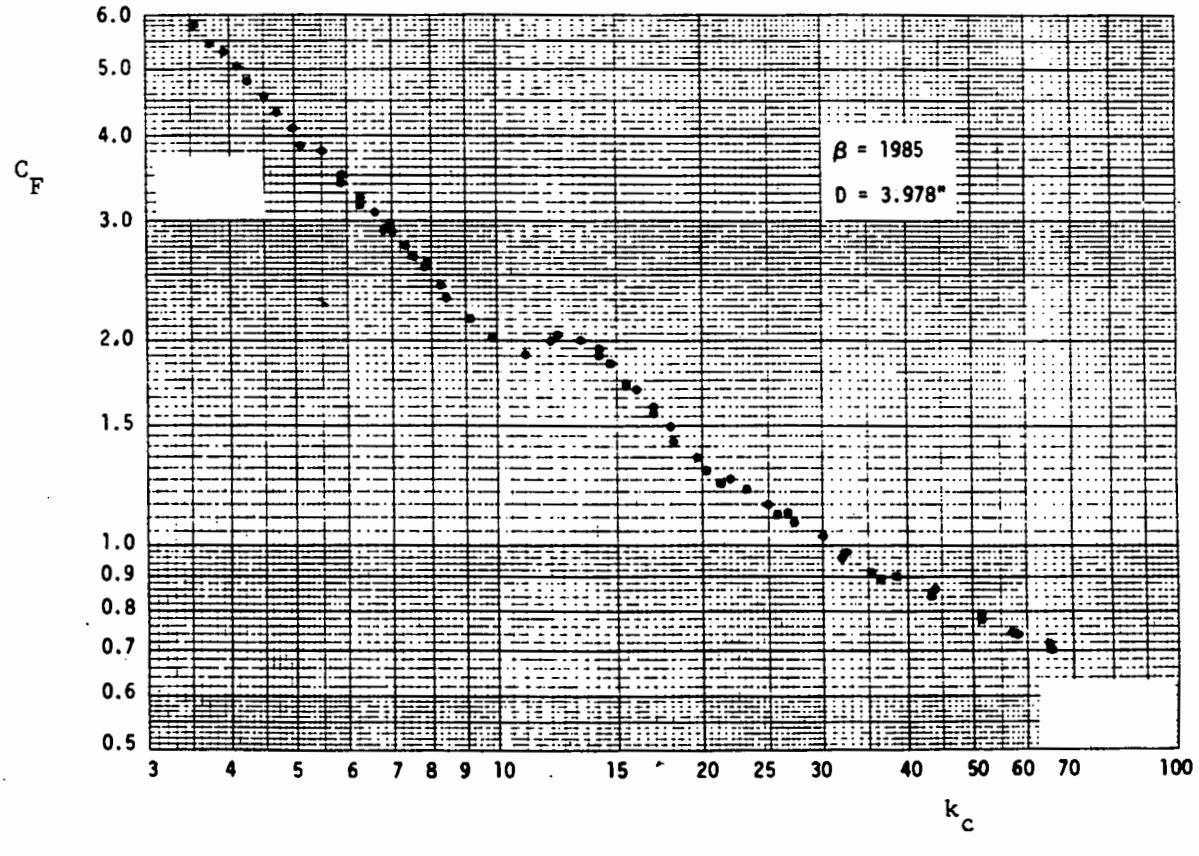

Figure 2.42 : Typical scatter found when measuring C_F.

2.4.2 Differences in C_F between two- and three-dimensional flow

Since the data was gathered in two-dimensional flow, there may be variations in three-dimensional flow. Stansby's experiments (1983) showed a large amount of scatter when applied to C_M and C_D (Section 2.1.3.3, Figs. 2.22 and 2.23), but when applied to C_F it was found that the C_F values approximated closely to Sarpkaya's curve, apart from Ω = 0,9 (i.e. an orbit which is close to circular)(see Fig. 2.43)(from Stansby, 1983). Note in this figure that $C_F' = (f_{max})_{RMS}/\frac{1}{2}\rho\,(u_{RMS})^2 D$. It is still uncertain what effect three-dimensional flow has on Sarpkaya's values for C_F.

2.4.3 Total force coefficient C_{F*}

The total force coefficient, C_F, tends towards very high values at low k_c, so that small errors in the k_c number might tend to large errors in C_F. Therefore a new coefficient, C_{F*}, was proposed, that approximates the inertia coefficient, C_M, at low k_c values, and approximates C_F at high k_c values (note that C_F in turn approximates C_D at high k_c, so that C_{F*} also approximates C_D). C_{F*} is defined as

$$C_{F*} = \frac{f_{max}}{\frac{1}{2}\rho D \{u^2 + \frac{\pi D}{2}\dot{u}\}}$$

where u and $\dot{u}$ = the velocity and acceleration values corresponding to f_{max}

A root mean square value of C_{F*} was used by Bishop (1980) to analyse field test results from the NMI test rig at Christchurch Bay. Thus,

$$(C_{F*})_{RMS} = \left[\frac{\overline{(f_{max}^2)}}{(\frac{1}{2}\rho D)^2\{u^4 + (\frac{\pi D}{2})^2 \dot{u}^2\}}\right]^{\frac{1}{2}}$$

which is plotted against a k_c number in Fig. 2.44 (from Bishop, 1980).

In this figure, each ringed area represents 24 measurements during a 20 minute run. Note that run 3 consisted of small waves and a strong tidal current. The average C_{F*} values are compared to other data in Fig. 2.45 (from Standing, 1984). These values agree well with each other.

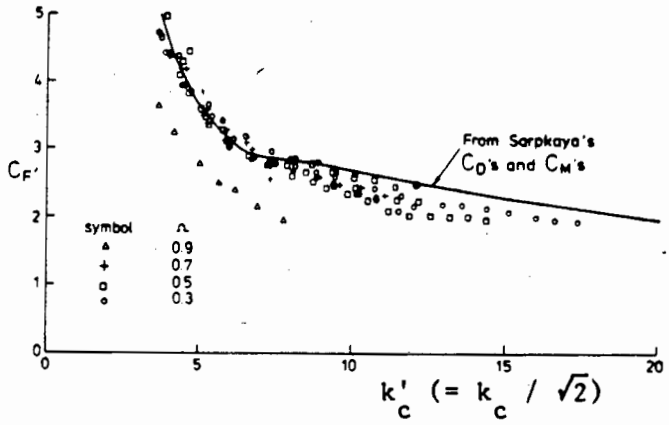

Figure 2.43 : C_F versus k_c for various Ω

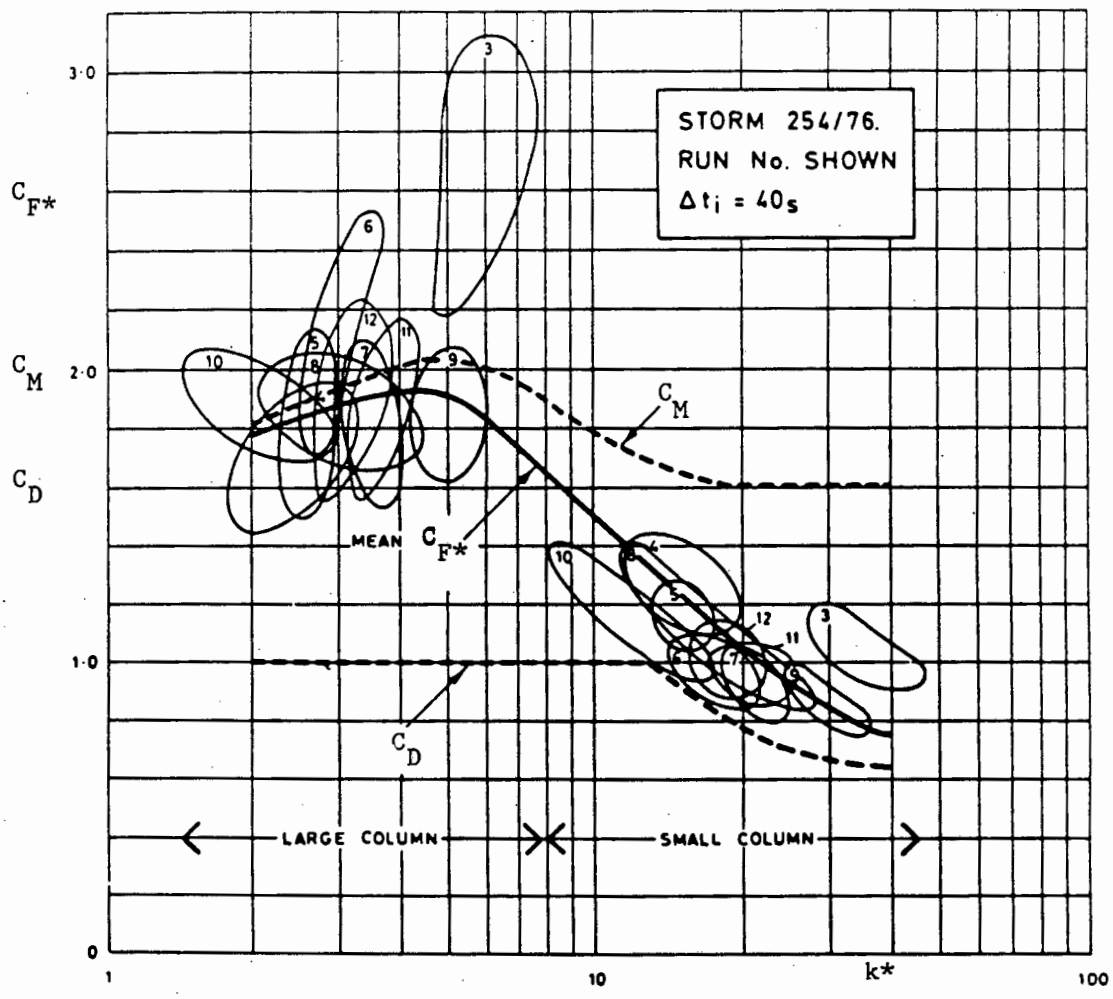

Figure 2.44 : C_F* versus k* from field test.

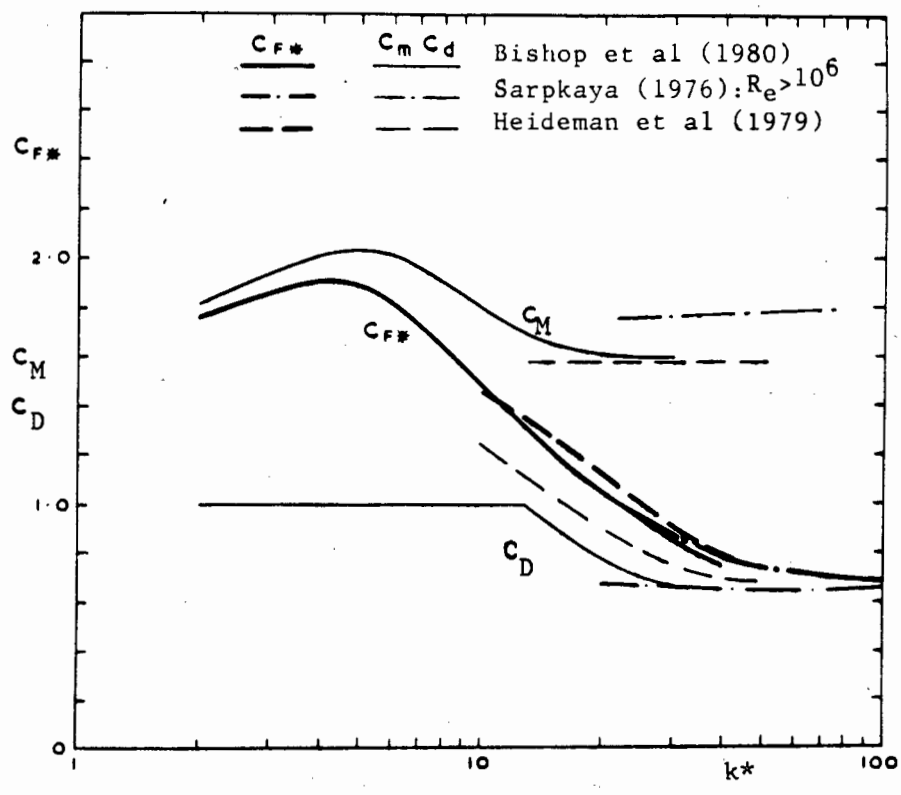

Figure 2.45 : Comparison of C_F*, C_M and C_D from three different authors, including two field tests.

CHAPTER 3

DIFFRACTION THEORY

If a pile is small in relation to the wave length then the largest force exerted on it is the drag force. As the pile diameter increases (in relation to the wave length) the inertia force becomes predominant. Finally, when the diameter becomes a significant proportion of the wavelength (D/L > 0,2) then forces due to the diffraction and reflection of the incident wave are important. In this case the drag force is negligible.

The diffraction theory assumes that the water is non-viscous and the motion irrotational and the flow can therefore be described by a velocity potential. Superimposed on the incident potential is the potential due to the scattered (reflected and diffracted) wave such that

$$\phi = \phi_i + \phi_s \qquad (3.1)$$

where ϕ = velocity potential
ϕ_i = incident velocity potential
ϕ_s = scattered velocity potential

The pressure around the pile can be calculated from the velocity potential, and thus the force.

3.1 Linear Diffraction Theory

The linear diffraction theory (MacCamy and Fuchs, 1954) assumes, in addition to a frictionless fluid and irrotational motion, that the wave heights are small in relation to their lengths and thus can be defined by linear theory. In this case, the incident potential, ϕ_i, is given by the real part of

$$\phi_i = -\frac{gH}{2\sigma} \frac{\cosh k(d+z)}{\cosh kd} e^{i(kx - \sigma t)} \qquad (3.2)$$

where $\sigma = \frac{2\pi}{T}$

$k = \frac{2\pi}{L}$

d = water depth

and the Z-axis is directed positively upward from the still water level.

Using cylindrical co-ordinates (r, θ, z), and substituting for e^{ikx}, equation (3.2) may be written as

$$\phi = \frac{gH}{2\sigma} \frac{\cosh k\,(d+z)}{\cosh kd} \left[J_o\,(k \tfrac{D}{2}) - \sum_{m=1}^{\infty} 21^m \cos m\theta\, J_m\,(k \tfrac{D}{2}) \right] e^{i\sigma t} \qquad (3.3)$$

where $J_m\,(k \frac{D}{2})$ is a Bessel function of the first kind of the mth order and with argument $(k \frac{D}{2})$. Definitions of Bessel functions are given in Appendix A.

It is assumed that the potential of the scattered wave is given by

$$\left(\phi_s\right)_m = A_m \cos m\theta \left[J_m\,(k \tfrac{D}{2}) + Y_m\,(k \tfrac{D}{2}) \right] e^{i\sigma t} \qquad (3.4)$$

where $Y_m\,(k \frac{D}{2})$ is a Bessel function of the second kind.

The total velocity potential is given by the superposition of ϕ_i and ϕ_s. The coefficients A_m are determined by setting the water particle velocity normal to the cylinder equal to zero at the cylinder wall, i.e. $\frac{d\phi}{dr} = 0$ at $r = \frac{D}{2}$, which gives

$$\phi = \frac{gH}{2\sigma} e^{i\sigma t} \frac{\cosh k(d+z)}{\cosh kd} \left[J_o\,(k \tfrac{D}{2}) - \frac{J_o'\,(k \frac{D}{2})}{H_o^{(2)\prime}(k \frac{D}{2})} \right.$$

$$\left. + 2 \sum_{m=1}^{\infty} (i)^m \left(J_m\,(k \tfrac{D}{2}) - \frac{J_o\,(k \frac{D}{2})}{H_m^{(2)\prime}(k \frac{D}{2})} H_m^{(2)}(k \tfrac{D}{2}) \right) \cos m\theta \right] \qquad (3.5)$$

where $H_m^{(2)}( )$ is a Hankel function of the second kind, and primes denote derivatives with respect to the argument.

The pressure is now computed by using Bernoulli's equation,

$$P = \rho \frac{\partial \phi}{\partial t} - g\rho z \tag{3.6}$$

where all the squared and higher-order terms have been neglected.

The pressure may then be integrated around the cylinder to get the force at a depth z, so that

$$f = \frac{2 \rho g H}{k} \frac{\cosh k (d+z)}{\cosh kd} A (k \tfrac{D}{2}) \cos (\sigma t - \alpha) \tag{3.7}$$

$$\text{where } A (k \tfrac{D}{2}) = \frac{1}{\sqrt{\{J_1' (k\tfrac{D}{2})\}^2 + \{Y_1' (k\tfrac{D}{2})\}^2}}$$

$$\text{and } \tan \alpha = \frac{J_1' (k\tfrac{D}{2})}{Y_1' (k\tfrac{D}{2})}$$

A moment may be calculated from this force, and thus the special case for the moment on a pile hinged at the seabed is given by

$$M = \frac{2 g \rho J}{k^3} A (k\tfrac{D}{2}) \frac{(- k d \sinh dk + \cosh dk - 1)}{\cosh kd} \cos (\sigma t - \alpha) \tag{3.8}$$

Note that this moment is only evaluated up to the still water level. This is possibly due to the assumption of small wave heights. However, if greater accuracy is required, the integration can be continued to the water surface.

The linear diffraction theory has proved to be accurate. Fig. 3.1 (Chakrabati, 1972) shows experimental data measured at the crest and at the trough of a wave cycle compared to the theoretical values. The agreement is very good. Experiments have also been performed on models of large structures such as gravity oil rigs. Fig. 3.2 (Skjelbreia, 1979) shows the pressure at

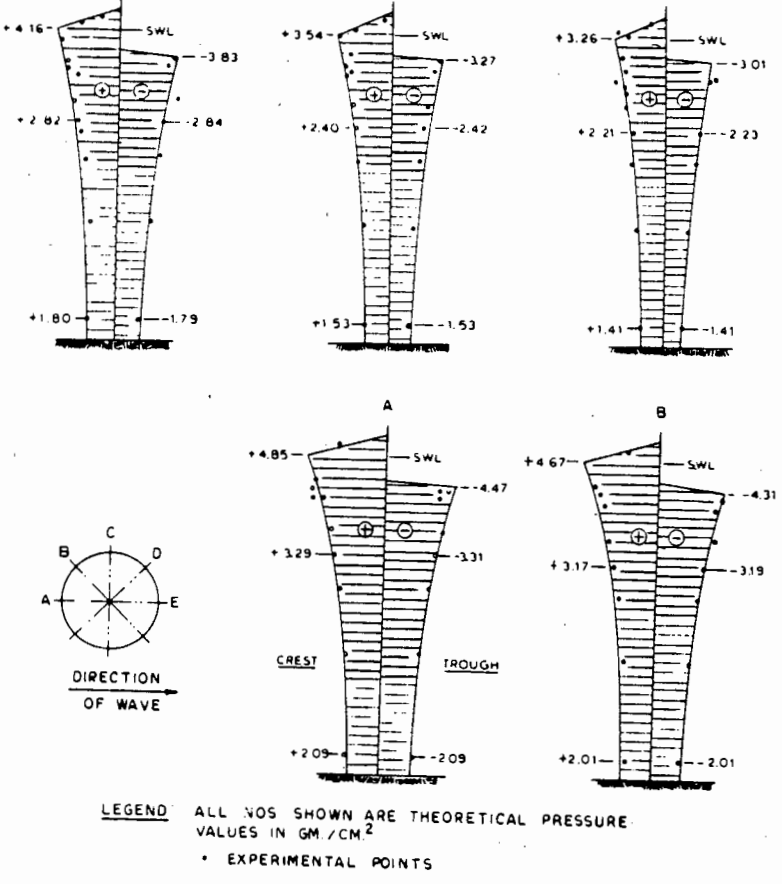

Figure 3.1 : Maximum and minimum pressures on a cylinder predicted by diffraction theory compared with measured values.

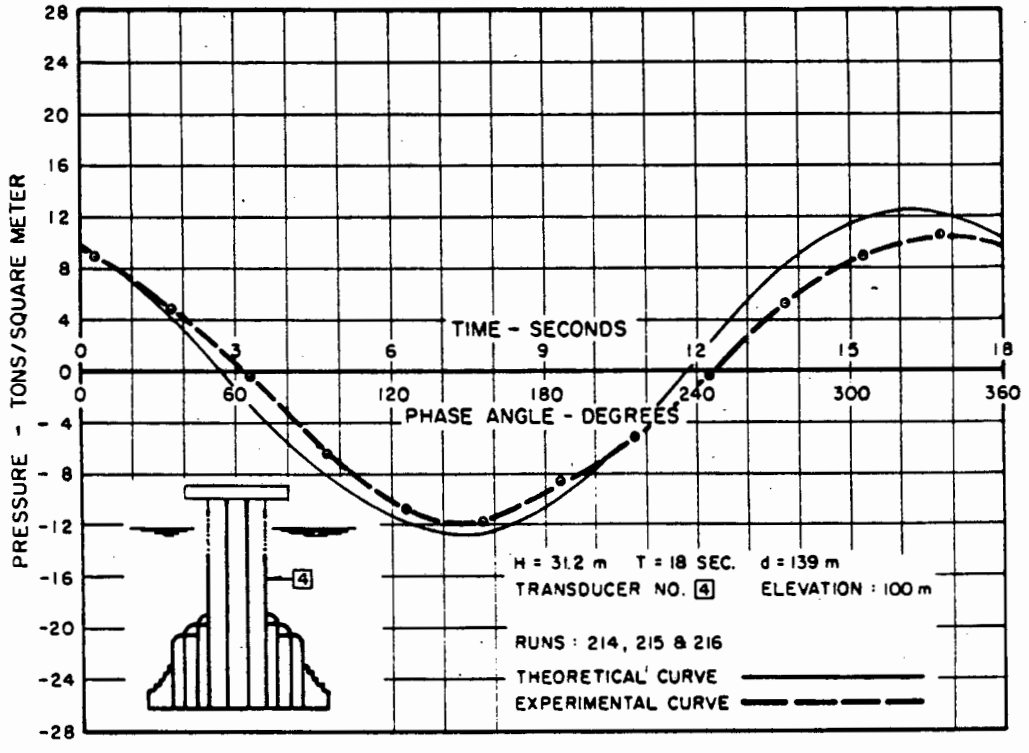

Figure 3.2 : Wave pressure on cylinder as a function of phase angle.

a point on a circular horizontal section of a gravity platform. There are significant differences between the theoretical and experimental pressures.These are probably caused by non-linearities in the wave: the maximum positive pressure is 100 kPa, and the maximum negative pressure is 120 kPa. H/L is approximately 0,10. A plot of the total horizontal force on the cylindrical section of the structure for a smaller wave (H/L ≈ 0,054) presented in Fig.3.3 (Skjelbreia, 1979) shows much closer agreement with the theoretical force.

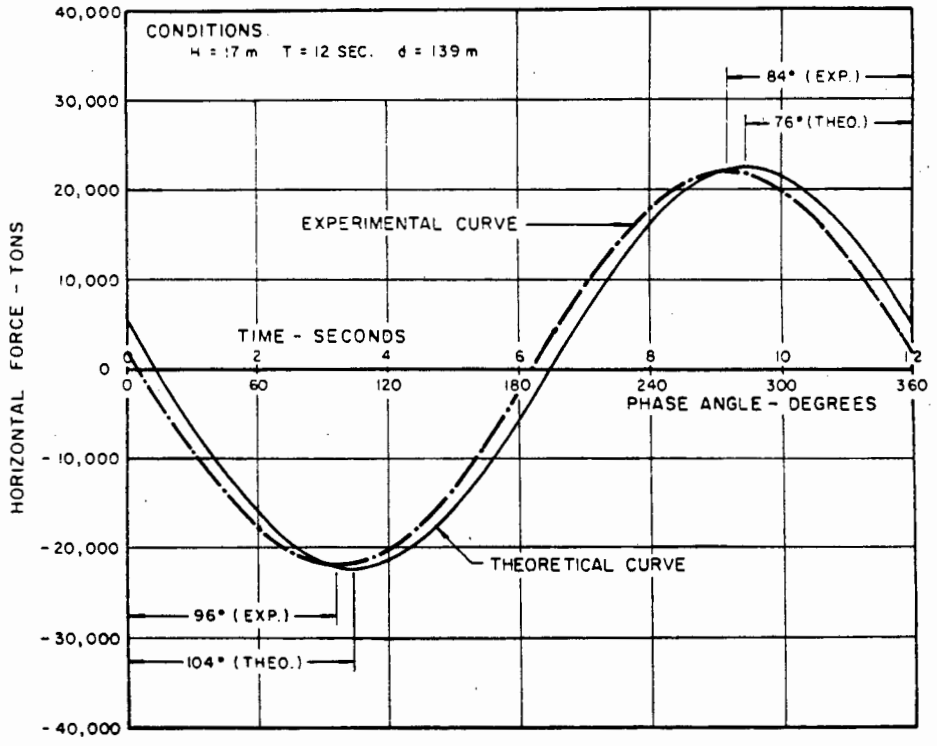

Figure 3.3 : Comparison of theoretical and experimental horizontal force as a function of phase angle.

3.2 Non-linear diffraction theory

The linear diffraction theory has proved to be a very accurate method of predicting forces on large diameter cylinders. Unfortunately this accuracy diminishes as the waves become non-linear. Several researchers (Chakrabati, 1972 and 1975, Roman and Venkatanarasaiah, 1976, among others) tried to adapt MacCamy and Fuchs' linear theory to non-linear waves, but they failed to create a mathematically rigorous theory.

A diffraction theory based on Stokes second order wave theory was eventually derived for deep water by Hunt and Baddour (1981). They found that

$$F = \epsilon F^{(1)} + \epsilon^2 F^{(2)} \tag{3.9}$$

where ϵ = the Stokes expansion parameter

F = the total force in the x-direction

$\epsilon F^{(1)}$ = the force component due to the first-order terms

$\epsilon F^{(2)}$ = the force component due to the second-order terms.

$\epsilon F^{(1)}$ represents the deep water linear force, which can be found using MacCamy and Fuchs' linear diffraction theory.

$\epsilon^2 F^{(2)}$ is made up of two parts - a steady force in the direction of wave propagation and an oscillatory force, such that,

$$\epsilon^2 F^{(2)} = \epsilon^2 \bar{F}^{(2)} + \epsilon^2 \tilde{F}^{(2)} \tag{3.10}$$

where $\bar{F}^{(2)}$ represents the steady second-order force

and $\tilde{F}^{(2)}$ represents the oscillatory second-order force and both $\bar{F}^{(2)}$ and $\tilde{F}^{(2)}$ can be found in terms of $F^{(1)}$.

The first term in eqn. (3.10), $\epsilon^2 \bar{F}^{(2)}$, is given by

$$\epsilon^2 \bar{F}^{(2)} = C_s \left(\max |\epsilon F^{(1)}|\right) \tag{3.11}$$

where C_s = a calculated, not an experimental, coefficient, shown in Fig. 3.4 (Hunt and Baddour, 1982)

The second term in eqn. (3.10), $\epsilon^2 \tilde{F}^{(2)}$, is given by

$$\epsilon^2 \tilde{F}^{(2)} = \max |\epsilon^2 \tilde{F}^{(2)}| \cos (2\sigma t + \delta) \tag{3.12}$$

where values of δ are shown in Table 3.1 (Hunt and Baddour, 1982)

Incident wave number-cylinder radius parameter, kD/2	Phase Angle
	Second order δ
0.0	−1.5708
0.5	−1.3742
1.0	−0.9254
1.5	−0.2579
2.0	+0.4952
2.5	1.4648
3.0	2.3588
3.5	3.2739
4.0	4.2931

Table 3.1 : Values of phase angle δ in radians.

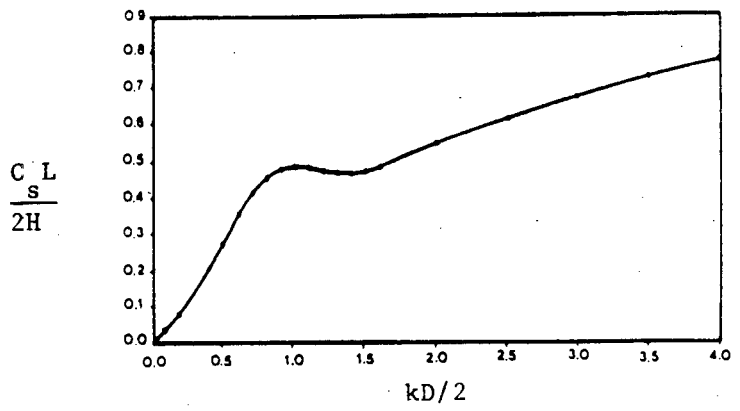

Figure 3.4 : Steady second-order force parameter, $C_s L/2H$ against kD/2

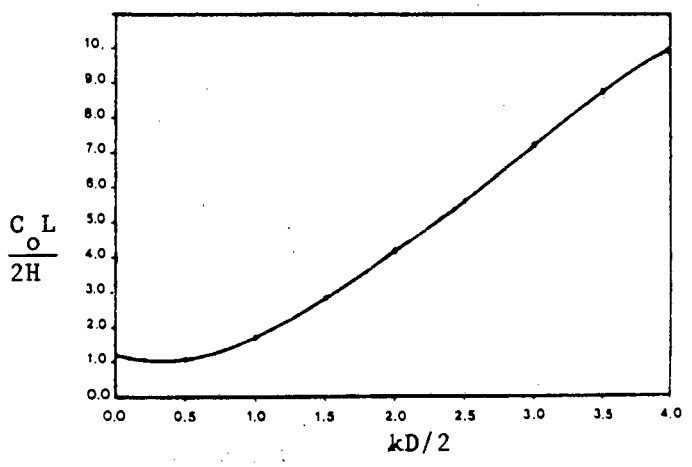

Figure 3.5 : Oscillatory second-order force parameter, $C_o L/2H$ against kD/2

and

$$\max |\epsilon^2 \tilde{F}^{(2)}| = C_o (\max |\epsilon F^{(1)}|) \qquad (3.13)$$

where C_o = a calculated, not an experimental, coefficient shown in Fig. 3.5 (Hunt and Baddour, 1982)

A detailed derivation of the above formulae may be found in Hunt and Baddour (1981).

The second order force may have a significant effect on the total force. For example, assuming $D \approx \frac{1}{3} L$ and $\frac{H}{L} \approx 0,1$ then the maximum force is increased by 12% compared with linear theory. As the wavelength decreases, the percentage increase in maximum force decreases, so that when the cylinder diameter equals the wavelength, the increase in maximum force is only 7%,

Note from Figs. 3.4 and 3.5 that the oscillatory second order force can be far bigger than the steady force. Therefore the maximum force in the direction contrary to the direction of wave propagation will be increased compared with linear theory. Furthermore, due to the phase shift between the first and second order forces, it will also be larger than the maximum force in the direction of wave propagation.

3.3 Extensions of diffraction theory

The diffraction theory has been extended to several other specific areas. Garrison and Chow (1972) extended it to non-circular underwater bodies, and Isaacson (1977) to shallow water using cnoidal wave theory.

3.3.1 Diffraction theory with shallow water cnoidal waves

Although MacCamy and Fuchs' linear theory is valid for shallow water as long as the waves remain linear (i.e. small wave heights compared to wave lengths), Isaacson (1977) developed a shallow water diffraction theory for cnoidal waves. He summarised the theory by plotting the ratio for the maximum force predicted using cnoidal theory to the maximum force predicted by linear theory, i.e. $R = \frac{F_{cnoidal}}{F_{linear}}$ in Fig. 3.6 (Isaacson, 1977).

Due to the assumptions made in this theory, it may only be used in shallow water.

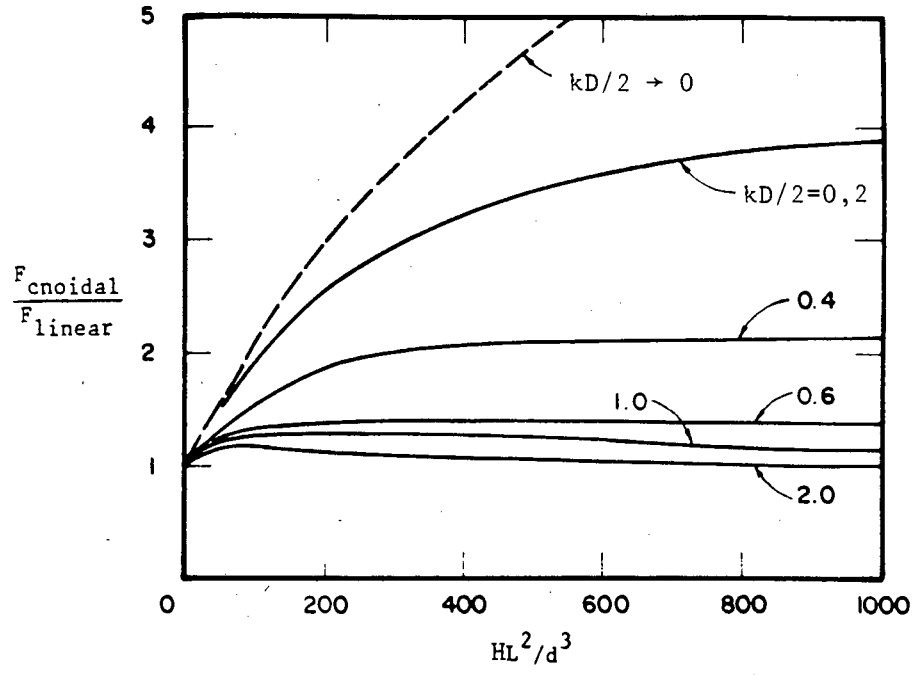

Figure 3.6 : Ratio of cnoidal to sinusoidal wave theory predictions for the maximum force on a vertical circular cylinder.

CHAPTER 4

TRANSVERSE FORCES ON A PILE

The transverse, or lift, force on a pile is that force which acts perpendicular to the direction of wave propagation, i.e. it acts at 90° to the in-line force. It is usually defined in the same manner as the drag force, i.e.

$$f_L = \frac{1}{2} C_L \rho D u^2 \qquad (4.1)$$

However, because the transverse force is somewhat irregular, both in period and in magnitude and because some residual vorticity often remains when $u \simeq 0$, the value of C_L may become very large. Therefore, several other definitions of C_L are used.

$$C_{L(max)} = \frac{\text{Maximum peak of the transverse force per unit length}}{0,5 \rho D u^2} \qquad (4.2)$$

$$C_{L(SPP)} = \frac{\text{Semi peak-to-peak value of the transverse force per unit length}}{0,5 \rho D u^2} \qquad (4.3)$$

$$C_{L(RMS)} = \frac{\text{rms value of the transverse force per unit length}}{0,5 \rho D u^2} \qquad (4.4)$$

The transverse force is caused by vortex action around a pile. In general, as a vortex is shed from one side of a pile, it causes a high local velocity and a low pressure, and thus a net force towards the shedding vortex. However, due to the inherent variability of vortex shedding, not only does the frequency of the transverse force vary, but also its magnitude. Fig. 4.1 (Chakrabati et al, 1976) shows a typical force trace for several cycles. The variability is noticeable.

Since different vortex patterns may form as the crest or trough of a wave passes, different lift forces may also result. This may lead to a situation where the net transverse force is non-zero, i.e. the average force is to one side of the pile. An example of this is given in Fig. 4.2 (Sarpkaya and Wilson, 1984). This shows that the force to one side of the pile is much greater than the force to the other side.

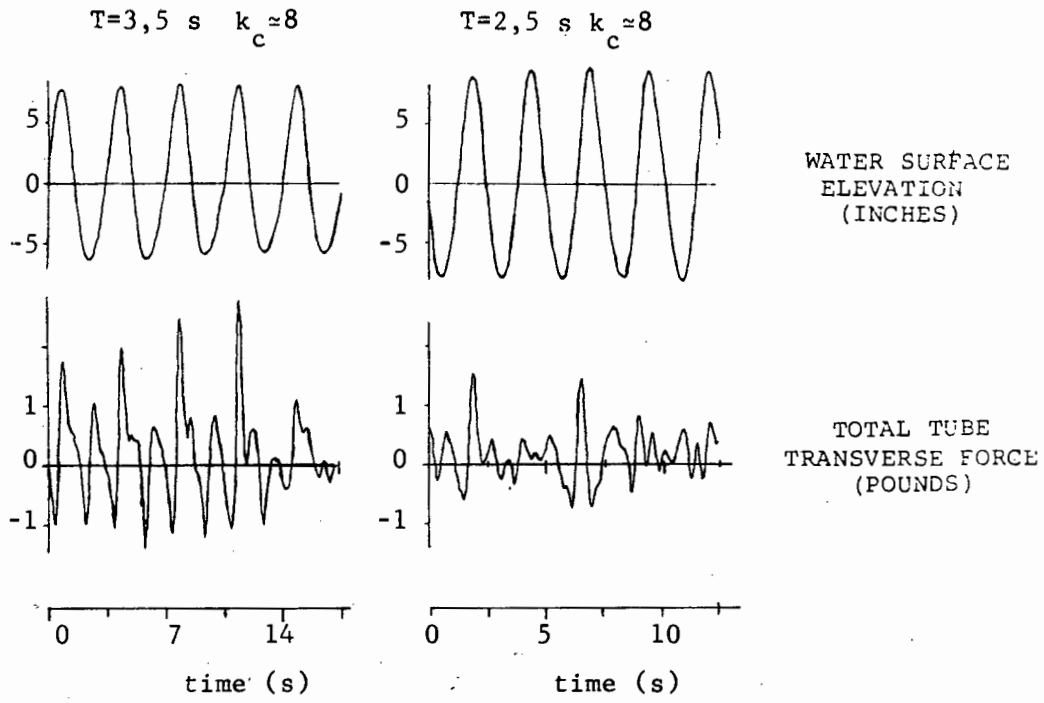

Figure 4.1 : Variability of transverse force.

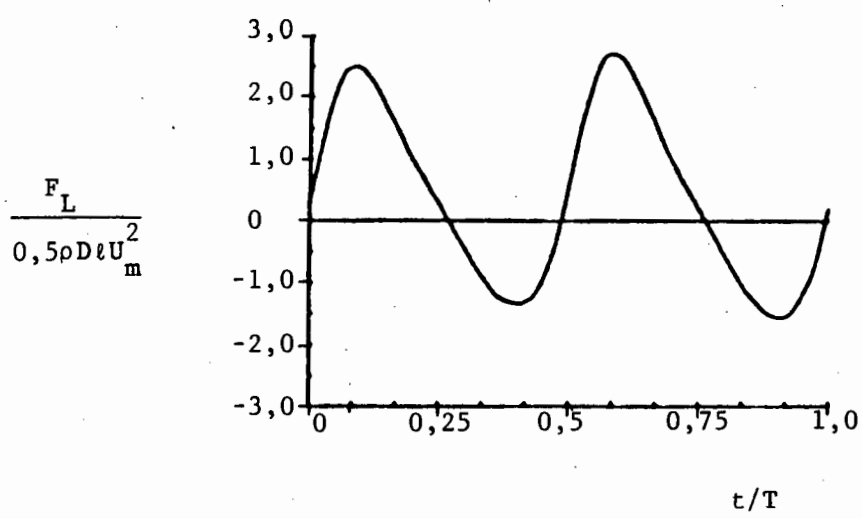

Figure 4.2 : An example of an asymmetrical transverse force $k_c = 12$

4.1 Parameters governing C_L

By using dimensional analysis, Isaacson (1976A), found that C_L was dependent on the Reynolds number, the Keulegan-Carpenter number, a depth parameter (kd) and a wave-steepness parameter (kH), i.e.

$$C_L = f(R_e, k_c, kd, kH) \tag{4.5}$$

However, Isaacson found that the wave steepness parameter (kH) had an insignificant effect on C_L, and therefore

$$C_L = f(R_e, k_c\ kd) \tag{4.6}$$

4.2 The magnitude of the transverse force

The magnitude of the transverse force can be a significant proportion of the total force on a pile, and may rival, or even exceed, the magnitude of the in-line force. Fig. 4.3 (Chakrabati et al, 1976) shows the resultant

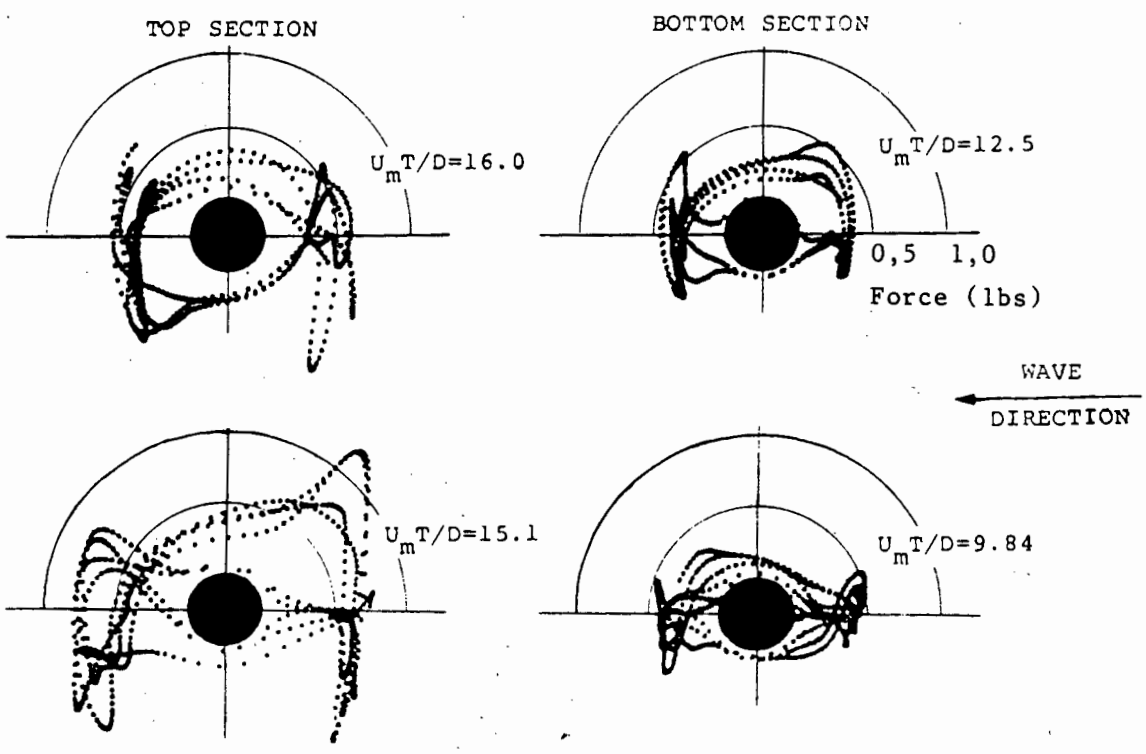

Figure 4.3 : Continuous plots of resultant measured force composed of in-line (inertia plus drag) and transverse forces for corresponding runs presented in figure 4.11

measured force on a pile for k_c = 15,1, where the transverse force is of the same magnitude as the in-line force.

4.2.1 The magnitude of C_L

4.2.1.1 C_L at low Reynolds number

Several authors (Bidde (1971), Chakrabati et al (1976), Isaacson (1976A) and Stansby et al (1983)) have examined the transverse force experimentally in wave flumes. Bidde found that the maximum lift force was 60% of the in-line force for $8 < k_c < 18$.

Both Isaacson (1976A) and Stansby et al measured $C_{L(RMS)}$ and plotted it against k_c and kd at low Reynolds number. Their results were almost identical, and are shown in Fig. 4.4 (Stansby, 1983 and Isaacson, 1976). C_L increases with increasing kd until kd reaches approximately 0,6 and then

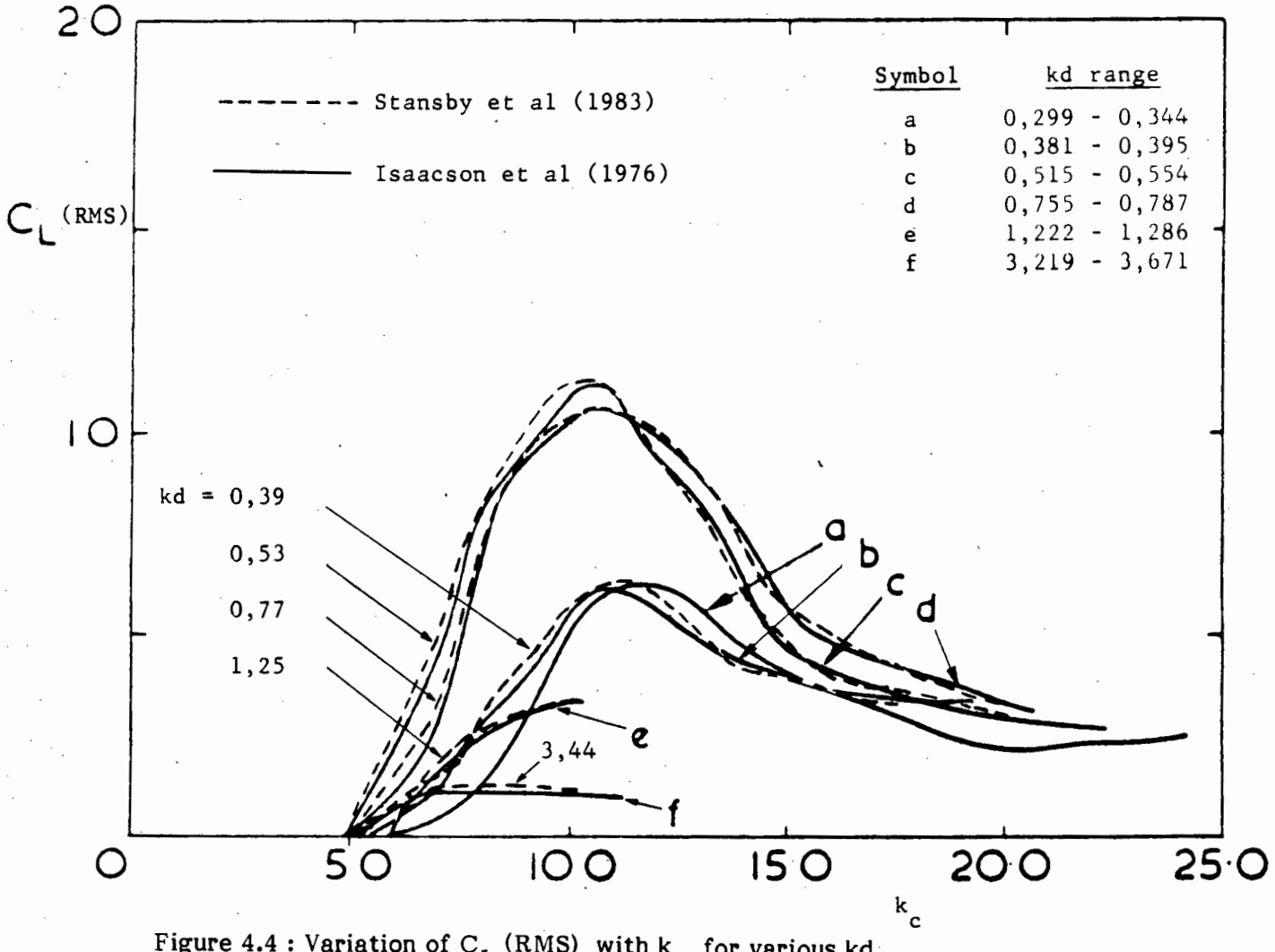

Figure 4.4 : Variation of C_L (RMS) with k_c for various kd.

decreases. (However, from the data it is also possible that kd indicates a step function, i.e. that C_L has one value for kd < 0,4 and another for 0,5 < kd < 1,0, and reduces thereafter). A typical plot of the data to show the amount of scatter is shown in Fig. 4.5 (Isaacson, 1976A), which also shows a relationship between $C_{L(RMS)}$ and $C_{L(SPP)}$. $C_{L(SPP)}$ is, very approximately, double $C_{L(RMS)}$.

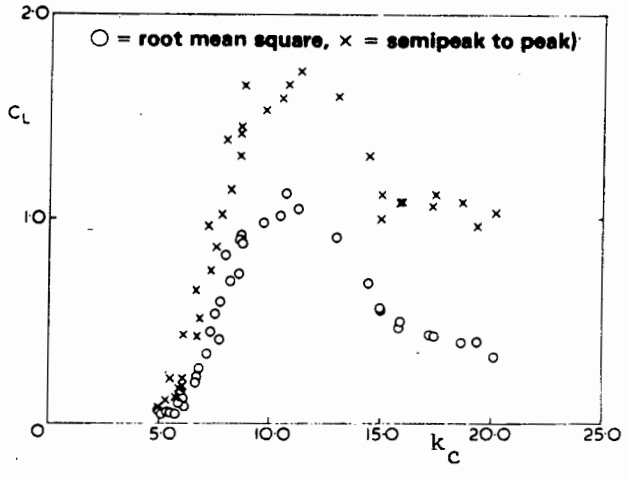

Figure 4.5 : Variation of lift coefficient with k_c for kd from 0.755-0.787

4.2.1.2 C_L at high Reynolds number

Sarpkaya (1976A) used a large U-tube to produce two-dimensional sinusoidal flow past a pile, i.e. flow with no velocity component parallel to the z-axis. Thus he approximated very shallow water conditions with both d, and thus kd, very close to zero. However, he was able to achieve very high Reynolds numbers. His results are shown (for $C_{L(max)}$) as a function of k_c, with Re and β as parameters in Fig. 4.6 (Sarpkaya, 1976A)), where $\beta = \frac{Re}{k_c}$. In Fig. 4.7 (Sarpkaya, 1976A), $C_{L(max)}$ is shown as a function of R_e with k_c as the parameter. Typical scatter is shown in Fig. 4.8 (Sarpkaya, 1976). Note that at high Reynolds numbers C_L is much smaller ($C_{L(max)} \lesssim 0,4$), but this still represents a significant force. At low Reynolds numbers, and especially at $k_c \approx 12$, $C_{L(max)}$ approaches 4,0. Isaacson and Stansby also found that the maximum of $C_{L(RMS)}$ occurred near $k_c = 12$.

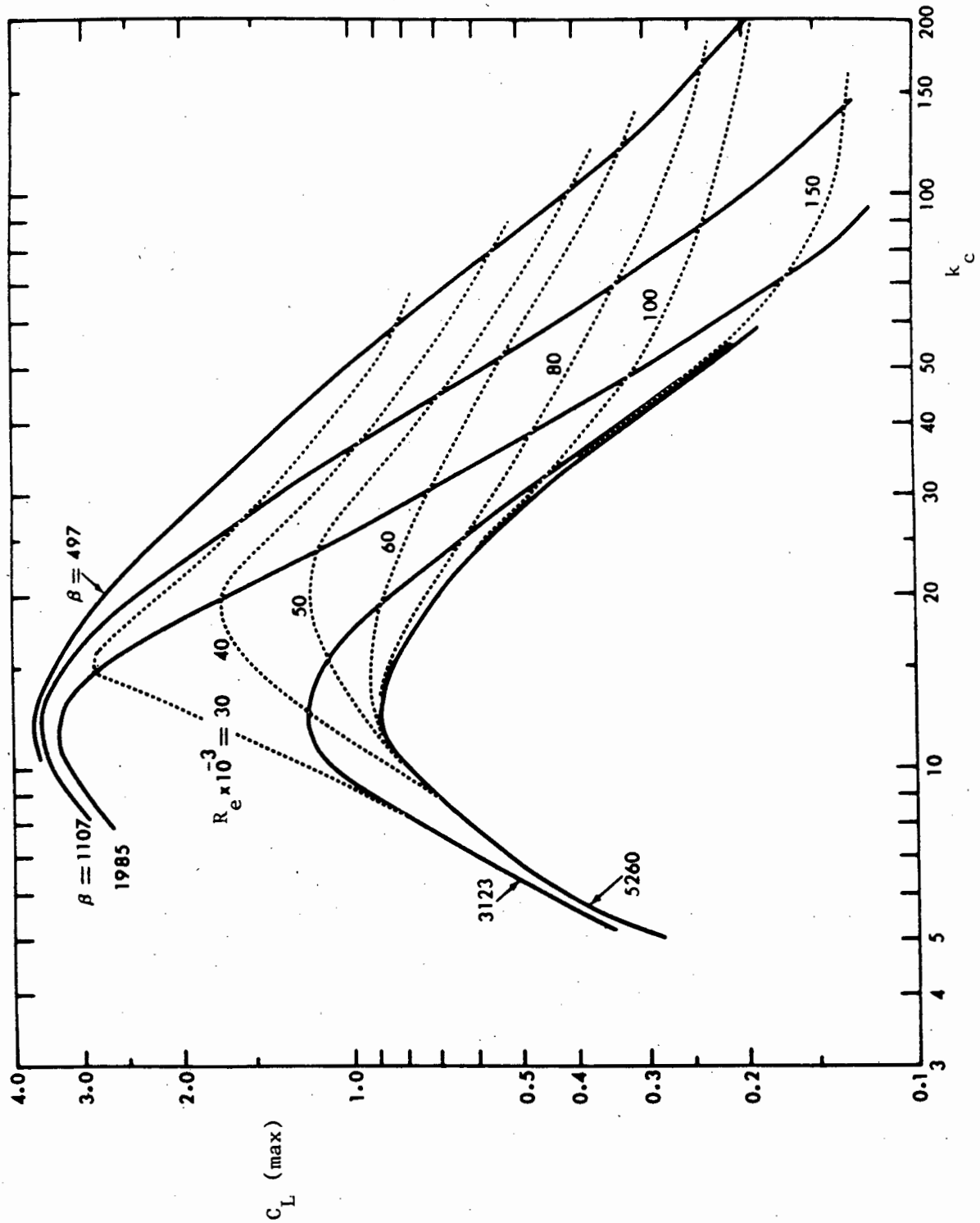

Figure 4.6 : C_L (max) versus k_c for various values of R_e and β

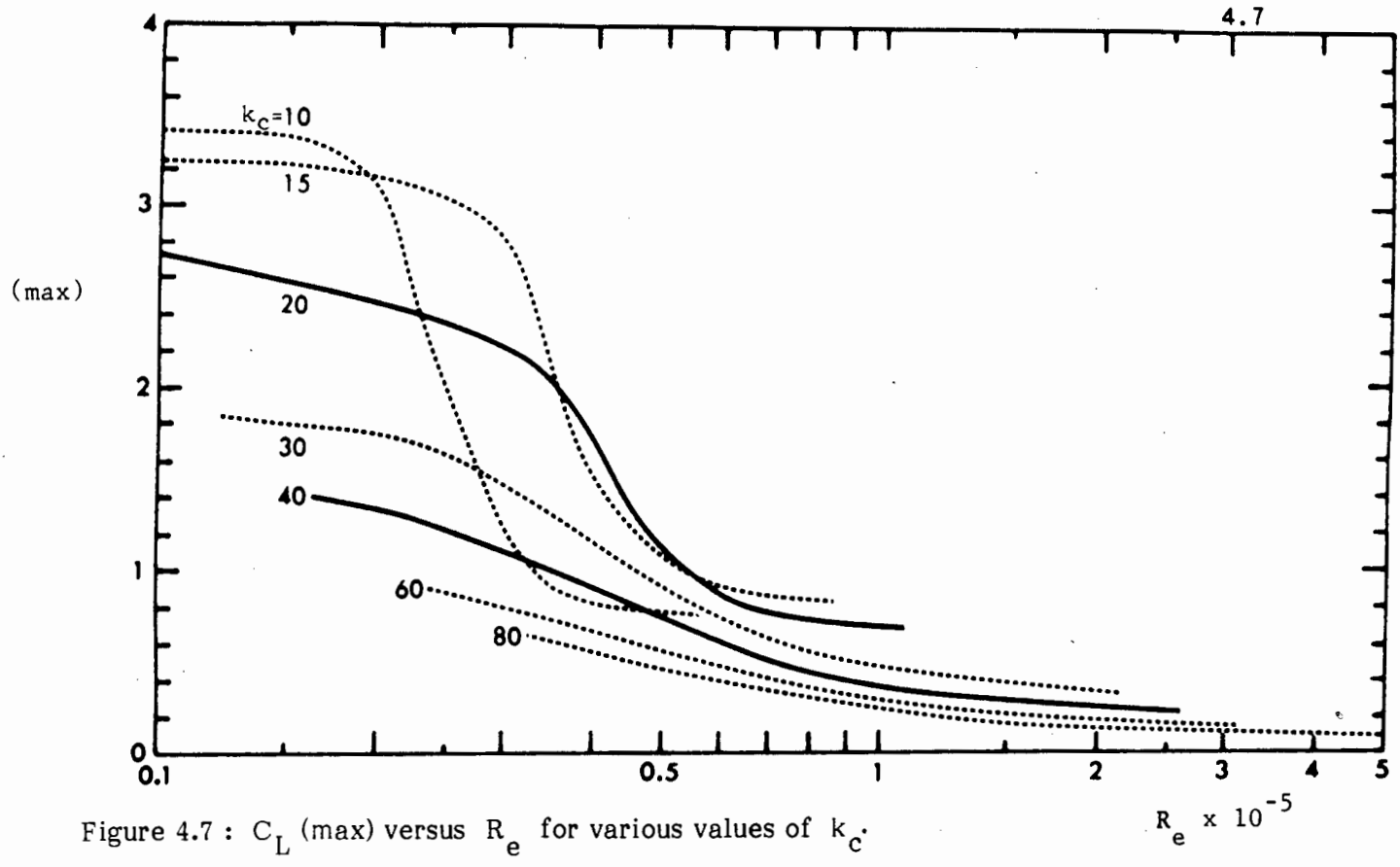

Figure 4.7 : C_L (max) versus R_e for various values of k_c.

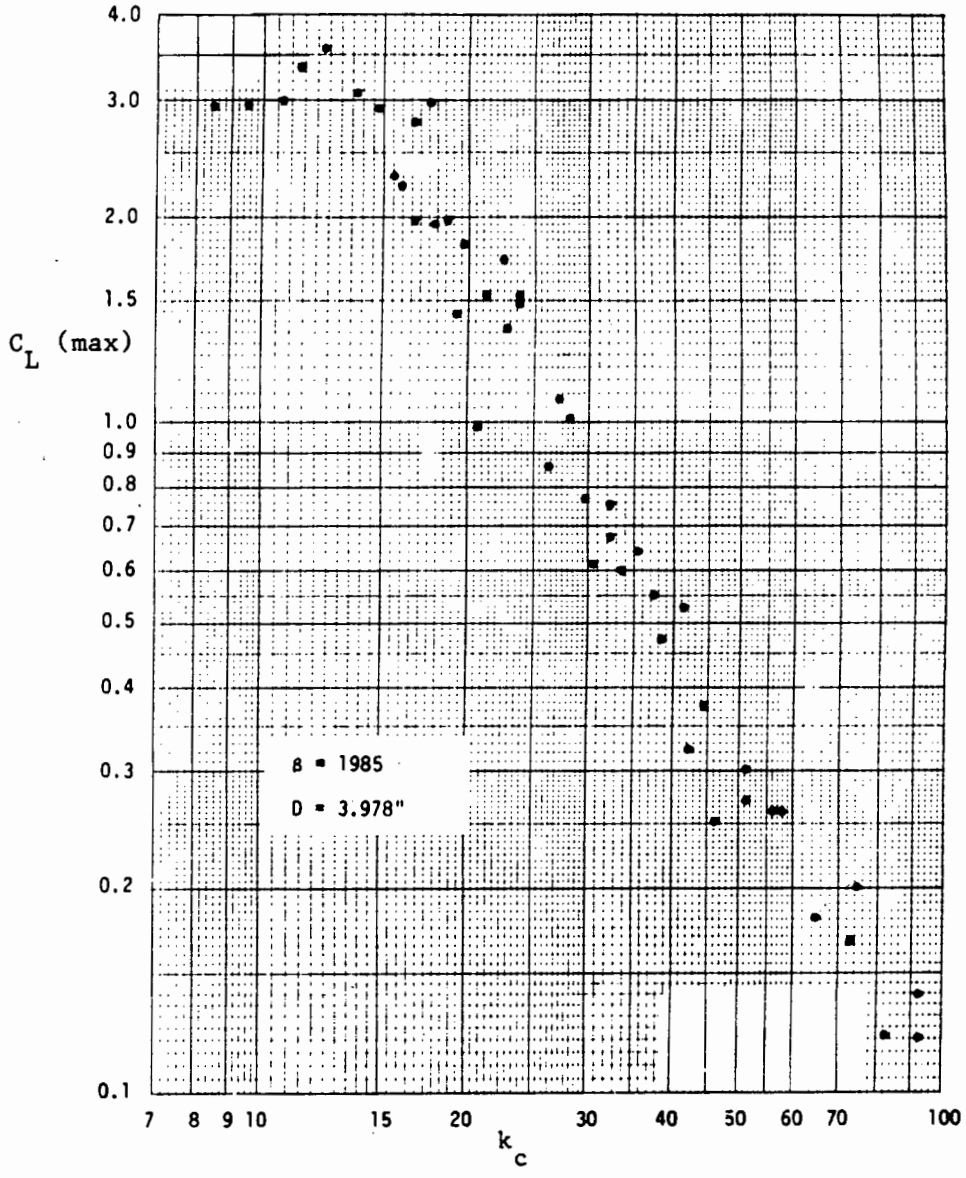

Figure 4.8 : C_L (max) versus k_c for $\beta = 1985$

Since Sarpkaya's results are limited to shallow water, it is difficult to predict C_L at high Reynolds number in deep or intermediate water. Isaacson's results indicate that kd becomes less important as a parameter when $k_c > 20$. If kd does, indeed, represent a step function, then Sarpkaya's data can be compared with kd < 0,4, but this has not been proven. Finally, Sarpkaya's data show $C_{L(max)} \approx 3,5$ at $\beta = 497$, $k_c = 12$, $R_e = 6 \times 10^3$, kd small, and the corresponding value from Stansby and Isaacson is $C_{L(RMS)} \approx 0,7$ for kd ≈ 0,3. Isaacson's maximum value of $C_{L(SPP)}$ is less than 2,0 (kd ≈ 0,77, Fig. 4.5). It is difficult to make further comparisons due to the incompatibility of the Reynolds numbers in each figure.

4.2.2 Field tests of the transverse force

Very few authors have been interested in measuring transverse forces in the field. However, Fig. 4.9 (Pearcey, 1979) shows a plot of the force vector,

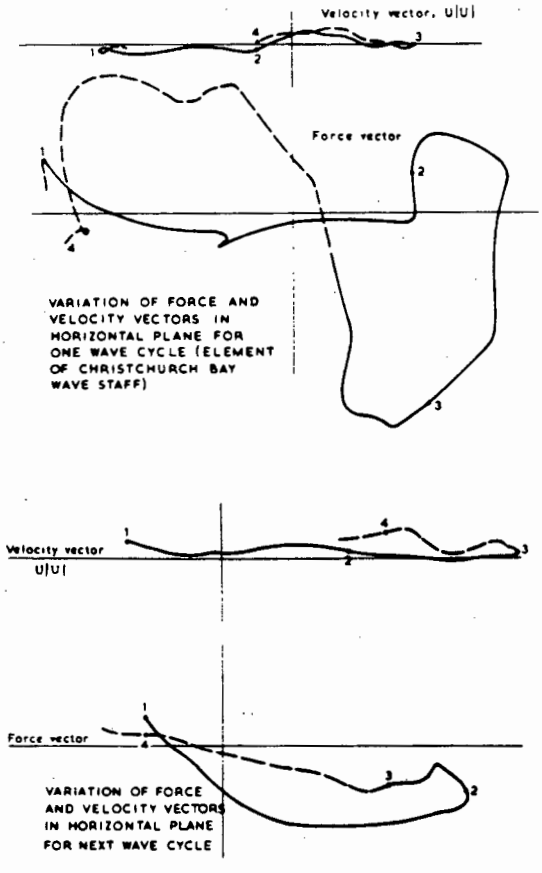

Figure 4.9 : Variation of force and velocity vectors for two consecutive wave cycles.

which reveals how important the lift force can be. A plot of the force vector for the next wave cycle also shows how irregular the lift force can be.

4.3 Frequency of the transverse force

The frequency of the transverse force is very heavily influenced by the frequency of vortex shedding. It is also susceptible to any vibration or resonance of the pile. Fig. 1.6 (page 1.8) shows the frequency of the transverse force per wave cycle as a function of R_e and k_c. This is for two-dimensional flow, but Iwagaki and Ishida (1976) agree with it for three-dimensional flow at low Reynolds number (Fig. 4.10, Iwagaki and Ishida, 1976). Note that both figures are approximate: the irregular nature of the transverse force means that occasionally a frequency (N + 1) will appear on the (N - 1) side of an f_t = N line, or vice versa.

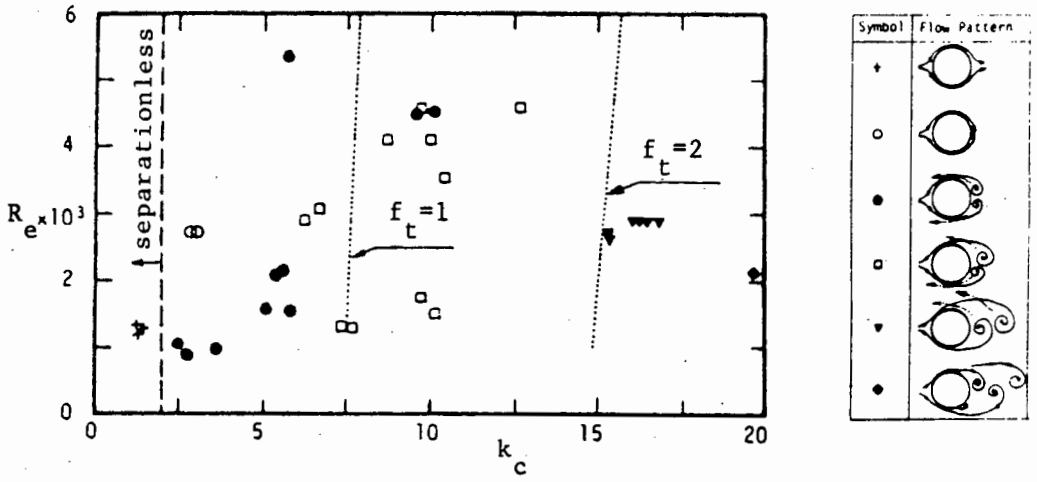

Figure 4.10 : Variation of vortex pattern and transverse force frequency with Keulegan-Carpenter number and Reynolds number.

4.3.1 Spanwise correlation of the transverse force

It can be seen from Figs. 1.6 and 4.10 that the frequency of the transverse force is a function of the Keulegan-Carpenter number, and therefore of depth. Therefore, although the presence of vortices, and any resonance or vibration of the pile, will tend to reduce this dependency, the frequency of

the transverse force can change along a pile. Chakrabati et al (1976) measured these frequencies at different horizontal sections of a pile and found that they varied (see Fig. 4.11, from Chakrabati et al, 1976). Thus the maximum lift force may well vary in phase as well as magnitude along the pile, which will reduce the maximum lift force.

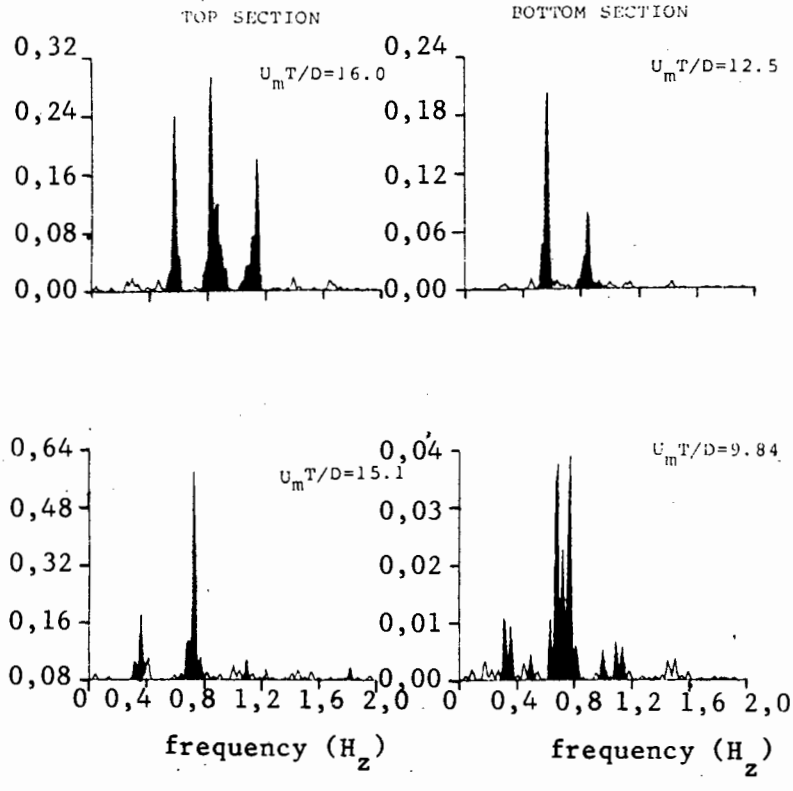

Figure 4.11 : Plots of lift force (half-amplitude squared) spectrum obtained by FFT technique for top and bottom sections for corresponding runs presented in figure 4.3

4.4 Vortex theory prediction of the transverse force

Since transverse forces are caused by vortices, it seems logical that vortex theory should be able to accurately predict them. Unfortunately, vortex theory has not yet progressed to the state where it can do this. Stansby (1977) attempted to do this, and his results are presented in Table 4.1 (Stansby, 1977). The vortex theory gives a reasonable value of C_L for k_c = 15, but gives poor results for other k_c values.

k_c	model	Experiment (Sarpkaya)	
	C_L (rms)	C_L (rms)	$R_e \times 10^{-4}$
15	0·68	0·64	8·0
20	0·50	0·33	10·1
25	0·45	0·23	13·6
30	0·46	0·16	16·4

Table 4.1 : Vortex model predictions of C_L compared with experimental results.

CHAPTER 5

CONCLUSIONS TO SECTION I: FORCES ON A SINGLE PILE

5.1 The dividing line between diffraction theory and the Morison equation is $D/L > 0,2$ for the diffraction theory to be valid and $D/L < 0,2$ for the Morison equation to be valid.

5.2 The Morison equation should be used to predict forces throughout a wave cycle (for $D/L < 0,2$) even for the region $8 < k_c < 20$ where it is inaccurate. No other method of force prediction has been proven more accurate under such a wide range of conditions.

5.3 The values of the coefficients C_M and C_D should be those given by Sarpkaya (Figs. 2.6 - 2.9) since two-dimensional flow and three-dimensional flow comparisons have only been performed at low Reynolds number, and Sarpkaya's are higher and therefore more conservative.

5.4 Although Sarpkaya's coefficients will give good average results, individual wave cycles may cause much larger or smaller forces than predicted. While most forces should fall within 25% of their predicted value, a 50% margin could be expected to account for almost all scatter. This does not take into account differences in force due to other sources such as currents, or marine growth, etc.

5.5 The total force coefficient C_{F*} has proved to be repeatable and is a good indication of the maximum force in a wave cycle. It is of the same order of accuracy as the Morison equation, i.e. most scatter would fall within 25% of the predicted force, and a margin of error of 50% should cover almost all forces. Again, this does not take into account forces due to other sources.

5.6 Other methods of force prediction either do not have a sufficient body of experimental evidence to ensure that they can be relied on or have obvious flaws that need to be corrected.

5.7 The transverse force should be calculated using Sarpkaya's coefficients (Figs. 4.6 and 4.7). These predict the maximum transverse force ($C_{L(max)}$) at high Reynolds number and also predicted higher forces, and were therefore more conservative, than other authors.

5.8 A need was felt for more research, especially in two main areas. These are:

5.8.1 Vortex theory. (If the nature and propagation of vortices was completely understood, variations in the in-line force and the transverse force on a pile could be understood much better.)

5.8.2 The magnitude of the transverse force, and the coefficient C_L, expecially in deep or intermediate water at high Reynolds number.

SECTION II : FORCES ON PILE GROUPS

CHAPTER 6

FORCES ON PILE GROUPS IN STEADY FLOW

Previous chapters have indicated that the force on a pile in steady flow is not equal to the momentary force on a pile in oscillatory flow at the same instantaneous velocity, and thus the force on a pile group in steady flow would be expected to differ from the force in oscillatory flow at corresponding velocities. However, a brief consideration of the steady flow condition can identify several factors that are important in oscillatory flow.

6.1 Forces on piles in a column

Piles in a column are placed such that the axes of the piles form a plane, or column, aligned to the direction of the flow. This is shown diagrammatically in Fig. 6.1.

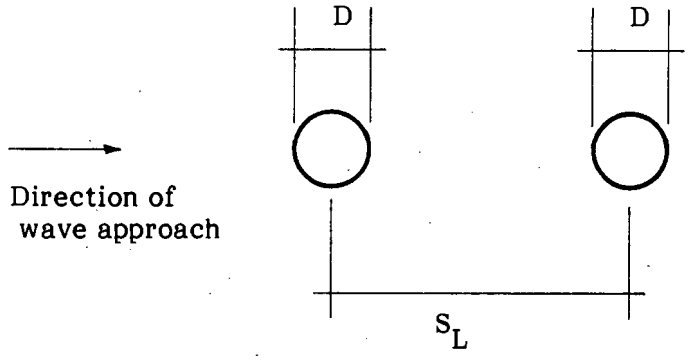

Figure 6.1 : Definition of a "column" of cylinders

6.1.1 Forces on two piles in a column

A pile situated directly downstream of another pile will have a lower drag coefficient than it would have alone. Ball (1974) quotes a reduction in the drag coefficient of 70% for piles from four to ten diameters behind an upstream pile. A plot of the drag coefficient against spacing for the downstream cylinder of a pair of cylinders is presented for several Reynolds

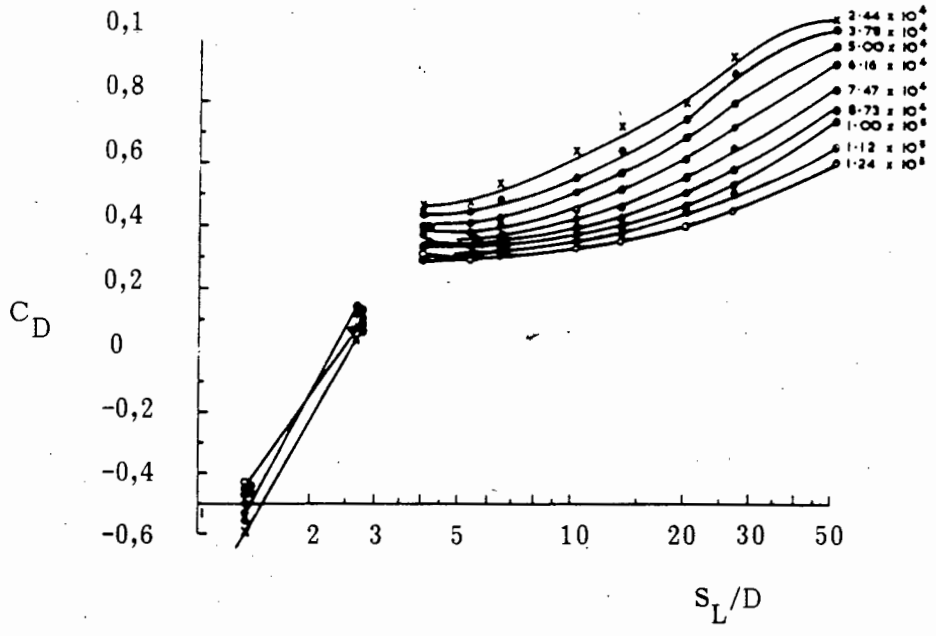

Figure 6.2 : Drag coefficient of the downstream cylinder for various Reynolds numbers

numbers in Fig. 6.2 (Zdravkovich, 1977). The notation is as shown in Fig. 6.1. Although the experimental data was obtained in a wind tunnel, it still shows several important features. First, the drag coeffi-cient is affected by the upstream cylinder for large spacings (up to 50 diameters). Second, for spacings greater than four diameters, increasing Reynolds number causes a decreasing drag coefficient. Third, the behaviour of the drag coefficient changes considerably as the spacing reduces to less than four diameters.

This last phenomenon is caused by a change in the behaviour of the flow in the "lane" between the two cylinders (defined in Fig. 6.3). If the two

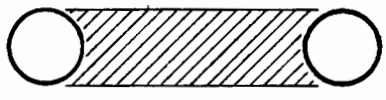

shaded area = "lane" between cylinders

Figure 6.3 : Definition of "lane" between cylinders

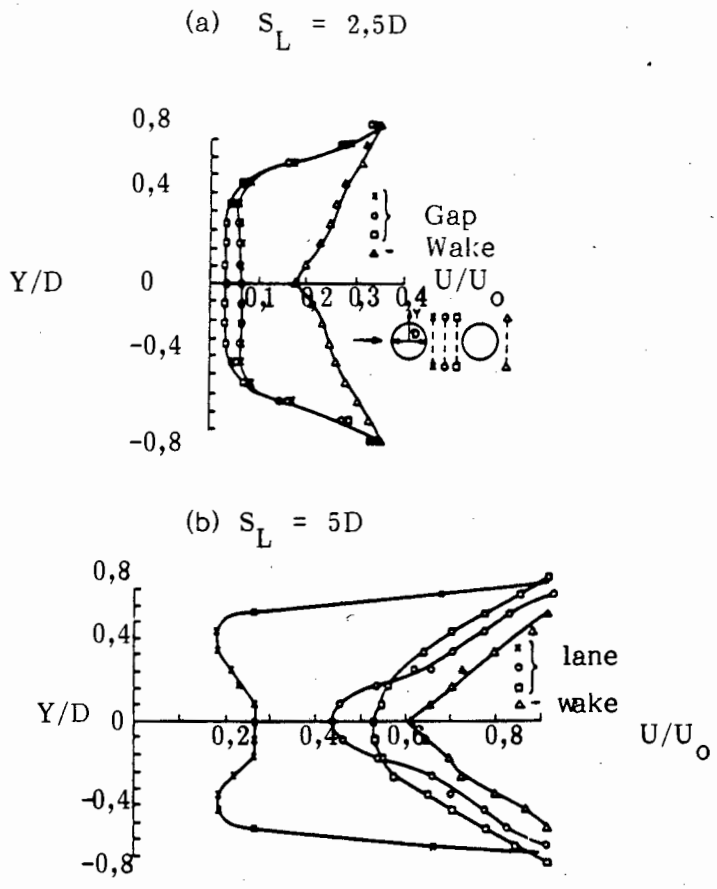

Figure 6.4 : Velocity profiles across the lane and wake

cylinders are close to each other ($S_L \leq 3D$) then the fluid in this lane has a very low velocity. Fig. 6.4 (Zdravkovich, 1977) shows velocity profiles at equal distances along the lane (i.e. at 1/4, 1/2 and 3/4 of the distance between the cylinders), and also at the same distance behind the downstream cylinder. This experiment was performed in water for two values of S_L, i.e. S_L = 2,5D and S_L = 5D. At the smaller spacing (S_L = 2.5D) there is a low, almost constant velocity in the lane, while at the larger spacing (S_L = 5D), there is a much greater, variable velocity. Furthermore, for larger spacings (S_L > 4D), vortices begin to form and to be shed from the upstream cylinder, which will also affect the drag coefficient of the downstream cylinder.

6.1.2 The force on multiple cylinders in a column

As cylinders are added to the downstream end of a column, the drag coefficient of the upstream cylinder tends to drop. Fig. 6.5 (Ball and Cox, 1978) shows the value of K_D for rows of plates at a spacing of S_L = 5D, where D = the width of the plate and K_D = Drag/(Drag for a single plate). (Note that though forces on plates are not equal to forces on cylinders, the same phenomena tend to occur, and thus studies using plates can be used to predict these phenomena on cylinders.) In this figure, the minimum force occurs at the fourth plate, independent of the number of plates. The force on any subsequent plate is always higher than the force on the plate immediately preceding it.

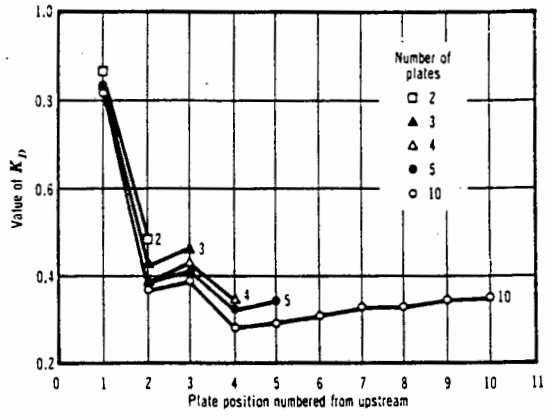

Figure 6.5 : Drag Factor Versus Number of Plates with Longitudinal Spacing, S_L = 5D

The effect of spacing on a fixed number of plates is shown in Fig. 6.6 (Ball and Cox, 1978). As the plates get closer together, the value of K_D tends to drop, as would be expected, except for the last two plates (plates number four and five) for the smallest spacings ($S_L \leq 4D$). This may be due to the changes in flow discussed for two cylinders at small spacings.

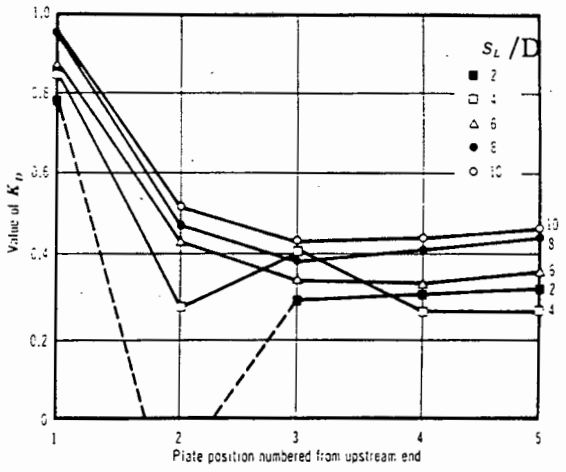

Figure 6.6 : Drag Factor Versus Longitudinal Spacing for Five Plates

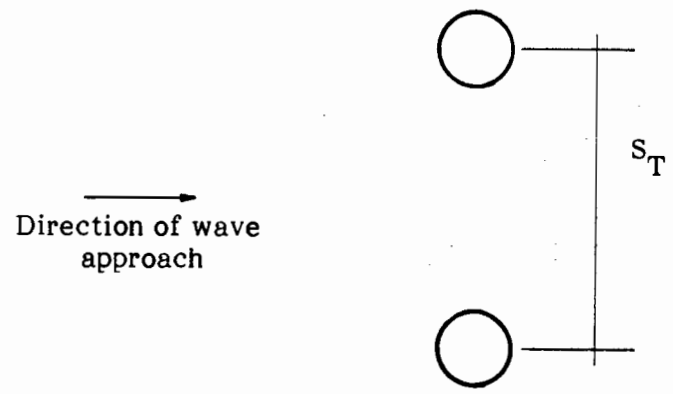

Figure 6.7 : Definition of a "row" of cylinders

6.2 Forces on piles in a row

A row of piles is defined such that the axes of the piles form a plane perpendicular to the direction of flow (Fig. 6.7).

6.2.1 Forces on two piles in a row

The value of the drag coefficient on two cylinders in a row is shown in Fig. 6.8 (adapted from Zravkovich, 1977). There are two important factors apparent from this figure. Firstly, as the two cylinders come closer together, the drag coefficient on both cylinders tends to rise. Secondly,

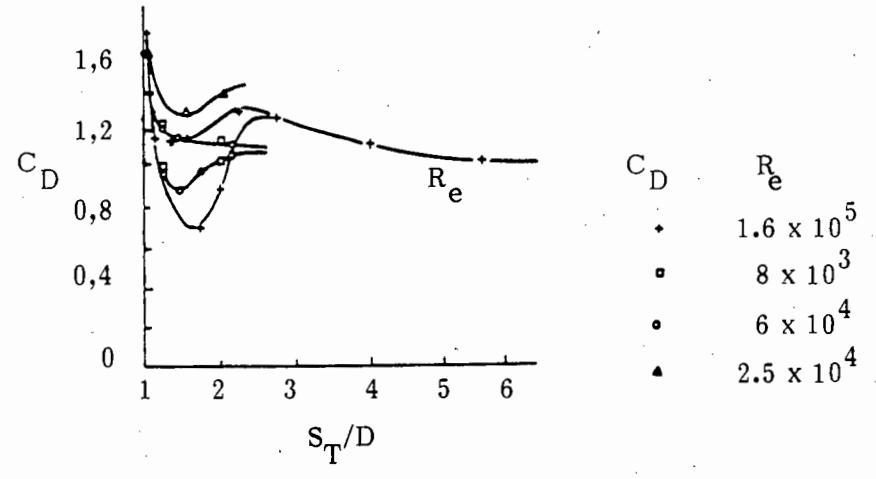

Figure 6.8 : Drag coefficients for a row of cylinders

when the cylinders are close together (S_T < 3D) the forces on the cylinders become unequal. The drag on the one cylinder will become significantly smaller than the drag on the other. The process is apparently random, and the higher force may exchange from one cylinder to the other, also at random. This situation may come about because, as the cylinders come close together, there is not enough room for two vortices to form between the cylinders (one from each cylinder). Thus vortex shedding will be suppressed behind one or other of the cylinders. This theory is supported by a plot of the Strouhal number of one cylinder (of a pair) versus spacing shown in Fig. 6.9 (Zdravkovich, 1977). The two values of the Strouhal number for $S_T \leq$ 2D means that there are two stable frequencies of vortex shedding behind each cylinder.

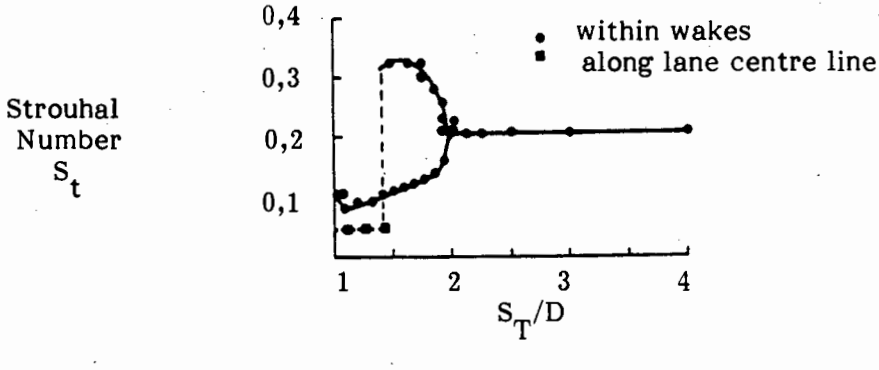

Figure 6.9 : Strouhal number for a row of two cylinders

6.2.2 Force on multiple cylinders in a row

Ball and Cox measured the forces on five plates in a row at various plate spacings. The results are shown in Fig. 6.10 (Ball and Cox, 1978). Both the centre and the inner plates show two alternative values of K_D at small spacing, but the outer plates appear always to have the smaller force. Furthermore, the values of K_D almost all exceed 1,0. Thus placing plates in a row increases the force by up to 40% for five plates.

6.3 The force on rectangular arrays

The force on several rectangular arrays, shown in Figure 6.11 (Ball and Cox, 1978) can be compared with the forces on single columns and rows (in Figs. 6.5 and 6.10). Interestingly, although placing plates in a single row tends

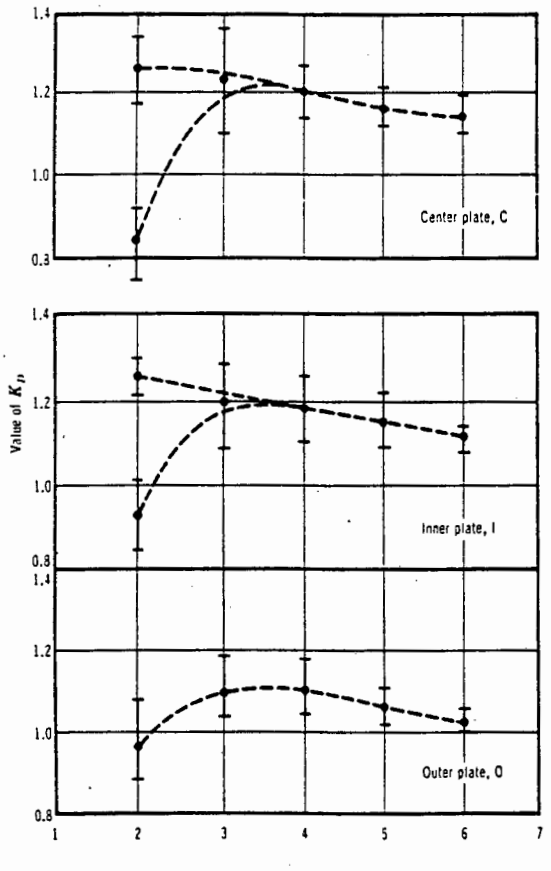

Figure 6.10 : Drag Factor versus Transverse Spacing for Five Plates

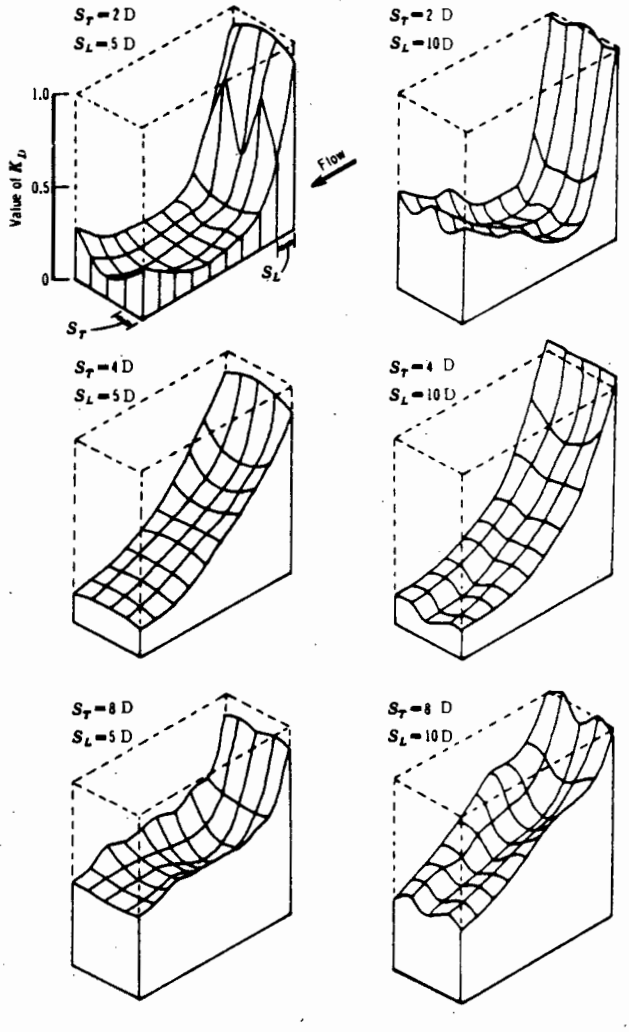

Figure 6.11 : Drag Factors for Group of Plates

to increase the value of K_D (compared to its value for a single plate) placing plates in an array tends to decrease the value of K_D compared to its value in a column, especially for $S_T \leq 4D$. Also, there is no evidence that any plates have two values of K_D, as a single row has. Furthermore, the force on the inner plates has reduced far more than the force on the outer plates - which tend to have a small force in a single row (compared to other plates in that row), but a large force in an array. For small S_T ($S_T \leq 2D$) the force on the individual plates begins to increase after a certain point downstream from the first plate, as with a single column. It is likely that this will also occur for larger values of S_T if the array was enlarged downstream (i.e. more rows were added).

6.4 Forces on two staggered cylinders

Two cylinders may be defined as staggered if the plane joining the axes of the cylinders is neither perpendicular nor parallel to the direction of flow as shown in Fig. 6.12.

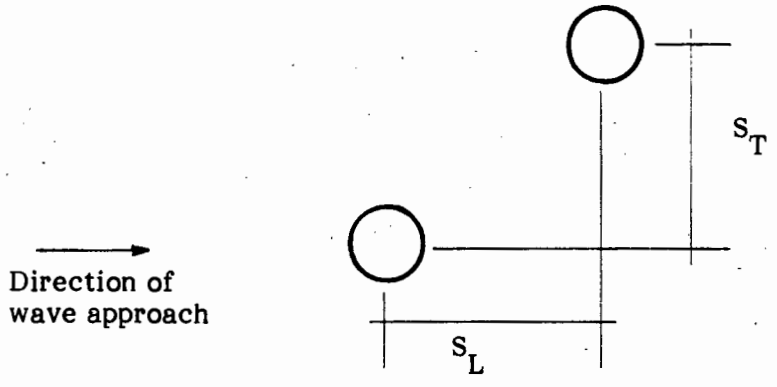

Figure 6.12 : A pair of "staggered" cylinders

6.4.1 The drag force

Zdravkovich has published experimental results of the drag coefficient for the downstream one of a pair of staggered cylinders, which is reproduced in Fig. 6.13 (Zdravkovich, 1977). The force contours tend to be parallel to the direction of the flow, except in the near vicinity of the upstream cylinder ($S_L < 1{,}5D$). Surprisingly, the minimum drag coefficient does not occur when it is directly behind the upstream cylinder ($S_T = 0$), but when it is slightly offset ($S_T \approx 0{,}25D$).

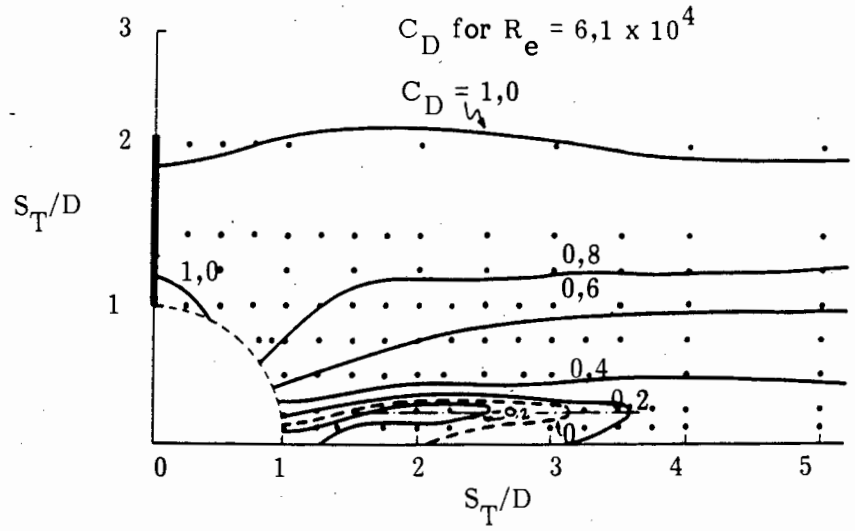

Figure 6.13 : Drag force coefficient for the downstream of a pair of cylinders for R_e = 6,1 x 10^4

6.4.2 The transverse force

The transverse force (Fig. 6.14, Zdravkovich, 1977) also has a major feature near S_T = 0,25D. Here the maximum transverse force coefficient $C_{L(max)}$ coincides with the minimum drag force. (Note that the transverse force is defined as positive when it tends to separate the two cylinders.) For large spacings (S_L > 4D) the contours of the transverse force coefficient appear to be parallel to the direction of flow.

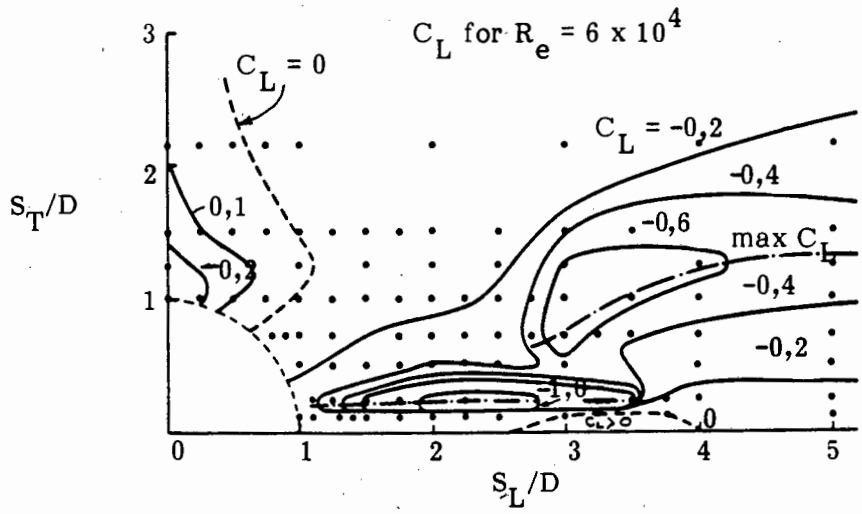

Figure 6.14 : Lift force coefficient for the downstream of a pair of cylinders for R_e = 6,1 x 10^4

6.5 The effect of Reynolds number

Fig. 6.8 shows the effect of Reynolds number on two cylinders in a row. The Reynolds number also affects a column of cylinders (Fig. 6.2).

CHAPTER 7

FORCES ON PILE GROUPS IN OSCILLATORY REAL FLOW

The prediction of forces on a group of piles is far more complicated than the prediction of forces on a single pile. Different arrangements for placing piles and the unknown direction of the incident waves (= θ_1) are only two variables which make it impossible to determine experimentally the forces on all possible arrays. Also, as has been seen in previous chapters, vortices play a large, and not totally understood, role in causing these forces. In an array of piles, there is usually a vortex street behind each pile, which can affect many downstream piles. As the ambient flow changes direction, those vortices which have not yet dissipated can be swept back around other piles, causing an area of confused vorticity in and around the pile group. This makes it difficult to predict forces even in simple arrays.

The method presently accepted for designing piles in arrays is to design each pile individually, i.e. to ignore the interaction between the piles. However, this can lead to under-prediction of forces on individual piles and over-prediction for the complete array. Figs. 7.1 and 7.2 (Laird et al, 1960B) show the in-line and transverse forces on the second of a pair of in-line cylinders (i.e. in a column) for different spacings compared to the forces on a single cylinder. Other results, not all shown in these figures, show that the in-line force varied from 150% to minus 20% of the minimum in-line force for a single cylinder, and the transverse force reached a maximum value of 90% of the maximum in-line force, or three times the maximum measured transverse force for a single pile.

Forces on a single cylinder are functions of k_c, R_e and θ (or t/T). Forces on arrays are, in addition, functions of the spacing between cylinders (usually measured in cylinder diameters) and the angle between the array and the incident wave (θ_1). A small change in this angle can cause a large variation in the forces on cylinders, especially those in the wake of upstream cylinders. In a wake, a cylinder usually experiences a reduced in-line force together with a much larger transverse force. If the cylinder moves out of the wake the in-line force should increase while the transverse force usually reduces. Therefore the maximum in-line and transverse forces seldom act simultaneously.

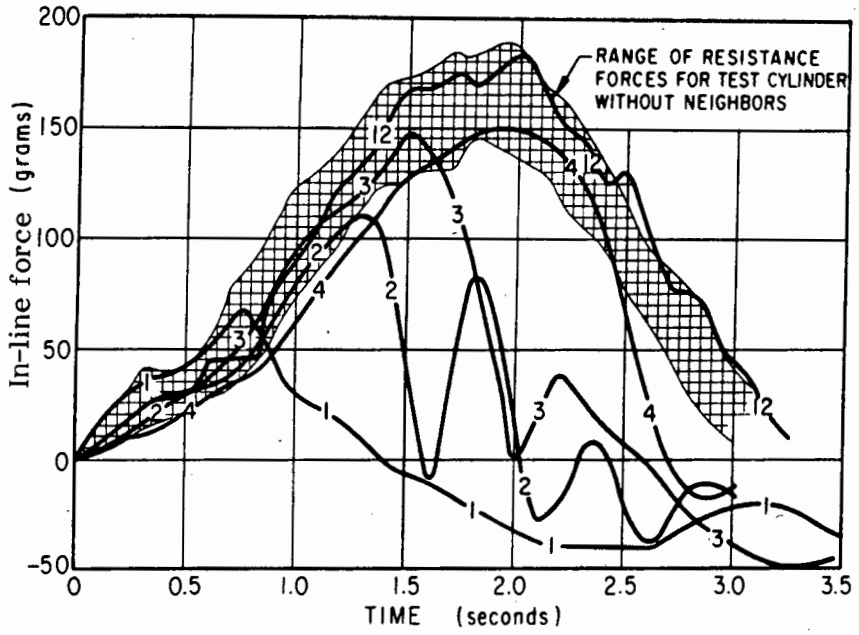

Figure 7.1 : In-line force on the second of a pair of cylinders as a function of time, with the spacing between cylinders (in diameters) as a parameter

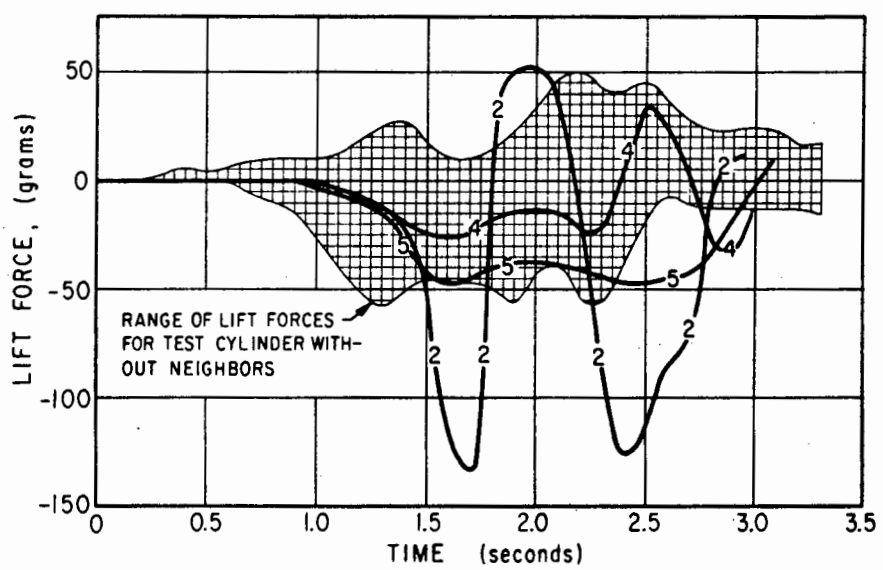

Figure 7.2 : Lift Force on the second of a pair of cylinders for the same runs shown in fig. 7.1 with spacings of 2, 4 and 5 diameters

7.1 Forces on a line of cylinders in oscillatory flow

7.1.1 Forces in a column

The total force coefficient, C_F, is shown in Fig. 7.3 (Chakrabati, 1979,), for three different arrays and for several S_L. The results for a single cylinder of approximately the same Reynolds number (Sarpkaya 1976) have been superimposed. These show that for $k_c > 10$, the forces on all cylinders in the column have been reduced, even for the leading cylinder of a pair. The

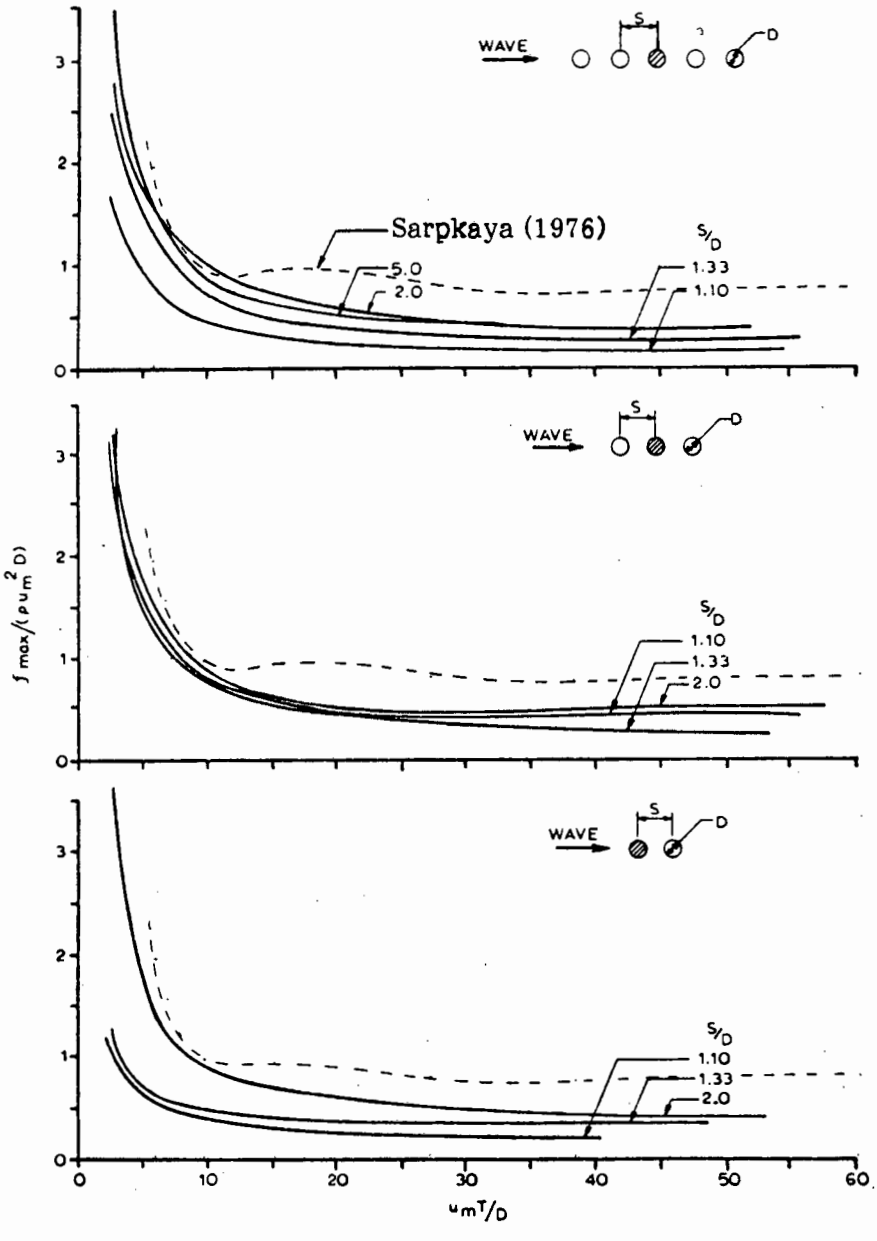

Figure 7.3 : Forces on cylinders in columns as a function of k_c and spacing

effect of the spacing is clear. The smaller the spacing, the lower the forces, as would be expected. Also, the forces on a single cylinder approximate those on the cylinder in the array for some spacings for k_c < 10. At k_c = 10, assuming linear wave theory, the horizontal distance a water particle travels is 3,2 D. Therefore, no cylinders with S_L > 3,2 should be affected by interference below k_c = 10.

Both the in-line and transverse forces on the second cylinder of a pair (S_L = 3 D) are shown in Fig. 7.4 (Bushnell, 1977). The interference coefficient is the force on the cylinder in the array divided by the force on a single cylinder. The forces on one cylinder of a pair throughout a wave cycle are shown in Fig. 7.5 (Bushnell, 1977). When a cylinder is in a wake, it has a flattened in-line force, together with a much magnified, regular transverse force. In the other half period, the in-line force is more peaked and the transverse force is small and irregular.

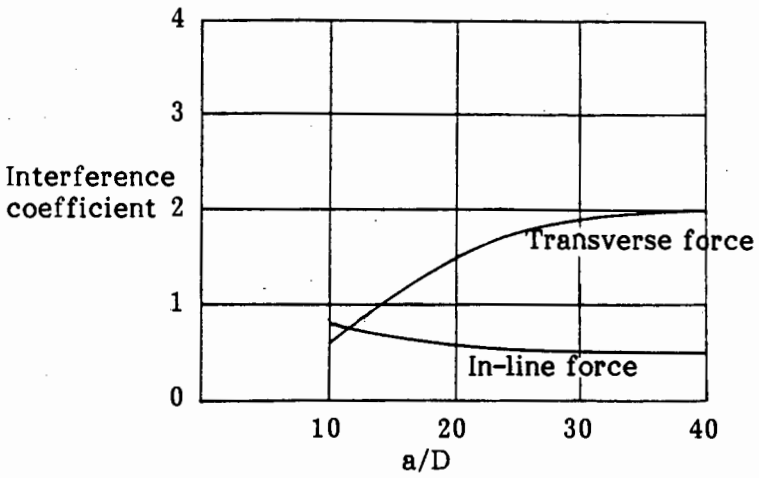

Figure 7.4 : Interference coefficient for the second of a pair of cylinders in a column with S_L = 3D

7.1.2 Forces on a row of cylinders

Forces on cylinders in a row are shown in Fig. 7.6 (Chakrabati, 1979), again with the approximate values from Sarpkaya (1976). These show that Chakrabati's forces for large spacing ($S_T \geq$ 2 D) are less than those on single

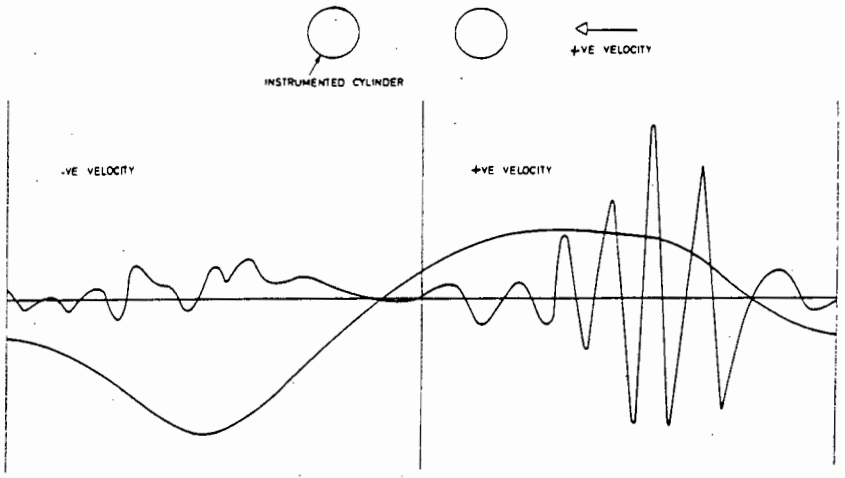

Figure 7.5 : Sample record of in-line and transverse forces for k_c = 104 and R_e = 6,0 x 10^4

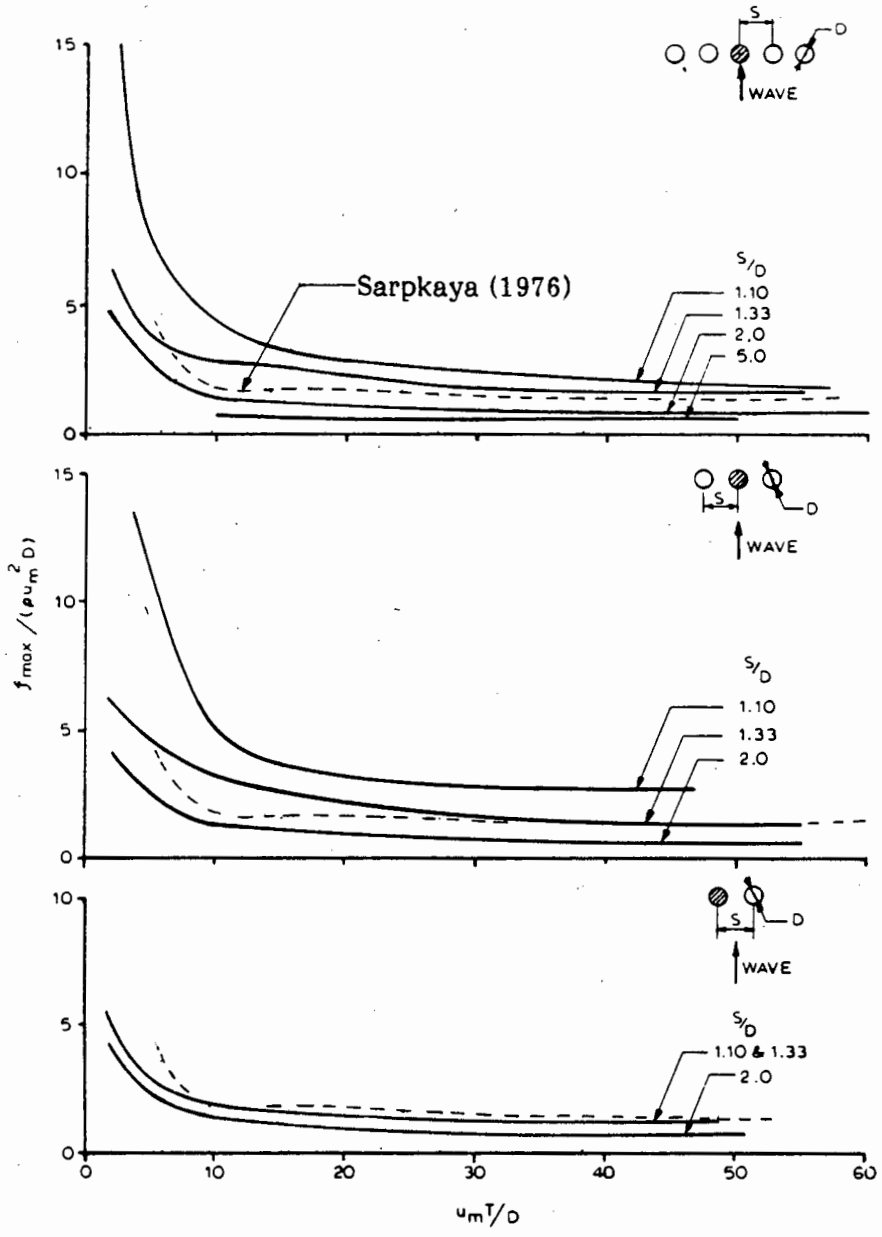

Figure 7.6 : In-line forces on cylinders in rows as a function of k_c and spacing

cylinders. This is unlikely to be true, and is probably due to experimental error. Chakrabati concluded that the forces on a cylinder of a row with S_T = 5 D were approximately those of a single cylinder. For cylinders in a row, increasing the spacing decreases the in-line force until it equals the force on a single cylinder.

The forces on each of the cylinders in a row of five cylinders is given in Fig. 7.7 (Chakrabati, 1979). This shows that the in-line force on the three inside cylinders is approximately equal (the exception being for S_T = 2 D) but that the end cylinders have a lower force at low spacing ($S_T \leq 1.33$ D).

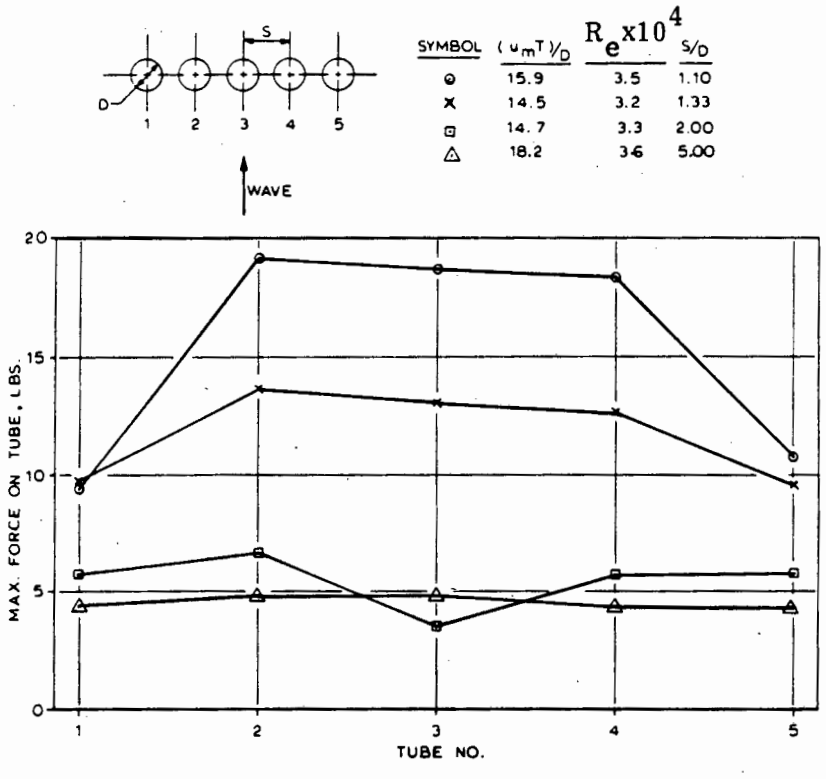

Figure 7.7 : Variation of maximum total forces on five tubes in a row at different spacings

The transverse forces on a row of cylinders are given in Figs. 7.8 - 7.10 (Chakrabati, 1982), and are compared with Sarpkaya (1976). These figures show that $C_{L(max)}$ can be far greater in an array than for a single cylinder, especially for a cylinder at the end of a row. However, the maximum lift forces in the centre of a row are not nearly as high, and are even, in some cases, reduced. It is also apparent that, even at the largest spacings (S_F = 5D), the transverse force is affected by the presence of other cylinders, especially at low k_c values.

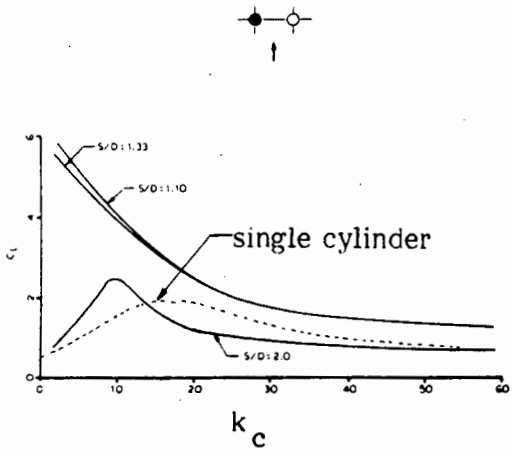

Figure 7.8 : Mean lift coefficients versus k_c number for 2 tubes in a row

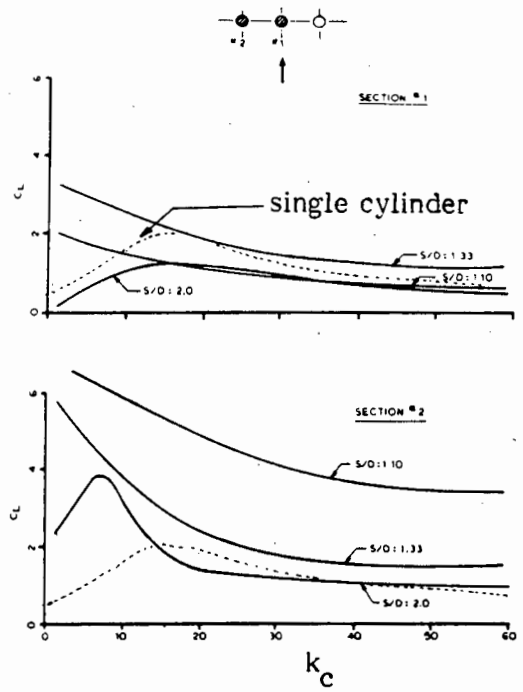

Figure 7.9 : Mean lift coefficients versus k_c number for 3 tubes in a row

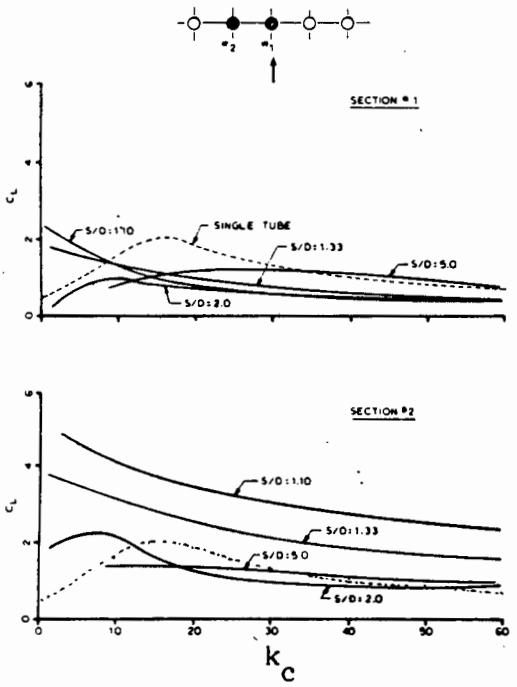

Figure 7.10 : Mean lift coefficients versus k_c number for 5 tubes in a row

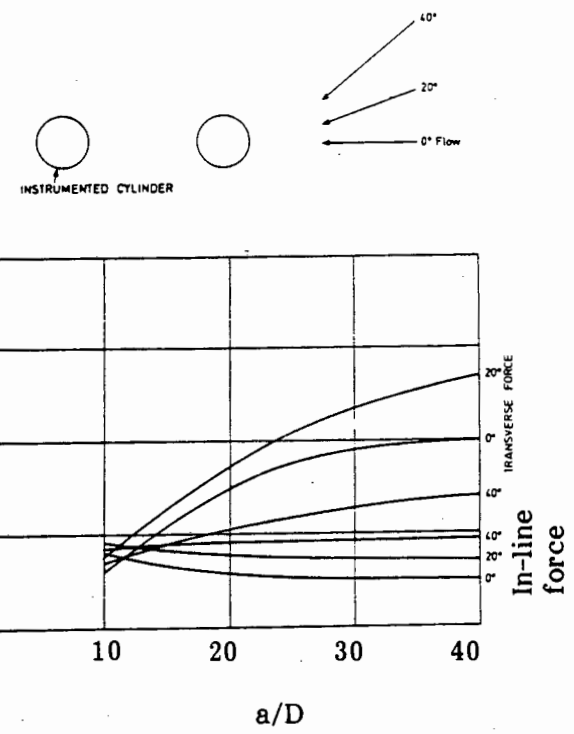

Figure 7.11 : Interference coefficients for two cylinders with spacing S = 3D

7.1.3 Forces on a line of cylinders angled to the direction of flow

Fig. 7.11 (Bushnell, 1977) shows the in-line and transverse forces on the second cylinder of a pair of cylinders at three different angles to the direction of wave propagation (0°, 20° and 40°) for S = 3 D. The in-line force tends towards the force on a single cylinder as it moves out of the wake of the upstream cylinder. However, the transverse force increases to a maximum and then decreases. This is probably because there is a high degree of turbulence and vortex action on the edge of the wake, and the highest transverse force occurs as the cylinder passes through this region. The in-line forces on cylinders, at different spacing and 45° to the direction of the propagation of the waves, are given in Fig. 7.12 (Chakrabati, 1979).

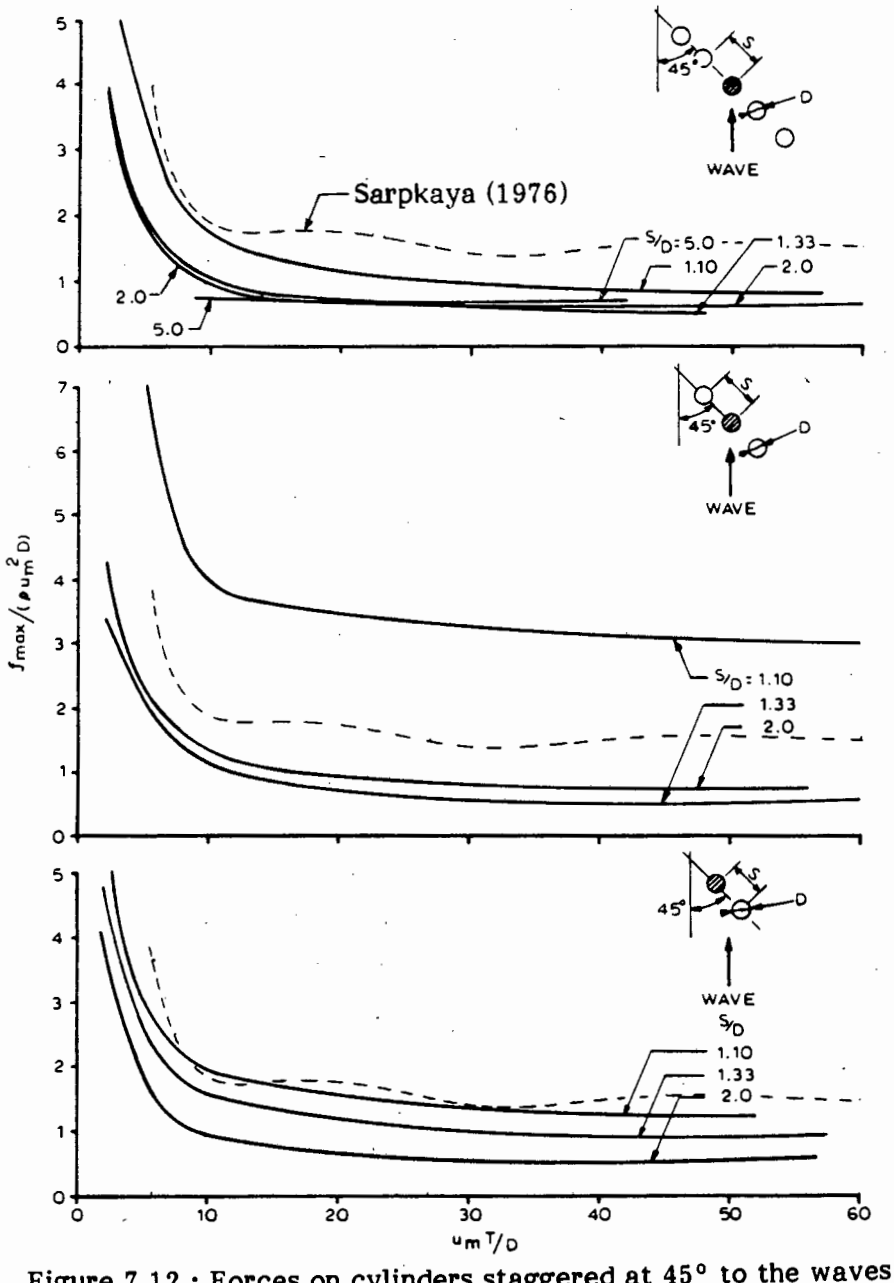

Figure 7.12 : Forces on cylinders staggered at 45° to the waves as a function of k_c and spacing

No trends with regard to S are immediately noticeable, although S = 1.10 D always has the highest force, especially for the three cylinder case.

7.2 Forces on a cylinder in a large array

Fig. 7.13 (Bushnell, 1977, Fig. 8) shows the interference coefficient for the centre pile of a square array with spacing $S_L = S_T = 3$ D. The coefficients are similar to those for the second cylinder of a pair (see Fig. 7.4), but both the in-line and the transverse forces are higher except for the in-line force when the angle of incidence = 0°. In this case the flow will tend to channel into the spaces between the cylinders, causing several relatively high speed streams of water parallel to the wave direction, as can be seen in Fig. 7.14 (Patel and Sarohia, 1982). In this figure, the longer dashes indicate faster flow.

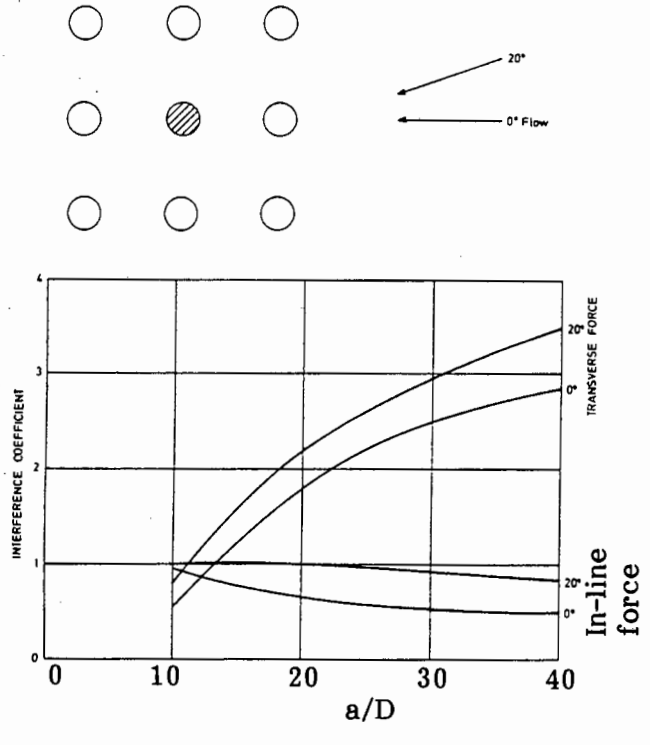

Figure 7.13 : Interference coefficients for centre position of array

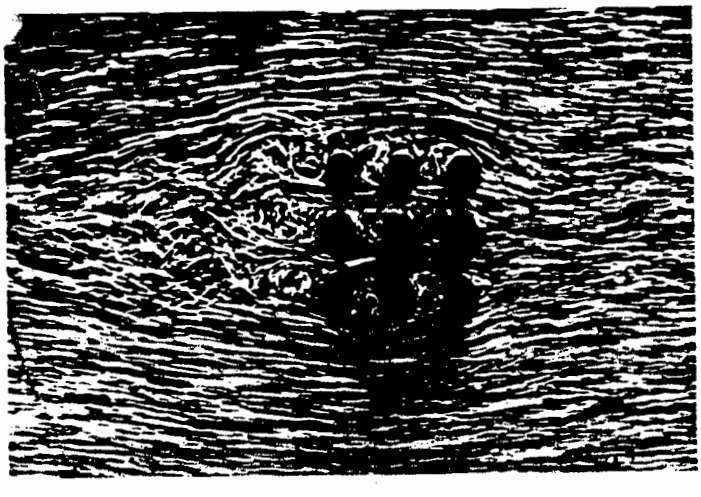

Figure 7.14 : Flow visualisation photograph for array with cylinders in line with wave direction $k_c = 15$

7.3 Forces on large arrays

7.3.1 Solidification

As a body of water becomes surrounded by piles, the enclosed water will be unable to exit the volume freely, and will remain relatively stationary. In the limit, if the water becomes completely enclosed by the piles, and thus is cut off from the incident waves, the effect will be to create one large pile. This phenomenon was investigated by Gibson and Wang (1977). For the cylinder arrangements shown in Fig. 7.15 (Gibson and Wang, 1977), they plotted C_M against a solidification ratio, $\Sigma D/\pi D_p$, which represents the solid proportion of the array perimeter. This is shown in Fig. 7.16 (Gibson and Wang, 1977). It shows very little effect on C_M for $\Sigma D/\pi Dp < 0,3$. The same data is shown in Fig. 7.17 (Gibson and Wang, 1977, Fig. 10), except that C_M is based on the array diameter D_p. Unfortunately, the nature of the

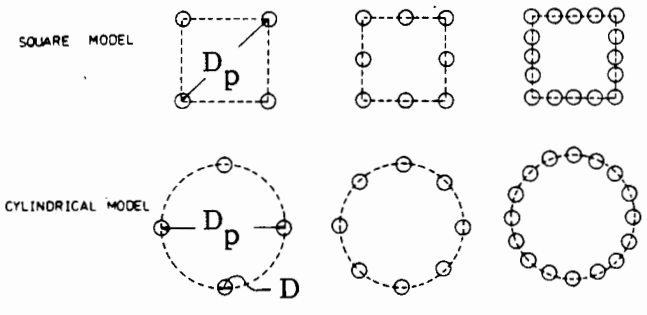

Figure 7.15 : Plan View of Spacings and Forms of Models

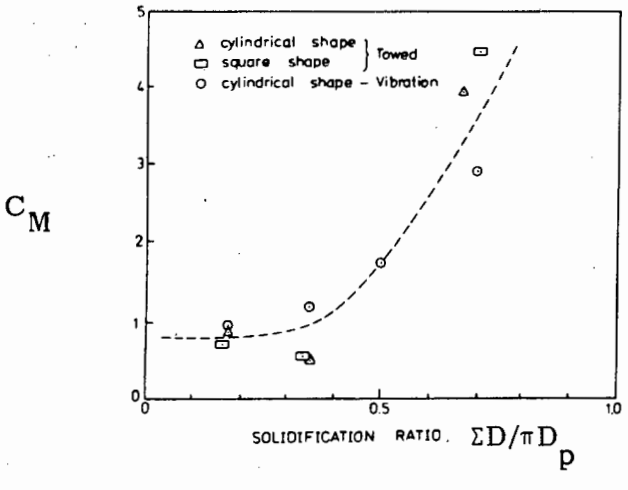

Figure 7.16 : C_M versus solidification ratio

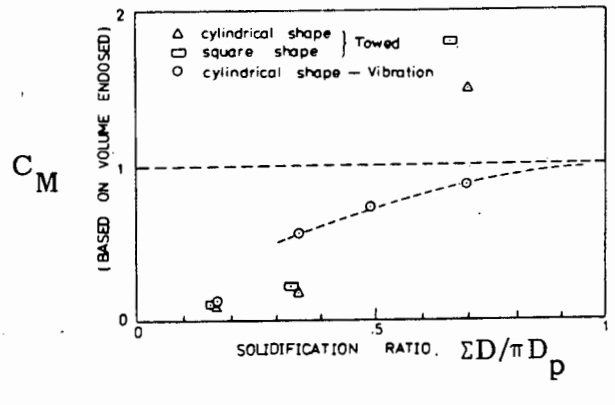

Figure 7.17 : C_M versus solidification ratio (based on volume enclosed)

experiments (the models were either accelerated linearly or vibrated at their own natural frequency) means that they are not directly applicable to oscillatory flow. However, the phenomenon does exist in oscillatory flow : Fig. 7.18 (Patel and Sarohia, 1982) shows how water can flow round an array, leaving almost still water within it, while forming large vortices around it. Note that the array, and the experimental conditions (apart from the approach angle of the incident wave) are identical to those in Fig. 7.14, where the water flows straight through the array.

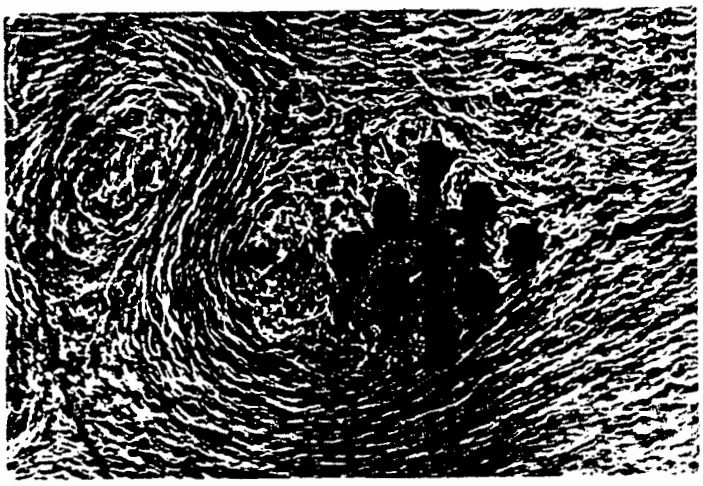

Figure 7.18 : Flow visualisation photographs for an array with cylinders at 45° to the waves $k_c = 15$

7.3.2 Resultant forces on complete arrays

7.3.2.1 In-line forces

The in-line forces on a complete array tend to be less than the sum of the calculated forces on all the individual cylinders, due to the shielding effects. Laird and Warren (1963) measured the forces on an array of 24 cylinders (shown in Fig. 7.19 (Laird and Warren, 1963)), which was oscillated in still water. Fig. 7.20 (Laird and Warren, 1963) shows these forces, as a function of cylinder spacing, in terms of F_A/F_o, where F_A = the measured in-line force on the complete array and F_o = twenty-four times the measured in-line force on a single cylinder in steady flow with U_o = the maximum velocity of oscillatory flow. Note there are 24 cylinders in the array. F_A/F_o tends towards 1,0 for S > 5 D.

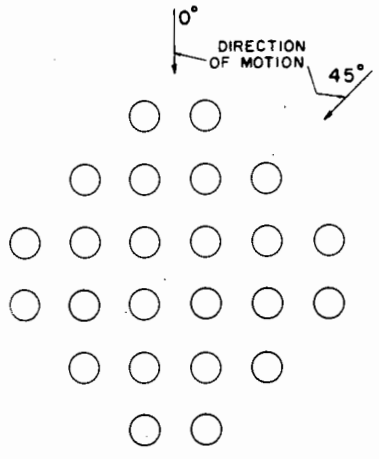

Figure 7.19 : Plan view of cylinder group

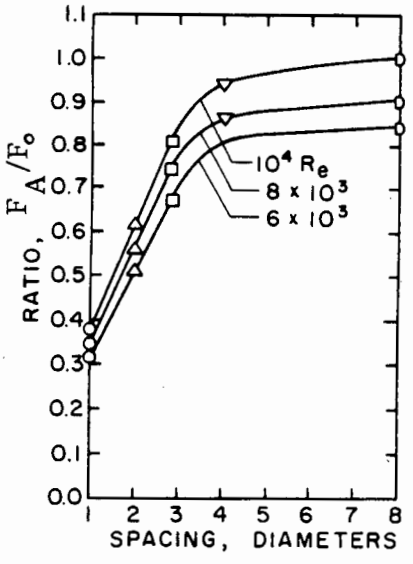

Figure 7.20 : In-line force ratios as a function of spacing

The total force on arrays was also measured by Heideman and Sarpkaya (1985). They measured the force on a square array with $S_T = S_L = 2$ D, and on a rectangular array with $S_T = 2$ D and $S_L = 5$ D, as a function of k_c for three angles of the incident flow ($\theta_i = 0°$, 15° and 20°).

The arrays were placed in a large U-tube in which the water oscillated around the cylinders, and the cylinders were slightly roughened to try to simulate high Reynolds numbers. Their results are shown in Fig. 7.21 (Heideman and Sarpkaya, 1985), where the total force coefficient, C_F, of the arrays is divided by the number of cylinders in the arrays to compare it with C_F for a single cylinder.

The results show very high forces on the arrays compared to the single cylinder. There could be several reasons for this : the width of the model array represented a significant proportion of the width of the flume and this may not only have forced the flow through the array, causing higher forces, but also inhibited the dissipation of the wake, which would also affect the forces, especially through several cycles. Also, the roughening cylinders cannot accurately model Reynolds number effects, but it will affect the forces on the cylinders.

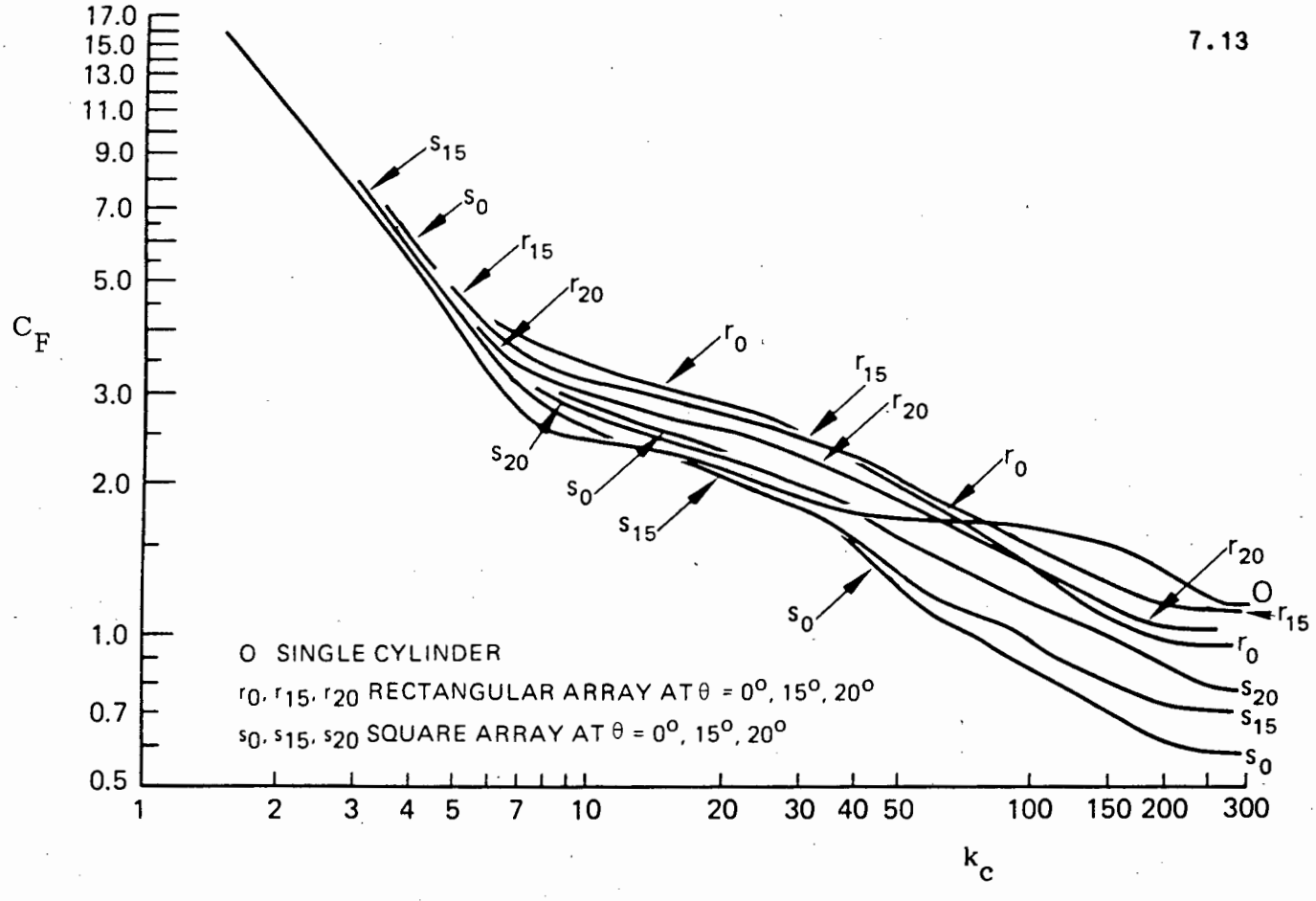

Figure 7.21 : Comparison of C_F for square and rectangular arrays and for single cylinders as a function of k_c

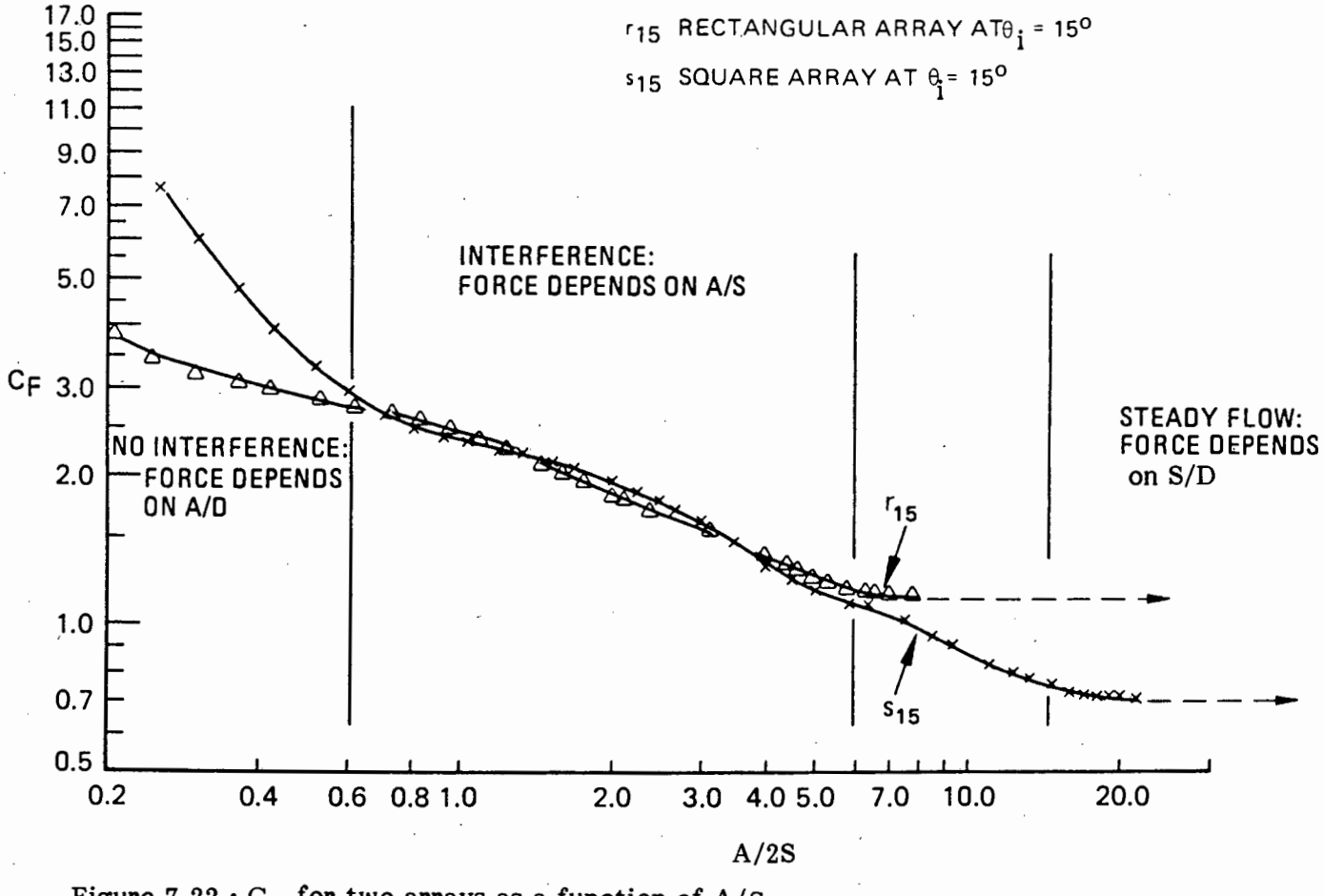

Figure 7.22 : C_F for two arrays as a function of A/S

Heideman and Sarpkaya replotted their data for two conditions (the square array at 15° to the incident flow and the rectangular array at 15° to the incident flow) against a new ratio, $a/2S_L$, where a = the horizontal distance a water particle moves. This is shown in Fig. 7.22 (Heideman and Sarpkaya, 1985). For small $a/2S_L$ (< 0,5) the cylinders are effectively isolated, and the C_F is independent of $a/2S_L$. For 0,6 < $a/2S_L$ < 6, C_F seems to be dependent on the ratio. For larger values the ratio does not seem to be important.

7.3.2.2 Transverse forces

Very few researchers have measured transverse forces on complete arrays. Laird and Warren did, however, for the array shown in Fig. 7.12, and published their results as a function of Reynolds number and cylinder spacing in Fig. 7.23 (Laird and Warren, 1963). Note here that the transverse force is amplified, even for S = 8 D.

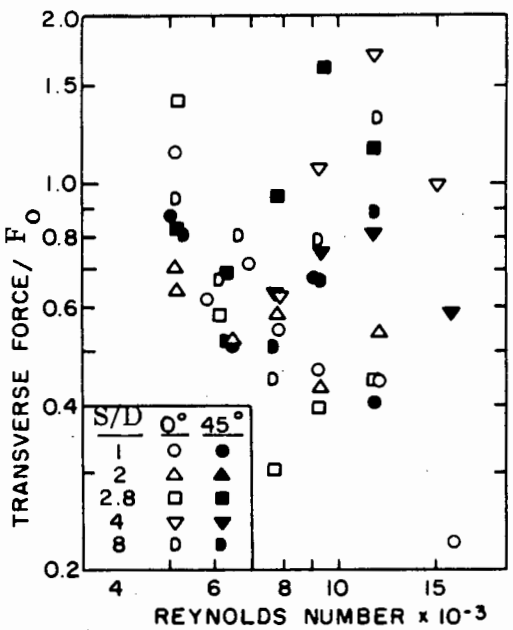

Figure 7.23 : Transverse force ratios for pile groups

It is important to note, for transverse forces in arrays, that the force is heavily influenced by the wake of previous cylinders, and therefore it is not safe to assume that the transverse forces on the individual cylinders

within the array are independent. Although it seems unlikely that all the cylinders will experience a maximum transverse force simultaneously, it may be possible at critical spacings.

7.4 Effect of Reynolds number

No author has performed experiments to reveal the effect of Reynolds number on the forces in cylinder arrays. Bushnell (1977) found no dependence on Reynolds number for low Reynolds numbers (shown in Fig. 7.24 (Bushnell, 1977)). He tried to simulate high Reynolds numbers by fitting tripwires to the instrumented cylinder, and the interference coefficient increased by approximately 30% (shown in Fig. 7.25 (Bushnell, 1977)). but this experimental method cannot be relied on. Heideman and Sarpkaya also tried to simulate high Reynolds number by inducing turbulence (by roughening the cylinders), and also measured high forces (Fig. 7.21), but again, this is not a proven method of simulating high Reynolds numbers.

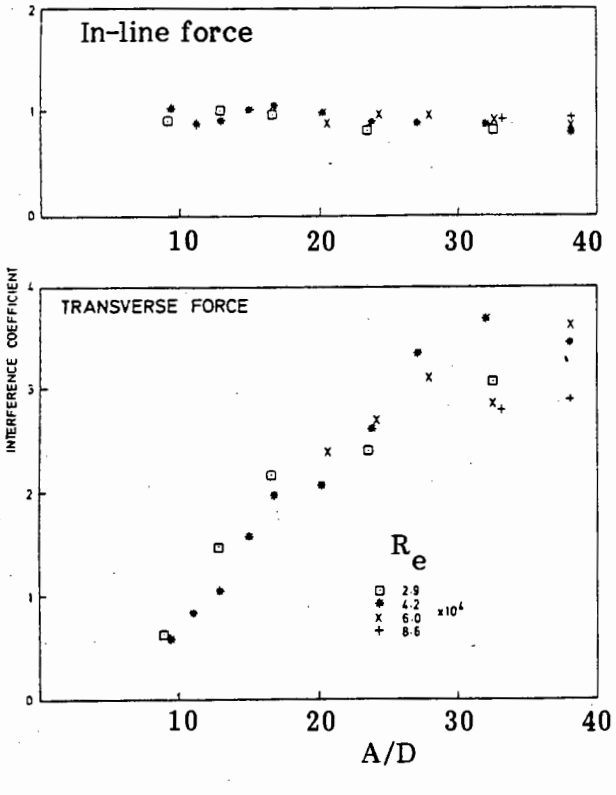

Figure 7.24 : Centre position interference coefficients for 20° flow

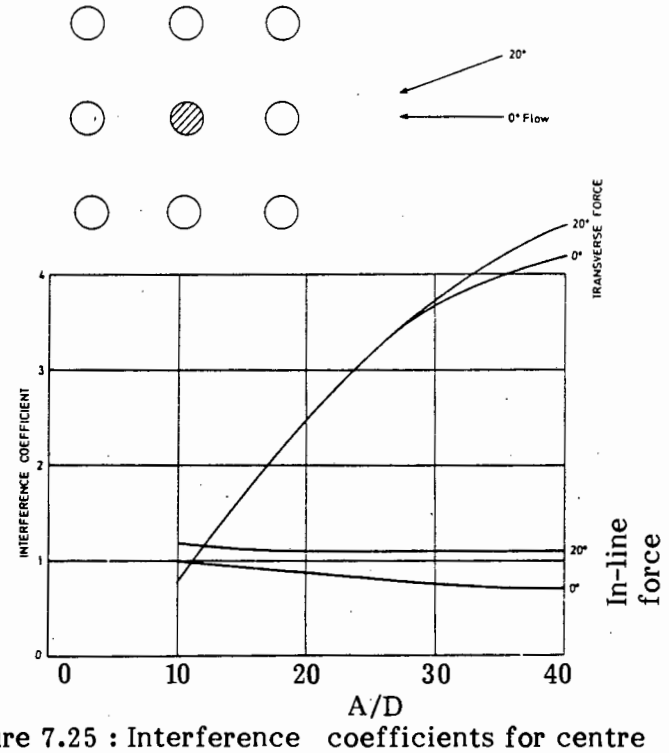

Figure 7.25 : Interference coefficients for centre position of array with tripwires

CHAPTER 8

POTENTIAL FLOW THEORY AROUND CYLINDER ARRAYS

Potential flow theory is only accurate if the viscosity of the flow is negligible. As stated in Chapter 1, this criterion is effectively achieved when the cylinder diameter is a significant proportion of the wavelength (typically $D/L > 0{,}2$). Therefore, the cylinders must be very large for potential theory to be applicable, and if this is the case, it is unlikely that the cylinder array would have a large number of cylinders. An oil platform, for example, with four large diameter circular legs is about the largest array that potential flow theory would be used on, and even then the inertia force from Morison's equation might be better suited to calculating the forces. The use of potential theory in arrays is, therefore, limited, and will not be dealt with in detail.

8.1 Diffraction theory on cylinder arrays

The diffraction theory of MacCamy and Fuchs was adapted by Spring and Monkmeyer (1974) to allow for the presence of other cylinders. They derived a formula for the velocity potential, ϕ, such that

ϕ = (velocity potential of incident wave)
+ (velocity potential of scattered wave of cylinder of interest)
+ (velocity potential of scattered saves from other cylinders)

This equation is set up in terms of a number of unknown coefficients, which are solved simultaneously by setting

$$\frac{\partial \phi}{\partial r} = 0 \quad \text{at all cylinder surfaces}$$

The pressure, and thus the force, on the cylinder is calculated in the same way that MacCamy and Fuchs used for a single cylinder, i.e. they used the Bernoulli equation to calculate the pressure, which is integrated over the cylinder to find the force on the cylinder.

Since this theory (Spring and Monkmeyer, 1974) is descended from MacCamy and Fuch's diffraction theory, it has the same limitations, i.e. it may only be used for linear waves in deep or intermediate depth water. However, it can allow for an unlimited number of cylinders. Unfortunately, for a large number of cylinders, the formulation of ϕ becomes very cumbersome and time consuming, even when using computers.

The complexity of the theory was addressed by McIver and Evans (1984) who simplified the process by replacing the scattered waves from surrounding cylinders with plane waves of appropriate amplitude. They also introduced a "correlation factor" to reduce the errors caused by this approximation. A comparison with Spring and Monkmeyer is shown in Fig. 8.1 (McIver & Evans, 1984). The two theories compare well, even for small spacings where the "plane wave" assumption would not be considered valid. It is also interesting to note the cyclical dependence of the in-line force on the spacing, which must therefore take up greater importance during design.

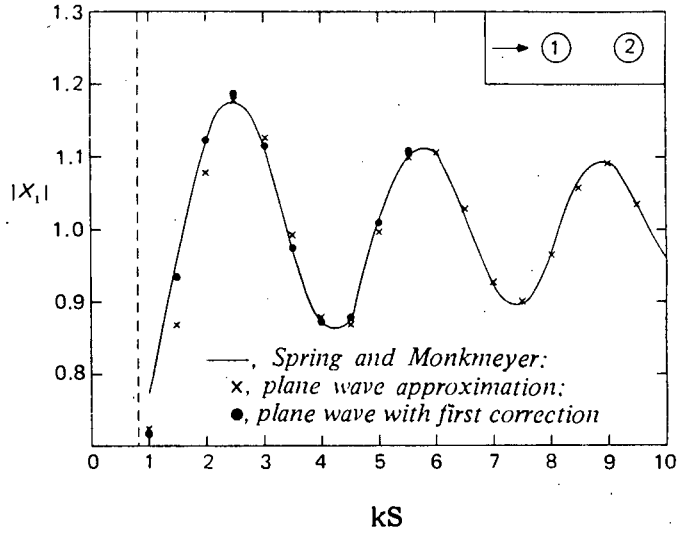

Figure 8.1 : In-line force on cylinder 1 $|X_1|$ as a function of cylinder spacing kS for two-cylinder case (ka = 0,8)

The diffraction theory for arrays has also been adapted specifically to calculate forces on infinite rows of cylinders. This has been done by Spring and Monkmeyer (1975) and Massel (1976).

CHAPTER 9

CONCLUSIONS TO SECTION II : FORCES ON PILE GROUPS

9.1 The presence of other piles in a group may cause significant deviations from the force on a single pile.

9.2 The in-line force on one pile in an array can be increased up to 300% of the in-line force on a single pile.

9.3 The transverse force on one pile in an array can be increased up to 400% of the transverse force on a single pile.

9.4 The in-line force on a cylinder in the wake of an upstream pile can be significantly reduced compared to the force on a single pile.

9.5 The total force on an array is usually less than the equivalent force on the same number of single piles.

9.6 Interference is negligible for piles with spacings greater than 5 diameters, and piles can be considered isolated for spacings greater than 10 diameters.

9.7 Diffraction theory can be used to calculate accurately the forces on groups of suitably large piles.

9.8 No definite conclusions may be drawn about the behaviour of the forces at high Reynolds numbers, since no clear data exists on this topic.

9.9 There has been no systematic research into forces on pile groups, but, instead, isolated research into individual problems or situations. Such research might reveal basic insight which is now lacking, especially with regard to the effect of Reynolds number and the correlation of the maximum force with the ratio a/S.

LIST OF REFERENCES AND BIBLIOGRAPHY

Ball, DJ	1974	Simulation of Piers in Hydraulic Models. *ASCE J. of the Waterways, Harbours and Coastal Engineering Div.*, 100, No. WW1, 23-24.
Ball, DJ and Cox NJ	1978	Hydrodynamic Drag Forces on Groups of Flat Plates. *ASCE J. of the Waterways, Port, Coastal and Ocean Div.*, 104, No. WW2, 163-173.
Bidde, DD	1971	Laboratory studies of Lift force on circular piles. *ASCE J. of the waterways, Harbours and Coastal Div.*, 97, No.WW4, 595-614.
Bishop, JR	1979	R.M.S. Force Coefficients derived from Christchurch Bay. Shaw TL (ed): *Mechanics of Wave-induced Forces on Cylinders*, Pitman, London, 334-345.
Bishop, JR Tickell, RG and Gallagher, K.	1980	The UK Christchurch Bay Project: A review of results. *12th Offshore Technology Conference*, paper No. OTC 3796.
Bushnell, MJ	1977	Forces on Cylinder Arrays in Oscillating Flow. *9th Offshore Technology Conference*, Paper No. OTC 2903, pp. 193-198.
Chakrabati, SK	1972	Nonlinear Wave Forces on Vertical Cylinders. *ASCE J. of Hydraulics Div.*,98, No. Hy 11, paper 9333, 1895-1909. Discussion 1973, 99, No. Hy 7, 1196, 1973, 99, No. Hy 11, 2135. Closure 1974, 100, No. Hy 7, 1073-1075.
Chakrabati, SK	1975	Second order Wave Force on Large Vertical Cylinder. *Technical Note, J. of the Waterways, Harbours and Coastal Eng. Div.* 101, No. WW3, 311-317.
Chakrabati, SK, Wolbert, AL and Tam, WA	1976	Wave Forces on Vertical Circular Cylinders, *ASCE J. of the Waterways, Harbours and Coastal Eng. Div.*, 102, No. WW2, paper 12140, 203-221. Discussion 1977, 103, No. WW1, 189. Closure 1977, 103, No. WW4, 567.
Chakrabati, SK	1978	Wave Forces on Multiple Vertical Cylinders. *ASCE J. of the Waterways, Port, Coastal and Ocean Div.*, 104, No. WW2, 147-161.

Chakrabati, SK	1979	Wave Forces on Vertical Array of Tubes. *Civil Engineering in the Oceans IV*, Vol. 1, pp. 241-259.
Chakrabati, SK	1980	Inline Forces on Fixed Vertical Cylinder in Waves. *ASCE J. of the Waterway, Port, Coastal and Ocean Div.*, 106, No. WW2, paper 15403, 145-155. Discussion 1981, 107, No. WW1, 45-46, 1981, 107, No. WW2, 127-128. Closure 1981, 107, No. WW4, 253-254.
Chakrabati, SK	1982	Transverse Forces on Vertical Tube Array in Waves. *ASCE J. of the Waterways, Port, Coastal and Ocean Div.*, 108, No. WW1, 1-15.
Chakrabati, SK	1985	Hydrodynamic Coefficients and Depth Parameters, Technical Note, *ASCE J. of the Waterways, Port, Coastal and Ocean Div.*, 111, No. 1, 123-127.
Chakrabati, SK , Libby, AR and Kompare, DJ	1986	Dynamic Pressures around a Vertical Cylinder in Waves. *18th Offshore Technology Conference*, Paper No. OTC 5102.
Dean, RG and Aagaard, PM	1970	Wave Forces: Data Analysis and Engineering Calculation Method. *J. of Petroleumn Technology*, 249, 368-375.
Dean, RG	1976	Methodology for Evaluating Suitability of Wave and Wave Force Data for Determining Drag and Inertia Coefficients. *Behaviour of Offshore Structures*, II, 40-64.
Dronkers, ML and Massie, WW	1979	Lift Forces on Cylinders. Shaw, TL (ed): *Mechanics of Wave-induced Forces on Cylinders*. Pitman, London, 510-520.
Garrison, CJ and Chow, PY	1972	Wave Forces on Submerged Objects. *ASCE J. of the Waterways, Harbours and Coastal Eng. Div.* 98, No. WW3, Paper 9098, 375-392.
Garrison, CJ, Field JB, and May, MD	1977	Drag and Inertia Forces on a Cylinder in Periodic Flow. *ASCE J. of the Waterways, Port, Coastal and Ocean Div.*, 103, No. WW2, Paper 12913, 193-204. Discussion, 1978, 104, No. WW2, 247-250, 1978, 104, No. WW4, 349.
Garrison, CJ	1990	Drag and Inertia Forces on Circular Cylinders in Harmonic Flow. *ASCE J. of the Waterways, Port, Coastal and Ocean Div.*, 116, No. 2, 169-190.

Gibson, RJ and Wang H	1977	Added Mass of Pile Groups. *ASCE J. of the Waterways, Port, Coastal and Ocean Div.*, 103, No. WW2, 215-223.
Havelock, TH	1940	The Pressure of Water Waves upon a Fixed Obstacle. *Proceedings of the Royal Society of London, Series A*, 175, pp. 409-421.
Hayashi, K and Takenouchi, T.	1985	Characteristics of Flow around a Vertical Circular Cylinder in a Wave. *Coastal Engineering in Japan*, 28, 207-222.
Heideman, JC, Olsen OA and Johansson, PI	1979	Local Wave Force Coefficients, *Civil Engineering in the Oceans IV*, II, 684-698.
Heideman, JC and Sarpkaya, T.	1985	Hydrodynamic Forces on Dense Arrays of Cylinders. *17th Offshore Technology Conference*, Paper No. OTC 5008.
Hogben, N	1974	Fluid Loading on Offshore Structures, A State-of-the-art appraisal: Wave Loads. *Maritime Technology Monograph No. 1*, Roy. Inst. Nav. Arch.
Hogben, N	1976	Wave Loads on Structures. *1st Conference on the Behaviour of Offshore Structures*, I, 186-219.
Hogben, N, Miller BL, Searle JW and Ward G	1977	Estimation of Fluid Loading on Offshore Structures. *Proceedings of the Institution of Civil Engineers, Part 2*, 63, pp. 515-562.
Hogben, N	1978	Wave Loads on Structures. *Marine Science Communications*, 4, Part 2, pp. 89-119.
Hunt, JN and Baddour, RE	1980A	Second Order Standing Waves Bounded by Circular Cylinders. *ASCE J. of the Waterways, Port, Coastal and Ocean Div.*, 106, No. WW1, 122-127. Discussion 1980, 106, No. WW4, 507-509, 1981, 107, No. WW1, 40-41. Closure 1982, 108, No. WW1, 116.
Hunt JN and Baddour, RE	1980B	Nonlinear Standing Waves Bounded by Cylinders. *Quarterly Journal of Mechanics and Applied Maths*, 33, 357-371.
Hunt, JN and Baddour, RE	1981	The Diffraction of Nonlinear Progressive Waves by a Vertical Cylinder. *Quarterly J. of Mechanics and Applied Maths*, 34, 69-87.

Hunt, JN and Baddour, RE	1982	Second order Wave Forces on Vertical Cylinders. Technical Note, *ASCE J. of the Waterway, Port, Coastal and Ocean Engineering*, 108, No. WW3, 430-434.
Isaacson M de St Q, and Maull, DJ	1976A	Transverse Forces on Vertical Cylinders in Waves. *ASCE J. of the Waterways, Harbours and Coastal Eng. Div.*, 102, No. WW1, Paper 11934, 49-60. Discussion 1976, 102, No. WW4, 491-493; 1976, 102, No. WW4, 493-495. Closure 1977, 103, No. WW2, 295-296.
Isaacson M de St Q	1977A	Shallow Wave Diffraction around Large Cylinder. *ASCE J. of the Water, Port, Coastal and Ocean Engineering Div*, 103, No. WW1, Paper 12756, 69-82.
Isaacson M de St. Q	1977B	Nonlinear Wave Forces on Large Offshore Structures. *Technical Note, ASCE J. of the Waterways, Harbours and Coastal Engineering Div.*, 103, No. WW1, 166-170. Discussion, 1977, 103, No. WW4, 568, 1978, 104, No. WW1, 93-94, 1978, 104, No, WW2, 245-246. Closure 1978, 104, No. WW4, 457-459.
Isaacson M de St Q	1979	Wave Induced Forces in the Diffraction Regime. Shaw T.L. (editor): *Mechanics of Wave-Induced Forces on Cylinders*, Pitman, London, 68-89.
Iverson, HW and Balent, R	1951	A Correlating Modulus for Fluid Resistance in Accelerated Motion. *J. of Applied Physics*, 22, No. 3, 324-328.
Iwagaki, Y and Ishida, H	1976	Flow Separation, Wake Vortices and Pressure Distribution around a Circular Cylinder under Oscillatory Waves. *15th Coastal Engineering Conference*, Chapter 137, 2341-2356.
Jen, Y	1980	Wave Force Analysis: An Alternate Procedure. Technical Note, *ASCE J. of the Waterway, Port, Coastal and Ocean Engineering*. 106, No. WW1, 117-121.
Keulegan, GH and Carpenter, LH	1958	Forces on Cylinders and Plates in an Oscillating Fluid. *Journal of Research of the National Bureau of Standards*, 60, No. 5, 423-440.
Laird ADK and Johnson, CA	1956	Drag Forces on an Accelerated Cylinder. *Journal of Petroleum Technology*, 8, 65-67.

Laird ADK, Johnson CA and Walker, RW	1960A	Water Forces on Accelerated Cylinders. *Transactions, ASCE*, 125, Paper No. 3038, 652-666.
Laird, ADK, Johnson, CA and Walker, RW	1960B	Water Eddy Forces on Oscillating Cylinders. *ASCE J. of the Hydraulics Div.*, 95, No. Hy 9, 43-54.
Laird, ADK and Warren, RP	1963	Groups of Vertical Cylinders Oscillating in Water. *ASCE. J. of the Engineering Mechanics Div.*, 89, No. EM1, 25-35.
Lamb	1906	*Hydrodynamics*, 3rd Edition, Cambridge University Press.
Lundgren, H.	1979	Wave Loading in the Drag/Inertia Regime with particular reference to Vertical Cylinders. Shaw TL (ed.) *Mechanics of Wave-Induced Forces on Cylinders*, Pitman, London, 55-67.
MacCamy, RC and Fuchs, RA	1954	Wave Force on Piles: A Diffraction theory. *United States Beach Erosion Board, Technical Memorandum No. 69.*
Massel, SR.	1976	Interaction of Water Waves with Cylinder Barrier. *ASCE J. of the Waterways, Harbours and Coastal Engineering Div.*, 102, No. WW2, 165-187.
McIver, P and Evans, DV	1984	Approximation of Wave Forces on Cylinder Arrays. *Applied Ocean Research.* 6, No. 2, 101-107.
McLachlan, NW	1934	*Bessel Functions for Engineers.* Oxford University Press.
Milne-Thomson	1938	*Theoretical Hydrodynamics.* Macmillan, London.
Miloh, T.	1980	Irregularities in Solutions of Nonlinear Wave Diffraction Problem by Vertical Cylinder. *Technical Note, ASCE. J. of the Waterway, Port, Coastal and Ocean Div.*, 106, No. WW2, 279-284. Discussion. 1981, 107, No. WW1, 42-43, 1981, 107, No. WW2, 125-126.
Morison, JR, O'Brien, MP, Johnson, JW and Schaaf, SA	1950	The Force Exerted by Surface Waves on Piles. *AIME Petroleum Transactions.* 189, 149-154.
Morison, JR, Johnson JW and O'Brien, MP	1953	Experimental studies of Forces on Piles. *Proc. of the 4th Conference on Coastal Engineering,* Chapter 28, 340-370.

O'Brien, MP and Morison, JR	1952	The Forces exerted on Waves by Objects. *Transactions, American Geophysical Union*, 33, No. 1, 32-38.
Ohmart, RD	1984	Hydrodynamic Loading of Steel Structures, *ASCE J. of the Waterway, Port, Coastal and Ocean Engineering Div*, 110, No. 4, 448-462. Discussion, 1987, 113, No. 4, 429. Closure, 1987, 113, No. 4, 430-431.
Patel, MH and Sarohia, S	1982	On the Dynamics of Production Risers. *3rd Conference on the Behaviour of Offshore Structures*, 1, 599-617.
Pearcey, HH	1979	Some Observations on Fundamental Features of Wave-Induced Viscous Flows Past Cylinders. Shaw, T.L. (editor): *Mechanics of Wave-Induced Forces on Cylinders*, Pitman, London, 1-54.
Raman, H and Venkatanarasaiah, P.	1976	Forces due to Nonlinear Waves on Vertical Cylinders. *ASCE J. of the Waterway, Port, Coastal and Ocean Engineering*, 102, No. WW3, 301-316. Discussion, 1977, 103, No. WW2, 299-300, 1977, 103, No. WW3, 404-406, 1977, 103, No. WW3, 406-407. Closure, 1978, 104, No. WW1, 91-92.
Rodenbush, G and Guitierrez, CA	1983	Forces on Cylinders in Two-Dimensional Flows. *Technical Progress Report BRC 13-83*, Belair Research Centre, Shell Development Co., Houson, Texas.
Sarpkaya, T	1976A	Vortex Shedding and Resistance in Harmonic Flow about Smooth and Rough Circular Cylinders at High Reynolds Number. *Naval Postghraduate School, Report No. NPS-59SL 76021.*
Sarpkaya, T	1976B	In-line and Transverse Forces on Smooth and Sand-Roughened Cylinders in Oscillatory Flow at High Reynolds Numbers. *Naval Postgraduate School, Report No. NPS-69SL 76062.*
Sarpkaya, T	1976C	Vortex Shedding and Resistance in Harmonic Flow about Smooth and Rough Circular Cylinders. *1st Conf. on the Behaviour of Offshore Structures*, I, 220-235. Discussion, II, 311. Closure, II, 312-315.

Sarpkaya, T.	1979	Wave Loading in the Drag/Inertia Regime with particular reference to Groups of Cylinders. Shaw, TL (ed.) *Mechanics of Wave-Induced Forces on Cylinders.* Pitman, London, 532-542.
Sarpkaya, T and Wilson, JR	1984	Pressure Distribution on Smooth and Rough Cylinders in Harmonic Flow. *Proc. of the Ocean Structural Dynamics Symp.*, Oregan State University, 341-355.
Sarpkaya, T.	1984	Discussion of "Quasi-2-D Forces on a Vertical Cylinder in Waves" by Stansby et al., *ASCE J. of the Waterway, Port, Coastal and Ocean Engineering*, 110, 120-123.
Sawamoto, M, Kikuchi, K, Ohba, M and Kasiwai, J.	1980	Forces on a Circular Cylinder in Oscillatory Flow. *Coastal Engineering in Japan*, 23, 147-158.
Sawaragi, T and Nakamura, T	1979	Analytical Study of Wave Force on a Cylinder in Oscillatory Flow. *Speciality Conference on Coastal Structures*, I, 154-173.
Skjelbreia, L.	1979	Wave Forces on Large North Sea Gravity Structures, *Civil Engineering in the Oceans IV*, I, 137-160.
Spring, BH and Monkmeyer, PL	1974	Interaction of Plane Waves with Vertical Cylinders. *Proceedings of the 14th Coastal Engineering Conference*, Chapter 107, 1828-1847.
Spring BH and Monkmeyer, PL	1975	Interaction of Plane Waves with a Row of Cylinders. *Proceedings, Civil Engineering in the Oceans III*, Vol. II, 979-998.
Standing, RG.	1984	Wave Loading on Offshore Structures: A Review. *Ocean Science and Engineering*, 9, part 1, 25-134.
Stansby, PK.	1977	An Inviscid Model of Vortex Shedding from a Circular Cylinder in Steady and Oscillatory Far Flows. *Proc. of the Inst. of Civil Engineers*, Part 2, 63, 865-880,
Stansby, PK, Bullock, GN and Short. I.	1983	Quasi-2-D Forces on a Vertical Cylinder in Waves. *Technical Note, ASCE J. of the Waterway, Port, Coastal and Ocean Engineering Div.*, 109, No. 1, 128-132. Discussion, 1984, 110, 120-123 Closure 1984, 110, 123.

Torum, A and Reed, K	1982	The Spanwise Correlation of Wave Forces on Slender Structures. *14th Offshore Technology Conf.* Paper No. OTC 4226.
Tranter, CJ	1968	*Bessel Functions with some physical Applications.* The English Universities Press.
Tsuchiya, Y and Yamaguchi, M	1974	Total Wave Force on a Vertical Circular Cylindrical Pile. *Proc. of the 14th Coastal Engineering Conference*, Chapter 105, 1789-1807.
Watson, GN	1948	*A Treatise on the Theory of Bessel Functions.* Macmillan.
Wehausen, JV	1980	Perturbation Methods in Diffraction. *Technical Note, ASCE J. of the Waterways, Port, Coastal and Ocean Div.*, 106, No. WW2, 290-291.
Wiegel, RL, Beebe, KE and Moon. J	1957	Ocean Wave Forces on Circular Cylindrical Piles. *ASCE J. of the Hydraulics Div.*, 83, No. Hy 2, Paper 1199.
Zdravkovich, MM and Namork, JE	1977	Formation and Reversal of Vortices around Circular Cylinders subjected to Water Waves. *Technical Note, ASCE J. of the Waterway, Port, Coastal and Ocean Engineering Div.*, 103, No. WW3, 378-383. Discussion, 1978, 104, No. WW2, 259-260.
Zdravkovich, MM	1977	Review of Flow Interference between two Circular Cylinders in Various Arrangements. *Journal of Fluids Engineering, Transactions of ASME*, 99, 618-633.

APPENDIX A

BESSEL FUNCTIONS

Bessel functions and their derivatives are listed below.

$J_v(z)$ = Bessel function of the first kind of order v and argument z

$$= \sum_{r=0}^{\infty} \frac{(-1)^r (z/2)^{v+2r}}{r!\, \Gamma(v + r + 1)}$$

$\Gamma(n)$ = $(n - 1)!$ if n is an integer

$Y_v(z)$ = Bessel function of the second kind of order v and argument z

$$= \frac{(\cos v\pi)\, J_v(z) - J_{-v}(z)}{\sin v\pi}$$

$H_v(z)$ = Hankel function, also called Bessel function of the third kind

$H_v^{(1)}(z)$ = $J_v(z) + i\, Y_v(z)$ = $H_v(z)$

$H_v^{(2)}(z)$ = $J_v(z) = i\, Y(z)$

Primes (e.g. $J_v'(z)$) refer to derivatives with respect to the argument (z).

APPENDIX B

Examinations were written by the author to complete the requirements of the degree.

Examination		Credit Rating
CIV 592F	Project Management in Civil Engineering (July 1988)	3
CIV 516F	Coastal Hydraulics (July 1988)	5
SEA 200F	Physical Oceanography (July 1988)	4
CIV 535S	Coastal Engineering Practice (November 1988)	5
CIV 525S	Contract Law (November 1988)	3
Thesis:	Wave forces on cylindrical piles and pile groups	20
	Total	40
Credits required for degree		40

UNIVERSITY OF CAPE TOWN

DEPARTMENT OF CIVIL ENGINEERING

CIV 592F POSTGRADUATE EXAMINATION

PROJECT MANAGEMENT IN CIVIL ENGINEERING

15 JUNE 1988 TOTAL MARK 100

NOTE

* The examination is three (3) hours
* Attempt all questions
* All writing to be in ink or ballpoint pen

1. Refer to Annexure A . Complete and hand in with the answer book.

2. Discuss the functions of a Project Manager. [20]

3. Describe the different types of information required by a Project Manager to plan a project. [20]

4. Discuss the problems which may arise when a Project Manager underestimates the cost of a Contract in his motivation to the Client for acceptance. [10]

5. Indicate , with comment , the cost items which may be affected in a contractor´s claim as also the reasons for a claim . [10]

Name..... 15 June 1988

ATTEMPT ALL THE FOLLOWING QUESTIONS WITH SHORT PRECISE ANSWERS

TOTAL MARK 40

a) What is the purpose of organising. [1]

.....

.....

b) Give four reasons why organisational charts are useful. [2]

1).....

2).....

3).....

4).....

c) For what reason are people motivated. [1]

.....

.....

d) Name two reasons why a Client would be motivated to undertake a project. [1]

1).....

2).....

e) Time and cost is interrelated but can be in conflict ,is this true or false ? [1]

True / false (circle the correct reply)

d) Indicate which of the following are procedural constraints : [3]

availability of local funding	yes/no
tendering	yes/no
detail design	yes/no
conditions of contract	yes/no
contractural incentives	yes/no
arbitration	yes/no

e) Give ten benefits of good planning : [5]

1).....

2).....

3).....

4).....

5).....

6).....

7).....

8).....

9).....

10).....

f) Indicate which of the following can assist with project control . [3]

personal commitment	yes/no
programme coordination	yes/no
review meetings	yes/no
project reports	yes/no
management support	yes/no
communication	yes/no

g) List six project management monitoring actions which should be excercised during construction. [3]

1).....

2).....

3).....

4).....

5).....

6).....

h) Indicate four normal reactions to which a person may resort if faced with a risk situation . [2]

1).....

2).....

3).....

4).....

i) Give three types of critical path charts for programming a project . [3]

1).....

2).....

3).....

j) Give eight reasons for providing a client with an estimate for a project . [4]

1).....

2).....

3).....

4).....

5).....

6).....

7).....

8).....

k) What should be considered when compiling a Schedule of Quantities for a project . [3]

1).....

2).....

3).....

4).....

5).....

6).....

l) Is the cummulative monthly payments made to a contractor a straight line , if not what shape is it ? [2]

.....

.....

m) Who takes the risk in a fixed priced contract. [1]

.....

n) On which cost elements in a contract are the inflation index values applied. [2]

1).....

2).....

3).....

4).....

o) What is the normal maximum percentage variation of a payment item that can be accepted before a Contractor may request a revision of the pay item rate , and for what reason. [2]

.....

.....

.....

p) What are statutory increases. [1]

.....

[4 PAGES]

UNIVERSITY OF CAPE TOWN

DEPARTMENT OF CIVIL ENGINEERING

M.Sc. in CIVIL ENGINEERING

CIV 516F : COASTAL HYDRAULICS

UNIVERSITY EXAMINATION : JULY 1988

ALL question may be attempted. TIME: 4 hours +

(OPEN BOOK EXAMINATION)

Constants

Sea water density = 1025 kg/m^3

Sea water weight = 10 kN/m^3

QUESTION 1

The standard alignment chart is attached and a new blank line has been inserted at the bottom of the page. This line is to be used for determining values of U_{max}, the maximum horizontal orbital velocity at the water surface, according to the Airy theory. If $U^*_{max} = \frac{U_{max}}{\pi H/T}$ is to be the dimensionless form of the variable on this line, mark off the correct positions of the $\overset{*}{U}_{max}$ values given in the following list.

$\overset{*}{U}_{max}$ = 1,01 2 6
1,10 3
1,40 4

Note that H is the local wave height throughout. Suggest a small change in the line label which would permit the scale to be used for maximum horizontal surface acceleration values. Use the new line to solve the following problem.

A swell of 10 second period with a deep water wave height H_o = 1,59 m approaches a beach with the wave crests parallel to the shore. Plot the value of u_{max} at the water surface for the following selected water depths.

65 m ; 34,4 m ; 15,9 m ; 6,8 m ; 2,86 m .

Use these calculations to estimate the water depth when the U_{max} value first reaches 1,5 m/s and check that the wave has not broken.

QUESTION 2

A sea platform consists of a square concrete slab positioned horizontally on four cylindrical vertical piles, each placed at a corner, the slab side being parallel to the local wave crest. The pile diameter is 1 m, the total pile height above sea bed is 6,4 m, and the slab dimensions are sides of 5 m with a thickness of 200 mm. The local wave characteristics are height 2 m, length 100 m, and period 12 s, the local water depth being 8 m.

(a) Considering the central 1 m high slice of any pile, calculate the horizontal forces per metre due to velocity and acceleration and by plotting these throughout one wave period or otherwise, identify the maximum force and the timing of its occurrence. Check that the velocity and acceleration distributions over the height of the pile are reasonably constant and thus estimate the total force on one pile.

Take C_D = 1,2 and C_M = 2,0 .

UNIVERSITY OF CAPE TOWN - JUNE EXAMINATION 1988

OCEANOGRAPHY SEA 200F

TIME: 3 HOURS TOTAL MARKS: 150

Answer ALL questions in SECTION A
Answer ONE question from SECTION B and THREE questions from SECTION C

SECTION A

Answer ALL questions in this section

1. Sketch the oxygen distribution in the deep ocean (4 km deep), at mid-latitude. (2)
2. What variables does the seawater density depend on? (2)
3. Define the "potential temperature". When should this be used in place of the "in situ" temperature? (2)
4. Is the ocean well stratified in the vertical? (2)
5. Give a labelled t,s diagram for the Atlantic ocean at 35^{o} S. (2)
6. Define "sigma-t" and the "standard ocean". (2)
7. Explain how a CTD works and what it measures. (2)
8. What is the "solar constant"? (2)
9. What is Group velocity and how is it related to the phase velocity of "deep water" waves? (2)
10. What is a "tsunami"? (2)
11. Define the terms "geopotential" and "dynamic metre". (2)
12. When does the diurnal inequality of the tide vanish? (2)
13. Sketch and describe the main elements of a Kelvin wave. (2)
14. Describe the terms "amphidromic point", "co-range lines". (2)
15. Give a simple definition of Salinity. (2)

TOTAL (30)

SECTION B

Answer EITHER OF the following questions:

(a) Describe with the aid of suitable diagrams, the characteristics of the major ocean current systems and the major bathymetric features around southern Africa. Include details of current speeds and surface temperatures. (30)

OR

(b) Write an essay on the phenomenon of El Nino - Southern Oscillation (ENSO) in the Pacific Ocean. (30)

SECTION C

ANSWER ANY THREE FULL QUESTIONS

(A) Discuss the main elements of the heat budget in the atmosphere and ocean, and give an indication of the relative importance of the terms in the heat budget equation.

Using the concept that a windstress in the y direction causes an Ekman flux or transport in the upper ocean in the x direction, describe how it is possible to set up an anticyclonic gyre in the South Atlantic ocean. (Hint: let y be positive north, and x positive west) (30)

(B) Discuss the method of dynamic sections to obtain the baroclinic, geostrophic velocity structure in the vertical in the Agulhas current. How can these relative velocities be converted into absolute currents?

If the surface slope on the current is 1 m in 100 km, up away from the coast, calculate the barotropic current speed and direction at 30^{o} S. (Use g=10 m s^{-2}, $f=2\Omega\sin(\theta)$, $\Omega = 7.29\ 10^{-5}\ s^{-1}$) (30)

(C) The dispersion of surface wind waves in the ocean is given by

$$\sigma^2 = gk \tanh(kd),$$

where $\sigma = 2\pi f = 2\pi/T$ is the radian frequency and
$k = 2\pi/L$ is the wave number, g = 10 ms^{-2}, d is depth.

Discuss the terms "deep water" and "shallow water" waves, and derive the phase velocities in these cases. What is the "deep water" wavelength of waves with a period of 15 s? What is the phase speed of these waves in 5m deep water?

Given that the approximate average power of the waves off the Cape coast is 40 Kw per metre of wave crest, calculate how many kilometres of wave crest must be harnessed by a wave absorbing device which is 50% efficient at extracting energy from the waves, to equal the power from a Power station producing 2 000 Mega watts. (30)

(D) Write short notes on:
The Phillips-Miles theories of wind wave generation,
South African tides,
Waves entering shoaling water,
Different types of breaking waves,
Fronts and convergences. (30)

UNIVERSITY OF CAPE TOWN

DEPARTMENT OF CIVIL ENGINEERING

UNIVERSITY EXAMINATION : 29 OCTOBER 1988

CIV 536 - COASTAL ENGINEERING PRACTICE

Time Allowed: 3 hours

Answer ALL Questions

There is a potential of 158 marks

SECTION 1 is to be handed in at the end of the first hour - CLOSED BOOK

SECTION 2 is "OPEN BOOK"

Name: .....

QUESTION 1

Briefly explain, in words and by means of annotated sketches, the meaning of the following terms:

1.1 Cope level [2]

1.2 Pendant fender [2]

1.3 Tidal prism [2]

1.4 Seiche [2]

1.5 Clinometer [2]

1.6 Show on a sketch plan of Hout Bay where you would expect to observe the effects of wave diffraction and refraction. Clearly indicate the physical cause of each effect and the form of the wave orthogonals and crests. [2]

1.7 Explain, by means of a sketch, the basic physical elements of airborne (single channel) linescan apparatus that could be used for remote sensing of the ground. [2]

1.8 Explain by means of a sketch how a dredger may be positioned using sextant resection. [2]

1.9 Explain the principle of subtense ranging using a sextant. Indicate the practical distance limit.

[2]

1.10 Explain by means of a sketch the principle of echo sounding for seabed profiling.

[2]

1.11 Give a sketch of the components and the arrangement that is used for tide recording at Granger Bay.

[2]

1.12 Explain the term "tidal residual". What is the cause of tidal residuals?

(2)

1.13 Explain the principle of the "Wave rider" accelerometer buoy. [2]

1.14 Show by means of simple sketches how field measurements of the following may be graphically presented in reports :

wind speed and direction [2]

Radioactive tracers [2]

Beach profiles [2]

1.15(a) Give a typical section of a rubble mound breakwater (annotate). [2]

1.15(b) Show the sequence of how this would be constructed in an exposed situation. [2]

1.16 Comment very briefly (<u>with a simple sketch</u>) on the adequacy or inadequacy of the following :

position of the slipway at Granger Bay [2]

boat "access" situation at harbour entrance in Hout Bay [2]

boat "access" situation at Kalk Bay harbour entrance [2]

a boat ramp at 1:6 [2]

a boat ramp at 1:15 [2]

1.17 Explain what you would look for in an aerial photograph of the coast to discern the direction of littoral drift. [2]

Total for SECTION 1 = 48 marks.

SECTION 2 - OPEN BOOK

2.1 Assuming that you are a Consulting Engineer specialising in coastal matters, reporting to the local authority responsible for the coast, write advisory notes to the responsible Committee on the following :

(a) It is September and the beach has steepened and eroded sufficiently for an adjacent parking area to appear to be in danger of being totally eroded.

Outline your proposed method of investigation, your preliminary advice as to what the Council should instruct you or Contractors to do, what alternatives measures are likely to be appropriate after completing the investigation. Give a staged breakdown of costs with time/construction expense justification. Assume the total beach length is 1 km and that the situation is as occurs at Fish Hoek.

[15]

(b) It is proposed that the harbour at Granger Bay be improved. Write a memorandum to the responsible Committee outlining the problems that occur at present and the approach you would take to improve the situation. Provide an approximate cost for the investigation and the development of a new construction plan. Give a breakdown of the work required. (Give sketch plans as needed).

[15]

(c) Describe the present situation and outline the approach you would take to investigate the cause of the tilt on the breakwater at Hermanus. Indicate two possible alternative causes, and how you would remedy the situation for each case. (In a sketch show the type of construction).

[10]

(d) Briefly explain how you would determine the directions of nett littoral drift and how you would estimate the littoral drift quantity at Hout Bay beach.

[10]

(e) Hout Bay harbour is to be extended to provide for an additional 500 floating berths for small craft. Present a breakwater and mooring layout, and show in plan details of boat ramps, harbour control and other infrastructure requirements that should be considered at a preliminary stage. State all assumptions.

[60]

Total for SECTION 2 = 110 marks

UNIVERSITY OF CAPE TOWN

DEPARTMENT OF CIVIL ENGINEERING

UNIVERSITY EXAMINATION - NOVEMBER 1988

COURSE CIV 525S - CONTRACT LAW

OPEN BOOK EXAMINATION

Time : 150 Minutes

PLEASE ANSWER ALL QUESTIONS, BEARING IN MIND THE NUMBER OF QUESTIONS, IT IS SUGGESTED THAT YOUR ANSWERS BE KEPT AS BRIEF AS POSSIBLE.

TOTAL NUMBER OF MARKS : 100 MARKS

10/11/88

106 01 01

QUESTION 1

"It must be conceded that the phraseology of Clause 54 (of the Standard Engineering Contract) is capable of bearing the construction placed upon it by the Court a quo. But in my opinion it is also open to a different interpretation". (Per Van Heerden JA in Melmoth Town Board v Marius Mostert (Pty) Limited 1984 (3) 718 at 728 F).

Comment on the above statement and deal with the powers of the engineer in terms of the said Clause 54.

10 Marks

QUESTION 2

You are a director of a construction company.

The construction company applies to an insurance company for the issue of a performance bond and the insurance company requires you to sign a suretyship for the obligations of the construction company in respect of that contract. However, in terms of the suretyship you bind yourself "as surety and co-principal debtor in solidum for the due and faithful performance by the construction company to the insurance company of all and whatsoever obligations undertaken by it on behalf of the construction company in connection with any matter whatsoever".

Shortly afterwards you resign from the construction company, and a year later you receive a letter from the insurance company advising you that in connection with another project carried out by the construction company after you had left its employ, the construction company was indebted to the insurance company, who are now looking to you for payment in terms of the suretyship signed by you.

You are very alarmed because you had not envisaged that you would be liable for obligations which were incurred after you had left the employ of the construction company. You decide to take legal advice.

What are you likely to be told?

10 Marks

QUESTION 3

You are a director of a construction company.

In terms of the construction contract, certain work was to be sub-contracted to a sub-contractor nominated by the architect.

The architect obtained a tender for this work from the sub-contractor and instructed your firm to accept the work. You sent an order on your standard printed form which contained on its reverse side printed conditions which included a clause reading as follows :-

"Payment of the amount due in terms of this order will only be effected after we (the main contractor) have received payment from the employer".

The sub-contractor wrote back to you thanking you for the order and the work was carried out.

The employer became insolvent before having paid for all the work.

The sub-contractor calls on you to obtain payment for all the work done by him.

What would you reply?

10 Marks

QUESTION 4

You are a director of a construction firm.

You contract with a development company (X Developers (Pty) Limited) to build houses on separate erven which are owned separately by individual owners who are clients of the development company, and with whom the the development company had entered into agreements for the building of these houses.

As the work progressed from time to time, each of the owners paid X Developers (Pty) Limited the amount required from them.

Unfortunately, X Developers (Pty) Limited find fault with your work and advise that they are not prepared to pay you any further sums until you have completed what they regard as the remedial work.

You dispute that in fact any remedial work is necessary, but you are not prepared to continue work until the amount due to you in terms of your contract with X Developers (Pty) Limited has been paid.

The individual owners need their accommodation urgently and decide to contract with another firm to build for them and finish off the work.

You do not want to give up possession of the building sites and the work thereon until you have been paid in full, and the individual owners institute action against your firm for an order claiming possession of the various sites. Your Board asks you for an outline of what your rights are in this matter.

Draw a short memorandum setting out your rights.

10 Marks

QUESTION 5

You are a director of a construction company.

It appears that your firm has failed to comply fully with performance of work undertaken in terms of the contract, but you wish to claim for the work which you have done.

You decide to take legal advice on your rights, and the attorney whom you consult says "Ah, this is a B K tooling case", and proceeds to give you certain advice.

On the basis that he knows what he is talking about, write a short memorandum for your managing director setting out what your rights are.

10 Marks

QUESTION 6

You are a director of a construction company.

Your firm has entered into a contract to build certain road works, and the contract is in terms of the General Conditions of Contract of 1982 as issued by the South African Institution of Civil Engineers.

Times are difficult - interest rates are rising - and your managing director advises you that it looks like it may be necessary to enter into an arrangement with the company's creditors.

He asks you to prepare a short memorandum for the Board setting out the rights of the employer under your contract, should your company decide to follow this course.

Prepare the memorandum.

10 Marks

QUESTION 7

You are a director of a construction company.

In terms of the contract your company has undertaken to pay your employer R10 000,00 a day for every day by which delivery of the completed works is delayed.

Due to internal disputes in the construction company, delivery of the completed works is delayed for a period of 3 months and your company's accountants make provision for the sum of R90 000,00 as being due by your company to the employer.

The managing director asks you to write a short memorandum for the Board setting out whether this is a liability, whether it can be reduced, and whether there would be any defence to a claim.

Write it.

10 Marks

QUESTION 8

In what circumstances may an extension of time be granted in terms of the General Conditions of Contract 1982.

10 Marks

QUESTION 9

You are a director of a construction company.

It is clear that a dispute is arising between the employer and your company, and the Board intends discussing whether the matter should go to arbitration or litigation.

You are asked to prepare a short memorandum discussing the relative merits of these methods of dispute settlement.

10 Marks

QUESTION 10

You are in practise as a consultant engineer.

You are appointed as the engineer in regard to a particular contract entered into in accordance with the General Conditions of Contract 1982.

One of the nominated sub-contractors complains bitterly to you that the main contractor has not paid him for work already done by such sub-contractor, for which you know the employer has already paid the contractor, and the nominated sub-contractor advises you that he is still working under the sub-contract and he would like you to protect him insofar as regards payment in the future.

What could you do?

Would your answer be any different if the sub-contractor was not a nominated sub-contractor?

10 Marks